ER-6219 ~~NG4 26527~~
NASA CR-57020

DEVELOPMENT OF A HELIOTROPIC ORIENTATION DEVICE FOR HIGH CONCENTRATION RATIO SOLAR POWER GENERATION SYSTEMS

FINAL REPORT
15 January 1964 — 10 August 1964

Prepared for
NASA Langley Research Center
Langley Station
Hampton, Virginia 23365

Prepared Under
CONTRACT No.: NAS 1-3588
CONTROL No.: L 3312

TRW ELECTROMECHANICAL DIVISION
THOMPSON RAMO WOOLDRIDGE INC.
8655 EUCLID AVENUE, CLEVELAND, OHIO 44117

OCTOBER 16, 1964

ER-6219

DEVELOPMENT OF A HELIOTROPIC ORIENTATION DEVICE FOR HIGH CONCENTRATION RATIO SOLAR POWER GENERATION SYSTEMS

FINAL REPORT

15 January 1964 – 10 August 1964

Prepared for

NASA Langley Research Center
Langley Station
Hampton, Virginia 23365

OCTOBER 16, 1964

Prepared Under

CONTRACT No.: NAS 1-3588
CONTROL No.: L 3312

By the

SOLAR ENERGY SYSTEMS GROUP
NEW PRODUCT RESEARCH DEPT.

TRW ELECTROMECHANICAL DIVISION
THOMPSON RAMO WOOLDRIDGE INC.
CLEVELAND, OHIO

FORWARD

This report was prepared by Thompson Ramo Wooldridge Inc. under NASA contract NAS-1-3588, Control No. L3312.

The TRW Program Manager was Mr. William J. Leovic, supervisor of the Solar Energy Systems Group. Members of the group who contributed significantly to the successful completion of the program include Mr. Milton W. Mueller, Project Engineer; Mr. William H. Reinhart, Research Engineer; Mr. Edward A. Maroli, Research Engineer; and Mr. Donald J. Paul, Designer.

The TRW Engineering Report Number is ER 6219.

ABSTRACT

A program directed towards the design and evaluation of a passive orientation device for use in alleviating the stringent sun vector alignment requirements associated with lightweight high quality paraboloidal solar concentrators has been completed. The orientation device fabricated and testing during the program is designed to sense the unbalance of solar energy impinging on sensors located adjacent to the focal plane of the concentrator. The device responds to this unbalance by producing corrective torques thereby relocating the concentrator and reducing the solar orientation error.

A variety of mechanisms using bimetallic and vapor pressure sensor-actuator elements were evaluated and the vapor pressure type was selected. A mercury filled sensor and bellows actuator mechanism was constructed and integrated with a calorimeter device which simulates a thermionic generator. Test results have shown that the mount is easily capable of reducing ± 5 degree alignment errors to less than ± 5 minutes when applied in a system consisting of a searchlight quality 5 foot concentrator and a simulated thermionic generator operating at 2000°K.

TABLE OF CONTENTS

LIST OF ILLUSTRATIONS

LIST OF ILLUSTRATIONS (Continued)

LIST OF ILLUSTRATIONS (Continued)

LIST OF ILLUSTRATIONS (Continued)

1.0 INTRODUCTION

Recent advances have made thermionic power conversion systems extremely desirable for space vehicle applications, particularly when highly accurate solar concentrators use the limitless energy of the sun to provide the required power. The advantages of not having to carry a fuel or heat source are obvious, but the requirement for high temperatures with thermionic energy conversion fosters a formidable solar orientation problem. The requirement that high precision concentrators be sun oriented to within tenths of a degree established the need for development of highly accurate and reliable orientation mechanisms.

Feasibility test models conceived and built in the past have shown that heliotropic mounts can provide the type of control action required to orient solar concentrators without using complex electronic or electromechanical devices. The models demonstrated that mount power requirements are very small, representing only the energy normally lost outside a thermionic generator cavity due to the image spread associated with paraboloidal reflectors. The simplicity of the design concept and the small number of parts in a passive heliotropic mount promote high performance and reliability. Also since many space power system generator concepts will involve the use of relatively small concentrator-generator modules, the heliotropic mount represents an ideal way of easing the structural alignment tolerances in the assembly of an array of modules since each module is independently oriented.

The heliotropic mount is a sun sensing and seeking device as is implied by its name. In practice it is possible to arrange many simple mechanisms, exclusive of any electronics or electromechanical components, which will exhibit a tropistic reaction when placed in view of the sun. The heliotropic mount concept is illustrated in Figure 1.0-1 for a mechanism using bimetallic strips to obtain the corrective action. The motion shown for the misaligned concentrator is greatly exaggerated since the mount mechanism can be made to be a very high gain device. The operating principle is, however, clearly illustrated. As the vehicle, and therefore, the concentrator, is misoriented with respect to the sun, the focal spot tends to move away from the concentrator axis and produce an unbalanced heating of the interposed bimetallic elements. These elements in turn produce restoring torque which minimizes the alignment error.

In early 1959, the Thompson Ramo Wooldridge Corporation (TRW) designed and tested several feasibility models of the heliotropic mount which used simple bimetallic sensor actuators to obtain concentrator alignment corrections. An improved model shown in Figure 1.0-2 was tested and found to possess a gain sufficient to limit concentrator alignment error to less than 0.1 degrees in the face of vehicle misorientation of up to 5 degrees. Other characteristics such as thermal response, mechanical strength or stiffness, and load capacity were somewhat deficient. The mounts were relatively simple and operation was confined to simple bench testing with little regard for the environmental conditions which would be encountered in an actual solar thermionic system.

HELIOTROPIC ORIENTATION SYSTEM SCHEMATIC

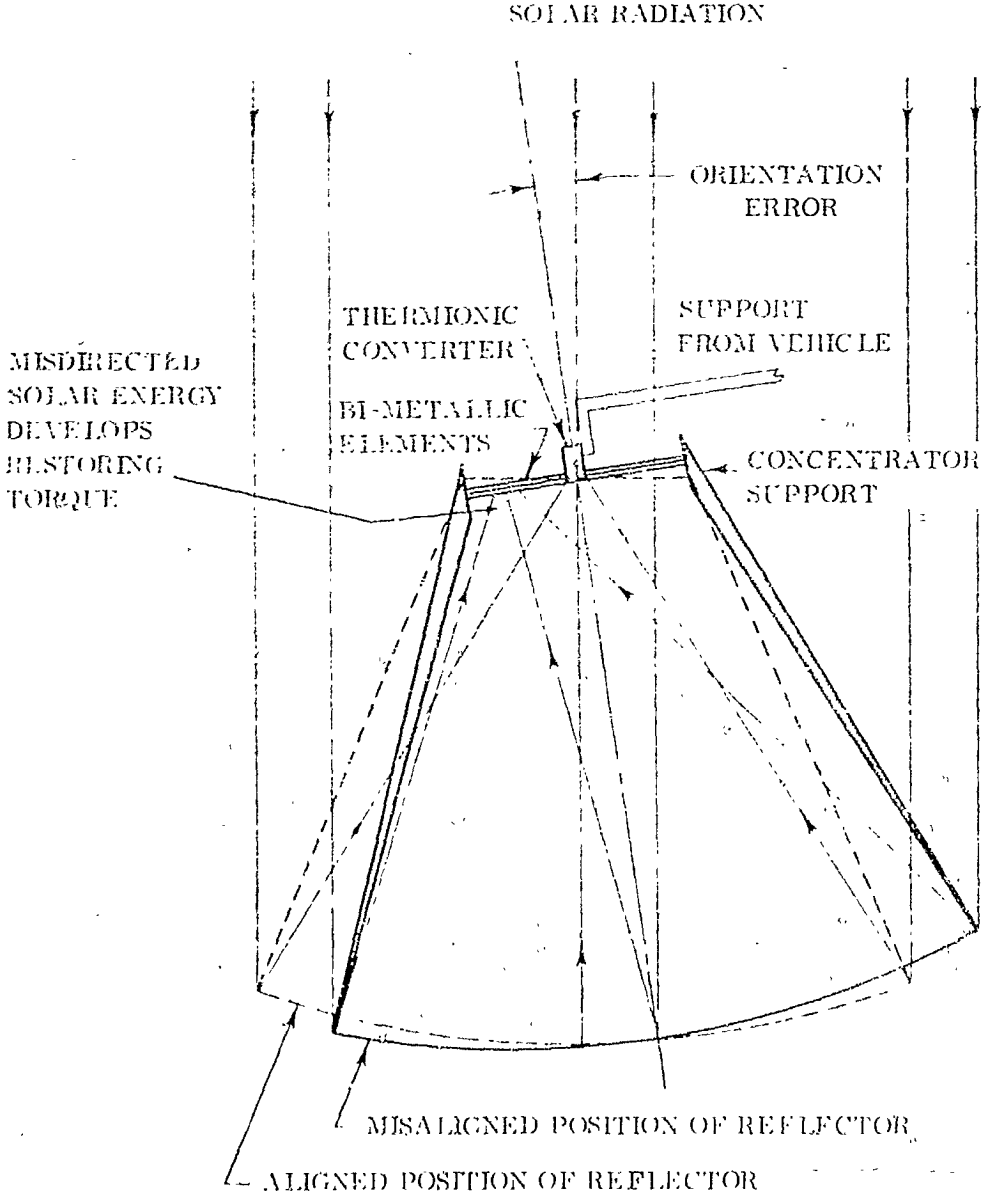

FIGURE 1.0-1

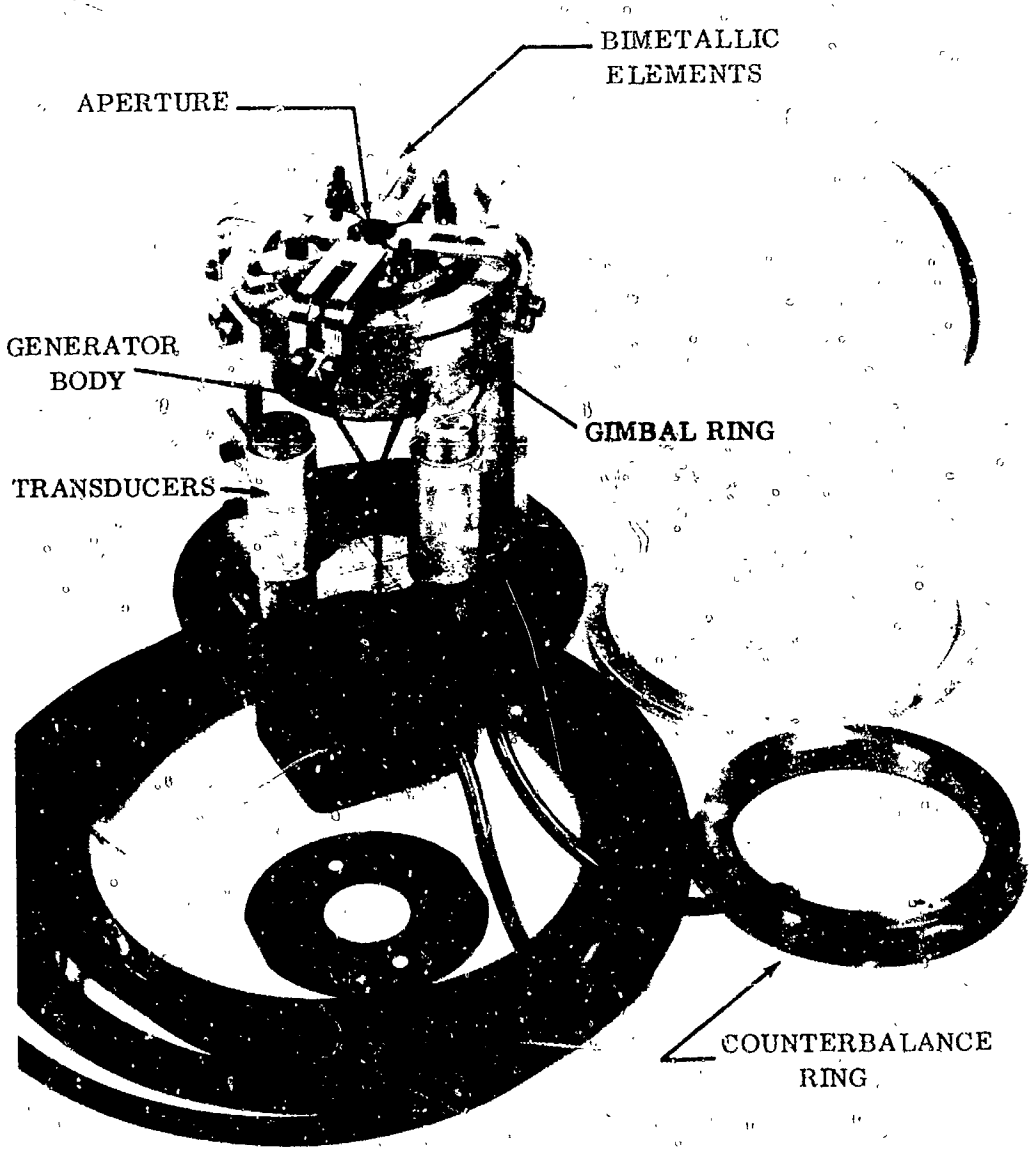

COMPLETE HELIOTROPIC MOUNT ASSEMBLY
INSTALLED ON A VACUUM PLATE

FIGURE 1.0-2

In recognition of the need for a passive type orientation device for future space power systems, a research program was awarded to TRW by NASA for the fabrication and testing of a typical device. Under the NASA sponsored program the objective was to develop a practical mount configuration which would operate with precision concentrators of up to 10 feet in diameter. The test mount design established during the program, is sized to operate with a 5 foot concentrator to facilitate testing of the mount with solar energy. This mount was to be fully compatible with the operating envionment and capable of reducing concentrator misalignment to ± 12 minutes or less in the face of vehicle orientation errors of ± 5 degrees. During the program, several mount concepts were reviewed and, based on the results of this review a specific concept was selected and designed. This design is as near prototype as possible and demonstrates that the selected configuration is entirely compatible with the operating environment and posses-es operating characteristics suitable for integration in anticipated future space power systems. The mount design was completely tested to determine all pertinent thermal, mechanical, and structural characteristics. Because of the nature of the tests and the complications of trying to simulate space vacuums, zero gravity conditions, thermal equilibriums, etc. the test activity represented one of the most critical and difficult undertakings in the program.

There are a number of configurations using both bimetallic and vapor pressure sensor-actuators which can be adapted to a solar power generating system to reduce orientation requirements by means of repositioning the concentrator. The principal configurations which were considered in detail under this program are reviewed in the following sections. In all cases the mount sensors were considered to intercept the tail or fringe zone of the flux profile at the generator cavity aperture. Other approaches using secondary lenses or mirrors are possible and would perhaps prevent mount or sensor destruction during initial acquisition or gross misorientation periods when very high flux levels prevail at the sensors. The use of the concentrated cone of flux is very desirable, on the other hand, since it provides for a very high and variable gain system and eliminates the problems of aligning the secondary mirror systems.

2.0 SUMMARY

The effort during this research project has been directed in seven major areas associated with the development, design, and evaluation of a near prototype heliotropic mount. These areas are:

1. A review of the basic considerations and design factors related to the many mounts and actuation concepts.

2. A detailed study of, and finalization of a preferred mount design concept.

3. The fabrication of all mount hardware along with the preparation of test facilities required for a comprehensive mount evaluation.

4. Conducting preliminary performance tests and calibration of the calorimeter device.

5. Modification of the mount as required.

6. A complete laboratory evaluation of the modified mount to determine all thermal, inertial, and gain characteristics.

7. Solar testing of the mount to confirm characteristics predicted during the design phase and the laboratory testing.

A review of the approaches to reorientation of misaligned solar concentrators led to the conclusion that the most satisfactory approach is to slew or rotate the concentrator about the generator assembly. Other approaches suffer excessive losses and are generally more difficult to mechanize. The basic heliotropic mechanisms, including various configurations of bimetallic elements and several vapor pressure mechanisms using bellows, bourdon tubes, and helix configurations, were evaluated on the basis of their particular characteristics and limitations. The results of this evaluation has led to the selection of the vapor pressure concept using bellows type actuators, mercury as the charging fluid, and flexure bearings as the prime components. This selection was made not because bimetallic and other vapor pressure concepts were unsuitable, but because the bellows actuator concept appeared to offer the best combination of desirable characteristics and the greatest flexibility and adaptability which will be required in anticipated future system applications.

A tentative design was carried out using the bellows concept built around a thermionic type module consisting of a five foot diameter solar concentrator and a 100 watt thermionic generator. Appropriate characteristics were assumed for the concentrator, generator and mount hardware. These characteristics were then used in an analog

computer program to permit a reasonably comprehensive study of the mount performance. Favorable computer study results including a parametric evaluation of various changes in component characteristics were subsequently obtained. Based on these results a heliotropic mount was designed and the necessary drawings prepared.

The fabrication of a power distribution calorimeter which simulates the thermionic generator, the special mounting plates and bracketry, and other components of the heliotropic mount was accomplished. The calorimeter device is intended to provide a good simulation of the operational environment associated with a thermionic generator and serves as the power absorbing and measuring device required for the solar testing phase of the mount evaluations. The actual mount hardware is designed as an attachment to the calorimeter assembly as shown in Figure 2.0-1, and possess all the features which would be required for a working space power system. The assembly including the vacuum enclosures for environment simulation and support structures have been designed to permit a complete test evaluation of all thermal, dynamic, and mechanical mount characteristics.

Preliminary tests conducted on the mount in the laboratory showed a number of defects in the assembly. The calorimeter, which consists of four conducting elements sized and instrumented with thermocouples to permit a measurement of heat flux, was found to be very erratic in its behavior. The calorimeter cavity attained very nearly its 1700°C design temperature with the proper power input simulated by electron bombardment heating, but an unstable mechanical junction between the sensing elements and the radiator sections within the calorimeter produced radical fluctuations in conducted power. The bellows selected for the mount actuators was also found to vary greatly in its characteristics with the application of pressure. The overall spring rate was found to quadruple at design pressures, deflection was limited, and the effective bellows area was determined to be half the value speficied by the vendors literature. Most important of all, the sensors used in detecting concentrator alignment errors were found to be several hundred degrees too hot due to the direct thermal input from the adjacent hot cavity of the calorimeter.

The mount was reworked to eliminate or reduce the problems encountered during preliminary testing. The poor thermal joint at the calorimeter shaft to radiator junction was brazed to form a one piece assembly. The bellows length was doubled by welding on an identical bellows and lengthening the bellows housing and other linkages. Both changes were found satisfactory in that the calorimeter output was stabilized and the mount spring rate reduced by a factor of two. The doubling of the bellows length also increased the allowable deflection to a full ± 5° of mount motion which had at first been found deficient to the extent that a slight yielding of the bellows occurred when the mount was rotated over 4°. The sensor overtemperature problem was not overcome by attempts at improved shielding and heatsinking. The final solution required the removal of the sensor to a location outside the simulated generator body to a point nearly 1/2 inch forward of the focal plane and

HELIOTROPIC MOUNT

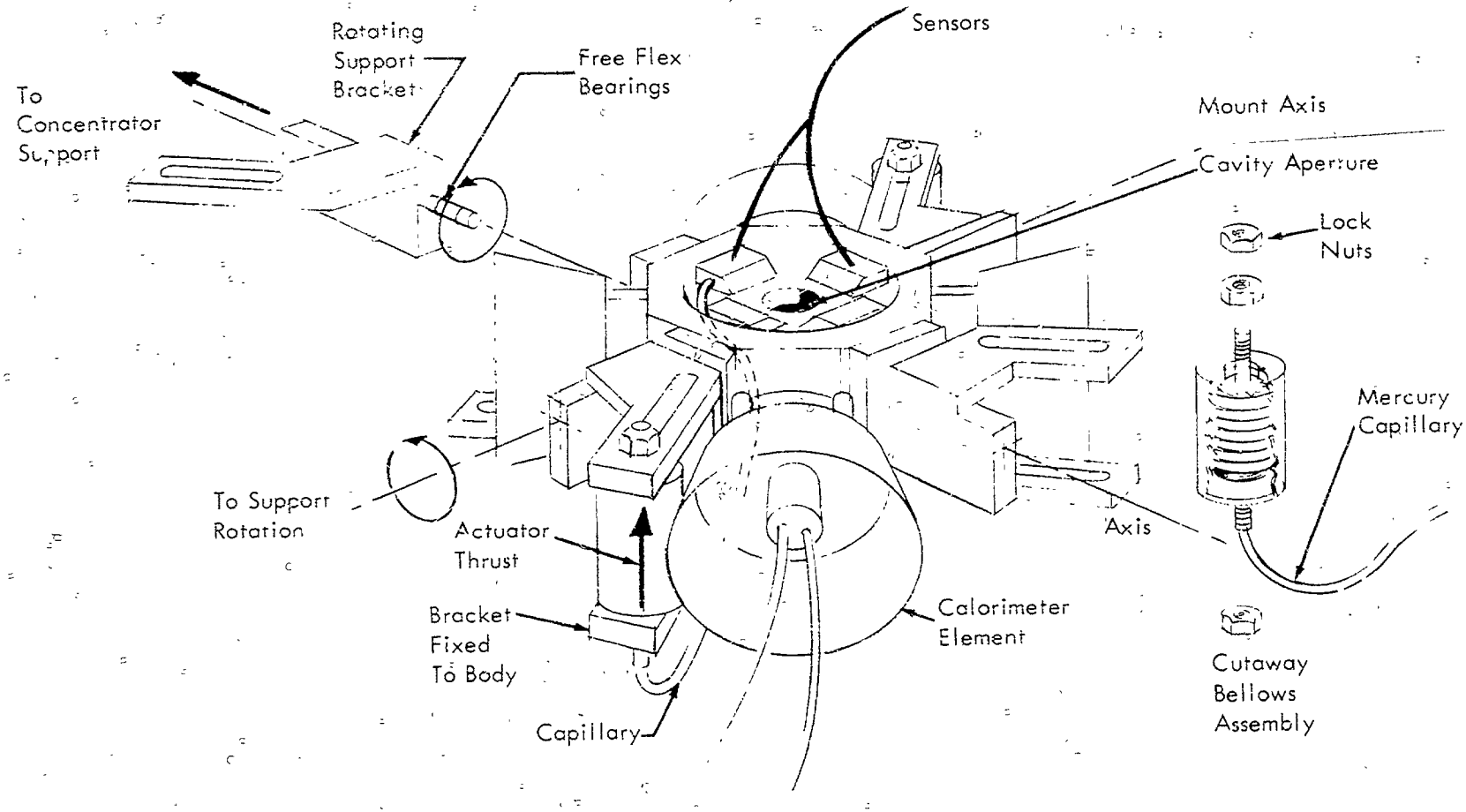

FIGURE 2.0-1

the cavity aperture. There was considerable concern that the flux profile or distribution so far forward of the focal plane might not be suitable to insure high sensitivity to small concentrator alignment errors thereby reducing the mount gain to an unsatisfactory level. Preliminary estimates of this flux distribution indicated a reasonable chance for obtaining good mount performance, however, and the very favorable solar test results have since born out the wisdom of this relocation.

The reworked mount was subjected to a series of laboratory tests to obtain as much performance data as possible. The tests were divided into several discrete classifications because of the complications of trying to test space qualified hardware under an earth bound environment. Static and dynamic tests of mount rotation as a function of sensor temperature were carried out in high vacuum using combinations of electron bombardment and resistance heating techniques to simulate input power levels under solar operation. Inertial tests, simulating the mass of the concentrator, were of necessity carried out outside the vacuum enclosures with simple electrical heating elements used to force sensor and other key components to the desired temperature levels. Dynamic frequency response data was obtained for a considerable range of temperatures and for several concentrator inertial values simulated by simple weighted lever arm systems The range of frequency response data was severely limited because of the sensor heater masses but data obtained for frequencies up to 0.05 cps compared favorably with previous computer study performance values.

Under actual solar energy tests using the TRW solar tracker rig and a 5 foot diameter glass concentrator mount performance was found to be satisfactory. With the sensors free of the added thermal inertia of the heaters and operating in the high vacuum of the tracker environmental chamber, the mount response and gain were very close to the design values. The mount has demonstrated its ability to respond to signals which vary at frequencies up to 0.1 cps. The mount gain or measure of sensitivity has been found to be better than 1 degree rotation per 1 minute of misorientation signal. With this gain it is easily possible to maintain concentrator alignment within $\pm$ 5 minutes while subjecting the vehicle structure to orientation errors of $\pm$ 5 degrees.

A review of the performance test results leads to the conclusion that heliotropic devices can be developed and used satisfactorily in anticipated future space power systems. Such mounts should be able to correct for random orientation errors in stabilized vehicles or space stations, and may even be suitable for use with slowly rotating spin stabilized stations.

3.0 MOUNT CONCEPT EVALUATION

3.1 Review of Methods for Correcting for Concentrator Misalignment

An evaluation of two methods of concentrator and cavity alignment was performed. These methods include generator cavity translation and concentrator realignment by means of heliotropic devices.

Of the two approaches stated a stronger case may be made for the concept which slews or repositions the concentrator. The arguments which are presented for or against each concept are founded not only on an analytical evaluation but also upon practical physical and dynamic considerations appropriate to the mount mechanisms. Other factors which are given consideration are those pertaining to the environmental and operating conditions which are present in the typical space station or vehicle.

The chief advantage of repositioning the cavity is that it would not be burdened by the large inertias associated with the concentrator slewing mechanisms. Also, by the addition of a small weight penalty, it appears reasonable that such a mount could be made to withstand the spin loading associated with large rotating space vehicles or stations. However, the flux distribution with this mount arrangement is subject to considerable distortion and spread due to angular misalignments in the concentrator. This is shown in Figure 3.1-1 which indicates the spot shape and axial displacement for a 45° rim angle, 10 foot diameter paraboloid under several conditions of misorientation. The circular spot represents the aperture diameter which would be sufficient to intercept all of the solar flux assuming a perfect concentrator surface geometry. The spot outlines shown displaced from this circular aperture represent the effect of misorienting this concentrator in the amount of 3, 10, and 30 minutes of arc. It is immediately seen that even if the cavity aperture were moved to coincide with the center of the peak flux intensity of each spot there would be substantial losses due to the large proportion of flux falling outside the aperture. The area of the spot with 30 minutes misorientation is 175 per cent of the circular aperture area. This number is substantially increased for orientation errors approaching 5 degrees and for concentrators of higher rim angles.

The cavity translation requirements for a 26 inch focal length concentrator would be approximately:

$$\delta = 26 \sin \phi = 2.26 \text{ inches}$$

for ϕ equal to 5 degrees. If the alignment error occurs on a plane 45 degrees from the actuator axis, the required actuator stroke must be 3.2 inches. These numbers assume the solar ray from the center of the concentrator will be coincident with the center line of the altered flux distribution profile. Since this is not the case, the actuator motion must be even larger. In considering motions of this sort, it is almost mandatory that pistons, linear motor, jack screws, or similar components be utilized. Even if high flexure welded bellows could be employed the bulb sensor inventory volumes would become very large with an attendant loss in response and performance.

FOCAL SPOT DISTORTION DUE TO CONCENTRATOR
ALIGNMENT ERRORS

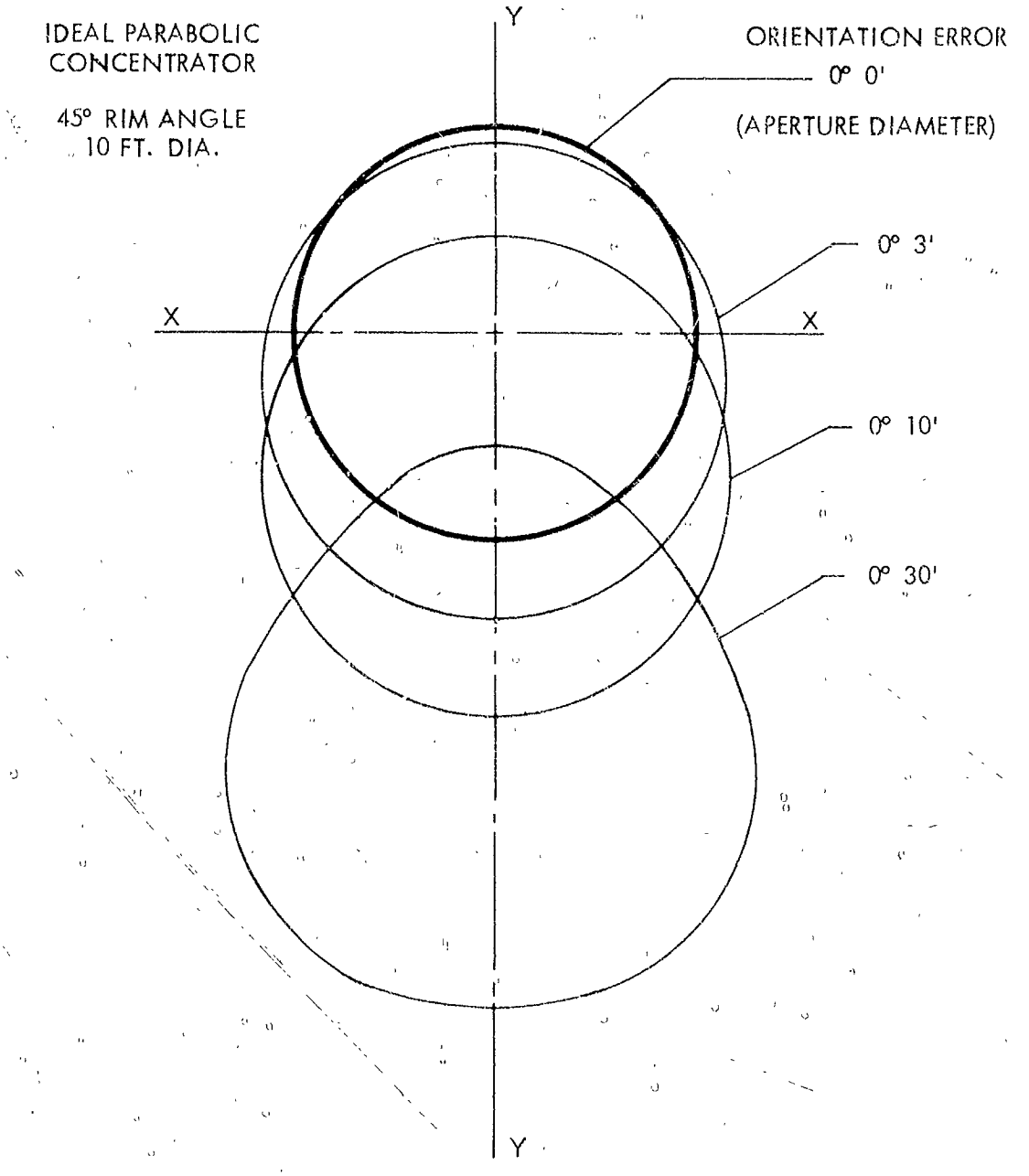

FIGURE 3.1-1

The fact that the focal spot is changed and the flux profile made unsymmetrical would also make it very difficult to determine a suitable sensor location. Even though the sensors would always seek a location where a force balance would exist in the mount actuator system the power input to the sensors would vary with misorientation error. This power input variation could easily be as much as 10 or 20 times the design value under oriented conditions and a mount failure due to overtemperature or overpressure might occur.

Because of the large amounts of power lost outside a properly sized cavity aperture, the excessively long actuator stroke requirements and the sensor location and equilibrium problems with angular misorientation it appears the translation type mount is unsatisfactory.

The approach to concentrator reorientation which uses concentrator alignment must be considered in light of three factors. One, the amount of power lost due to the rotation of the cavity aperture in the focal plane as part of the correcting action of the mount. Two, the variation in the image shape, location and percentage power loss due to concentrator alignment error. Three, the effect on sensor power input due to image spot changes with concentrator misorientation.

The amount of cavity power lost due to a rotation of the aperture plane relative to the concentrator axis has been found negligible compared to other image distortion or translation losses. The analysis performed to establish the extent of this loss involves several simplifying assumptions. These are: 1) that the concentrator is perfectly aligned with the sun, 2) the concentrator is a perfect parabola, and 3) the flux distribution is uniform over the focal spot.

With these assumptions it may be shown that the percentage of flux which fall outside the aperture circle for a single ray of light may be as high as 7.86 per cent. Figure 3.1-2a illustrates this prospect where y is the aperture circle radius established by the ellipse formed due to a solar angle of 32 minutes and a concentrator rim angle of 60 degrees.

Examination of Figure 3.1-2b which represents the concentrator-cavity relationship shows at once that only part of the elongated ellipse will fall outside of the cavity. This part of the ellipse possesses an area sufficient to produce a 7.86 per cent reduction in cavity power based on a uniform flux distribution.

This percentage loss is only true for a ray coming from the edge of the rim at a point in the plane perpendicular to x-x and on the concentrator axis. All other rays would be subject to a smaller or in most cases zero loss. An analysis of the concentrator geometry with respect to the inclined cavity aperture was made to determine what concentrator areas would actually cause ellipses with dimensions sufficient to produce an impingement of flux outside the cavity aperture limits. The results yield an effective concentrator area of 6.4 per cent and include a section of surface approximately as shown in Figure 3.1-2c.

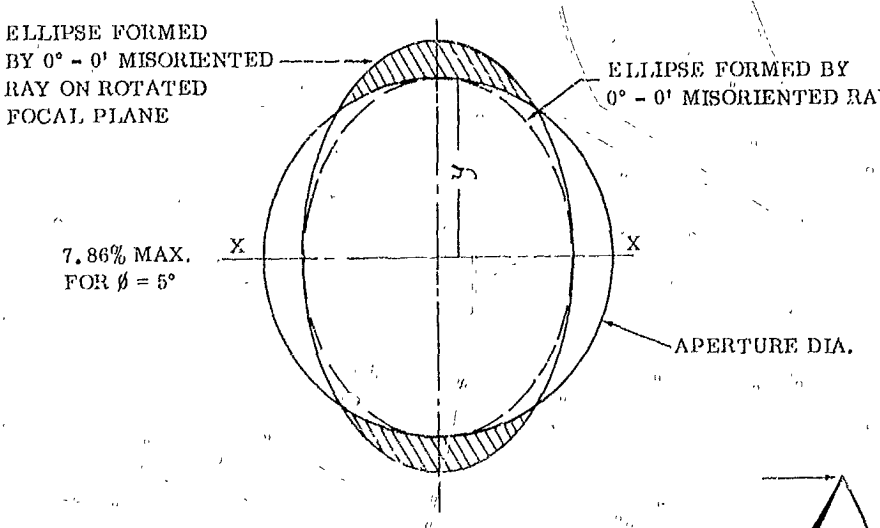

FIGURE 3.1-2a

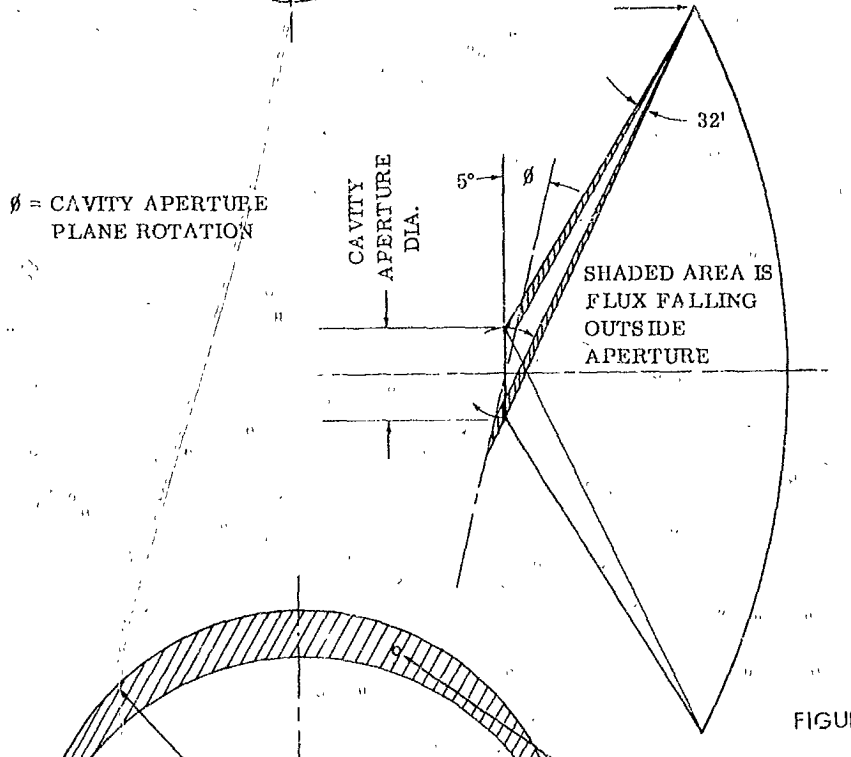

FIGURE 3.1-2b

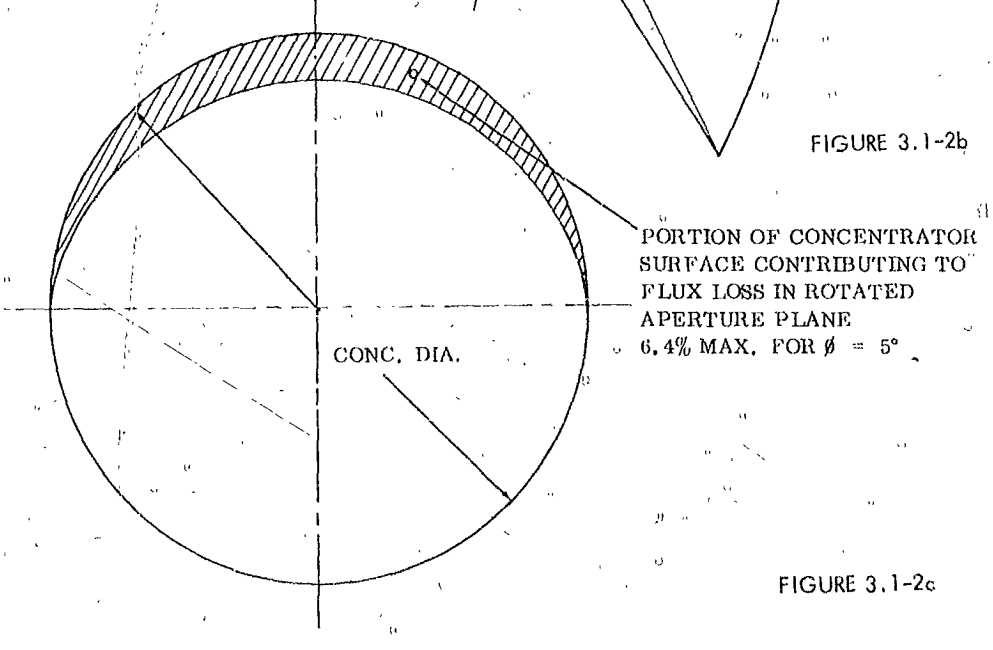

FIGURE 3.1-2c

With a uniform flux distribution the total loss is then 7.86 x 6.4 or 0.50 per cent. With a true non-uniform flux distribution this percentage will drop by an estimated factor of ten or more.

The power lost due to concentrator alignment error has been determined for a ten foot diameter concentrator and 45 degree rim angle using Figure 3.1-1. For a perfect paraboloic the change in shape and location of the image relative to a cavity aperture located on the concentrator axis is seen to be great for misorientation errors in excess of 3 minutes. A higher rim angle would of course increase these changes in shape and location. Assuming uniform flux over the spot areas an integration has been performed to develop a curve of cavity power versus misorientation angle as shown in Figure 3.1-3. In a curve which would be generated using a true flux profile for each image spot, the shape would be altered to maintain the total power at a higher level for misorientation angles up to 16 minutes and reduce total cavity power at a much faster rate for angles exceeding 16 minutes.

A more general evaluation of the effects of concentrator misorientation may be made from the plot of results of a computer study.[1] Figure 3.1-4 shows the reduction in percentage of focal plane power which results for several assumed area concentration ratios as a function of orientation error. The curve expressed for the 12,000 concentration ratio would be most appropriate for consideration with heliotropic devices. For this curve it is shown that even with the absence of concentrator surface and geometry errors the available power falls by 10% or more with an alignment error of 12 minutes. For most space power generation systems a 10 per cent decline in power would probably represent a tolerable limit.

Figure 3.1-5 represents a third evaluation of the effect of concentrator misorientation in terms of the measured power output from a thermionic cubical cavity generator as a function of concentrator orientation error. These curves are summarized in Figure 3.1-6. The band width is shown here to indicate the maximum variation in power output as a function of misorientation in several planes and with minor variations in the solar constant. The amount of power attenuation here indicates not only the effect of a reduction in cavity power but the effect of a change in generator performance due to a less favorable flux distribution and a reduction in generator efficiency due to the cavity temperature fall off.

The last factor concerning power input variations to the sensors due to changes in the image shape and flux distribution is the most difficult to evaluate. The misorientation of the concentrator, even when limited to 12 minutes, results in a general enlargement of the focal image spot and a distortion of the flux profile. The sensors will not

---

[1] The data in Figures 3.1-4 through 3.1-6 were obtained during TRW research activities prior to the initiation of the program reported herein.

CAVITY POWER EFFICIENCY VERSUS MISORIENTATION

45° 10 Foot Diameter Concentrator Assuming Uniform Flux Distribution

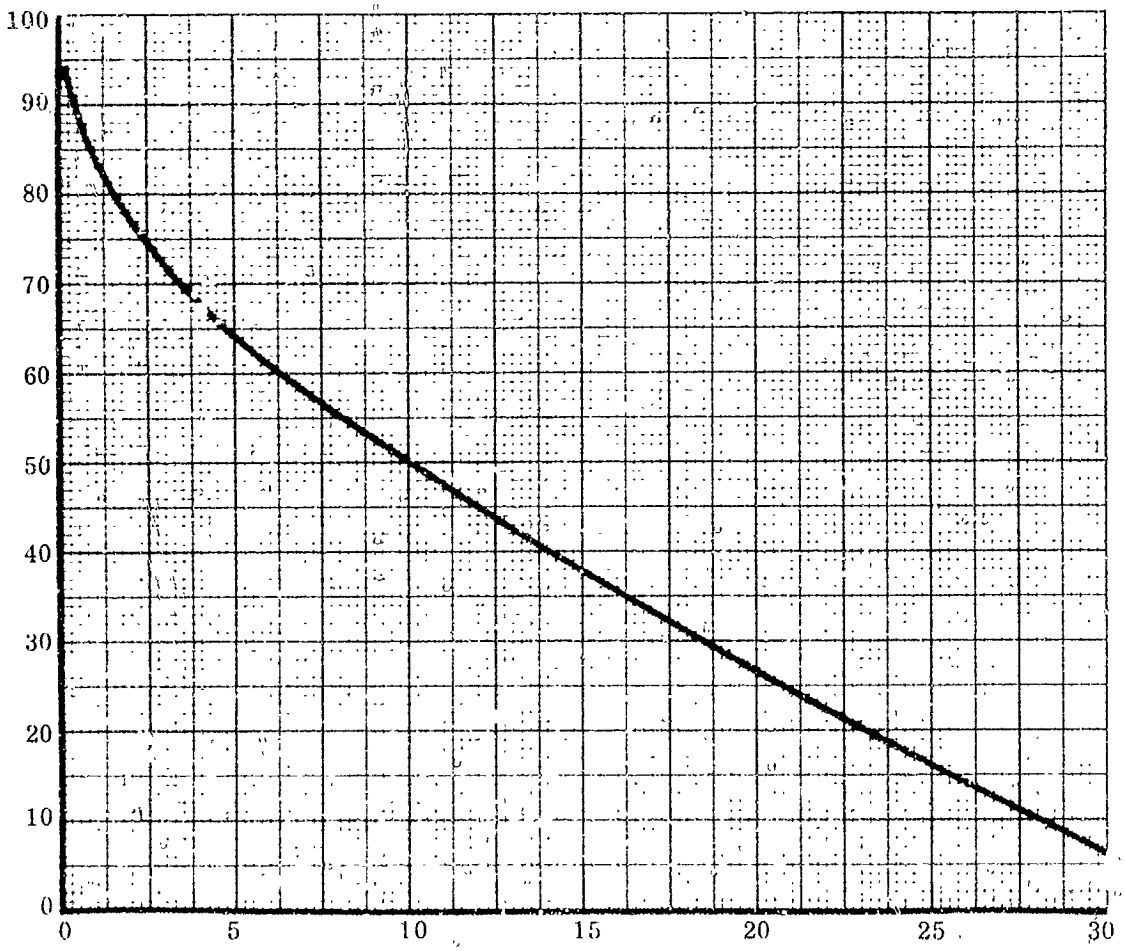

FIGURE 3.1-3

PER CENT ENERGY FALLING INTO APERTURE VS. CONCENTRATION RATIO

(Computed From Generalized Mathematical Model on IBM 7090)

Rim Angle - 60°

$\ell_R = \ell_\theta = 0$

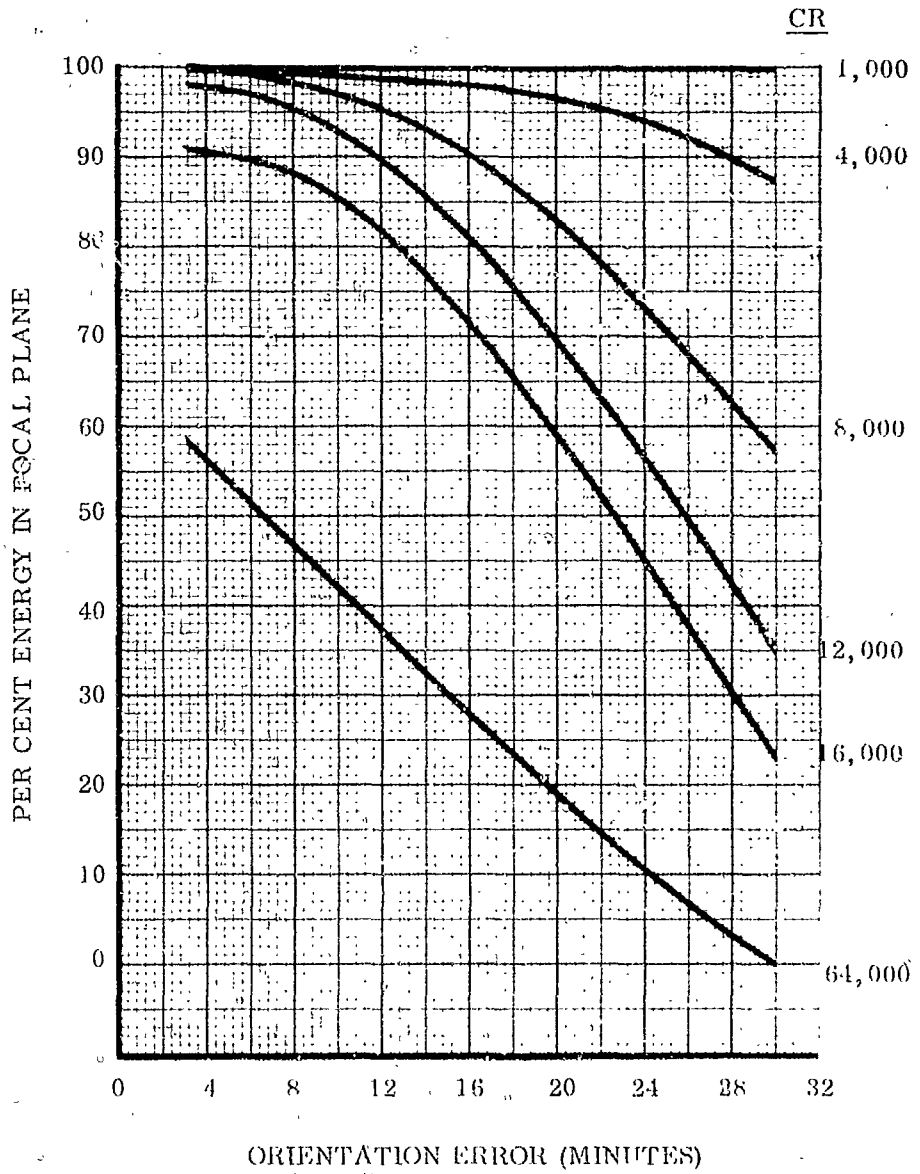

FIGURE 3.1-4

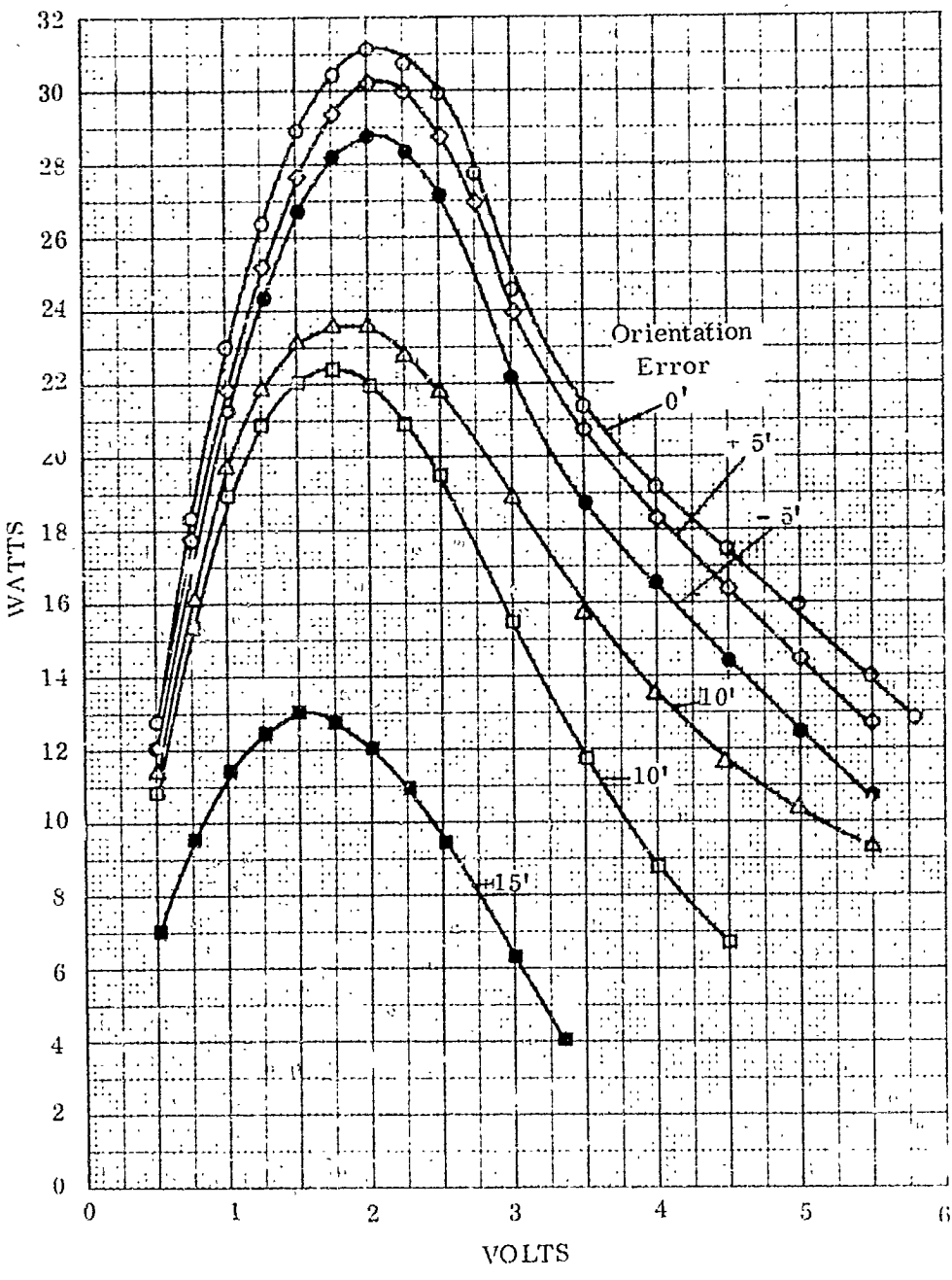

THERMIONIC GENERATOR POWER OUTPUT VERSUS VOLTAGE FOR VARIOUS SOLAR CONCENTRATOR MISORIENTATION ANGLES

FIGURE 3.1-5

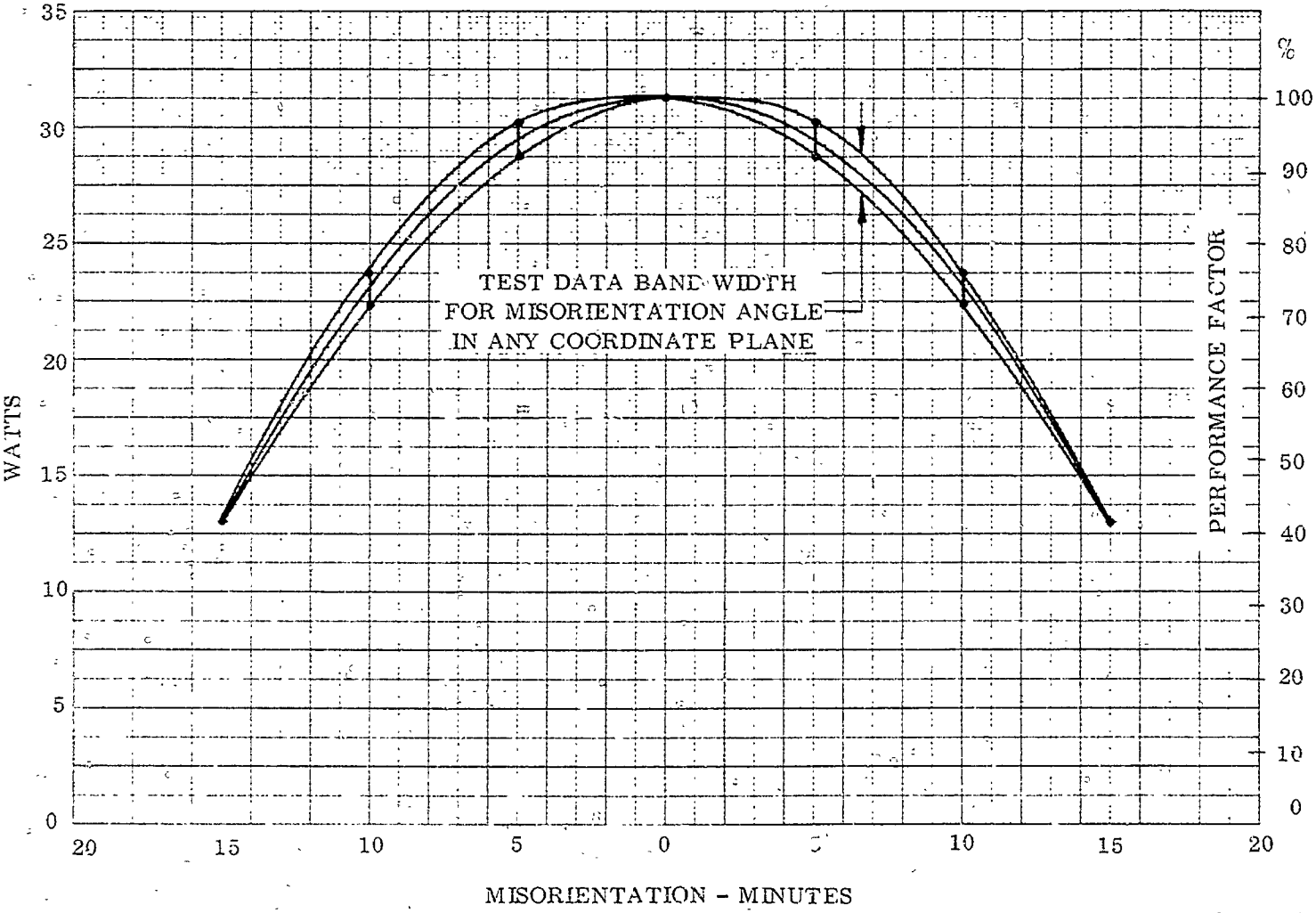

FIGURE 3.1-6

COMPOSITE PLOT OF MISORIENTATION EFFECTS - C. C. G.
(POWER & PERFORMANCE FACTOR VERSUS MISORIENTATION ANGLE)

introduce any additional alignment errors due to this change or distortion in the signal source. In fact the balancing action of the mount is such as to insure the direction of the maximum possible flux into the cavity under any condition of misalignment regardless of the type or extent of image or flux distortion. This is true because regardless of the flux profile or ambient level of the sensors, the actuation mechanism will always try to reduce the sensor power input to a minimum. Also for a balanced system each sensor in an opposing pair will be adjusted to have a comparable minimum input which requires therefore that the maximum flux be directed between these sensing points. Since the sensing points are located at the cavity aperture the flux must enter the cavity. The only real danger is that the increase in power input might raise the ambient sensor temperature above design limits and cause the destruction of the mount mechanism.

3.2 Review of Bimetallic Mechanisms

The most direct approach to passive solar orientation is to use simple bimetallic sensor actuators. Previously tested models(2) utilized these bimetals in the form of simple cantilever members with the tips protruding into the cone of concentrated solar flux and the rear end anchored to a gimbal ring arrangement. The operating mechanism involved the tilting of this gimbal ring by the unbalanced heating of opposed bimetal elements. These mounts worked well in most respects but possessed several weakenesses and performance limitations.

For example such arrangements require some means of supporting or fixing the tip end to the generator assembly without introducing large resisting torques in the plane 90 degrees removed which would render the elements in that plane inoperative. Also there was found to exist a conflict between requirements for mechanical stiffness and rapid thermal response. Further, the pivot bearing or support arrangements used in the gimbal ring assembly were not able to carry the required loads or withstand long term operations in vacuum at high temperatures. These factors and others indicated a need for a review of bimetal actuators to select more appropriate configurations. A summary of this configuration evaluation is presented in the following paragraphs, for: 1) cantilever strips, 2) gimbal-less mount, 3) spiral coils, 4) hairpins, 5) discs, 6) helical coils, and 7) flexure bearings.

Cantilever Concept

This concept shown in Figure 3.2-1a is of the type previously built and tested. The listing of advantages and disadvantages that follow are based on the experience with these previous test models.

(2) TRW Corporate Program.

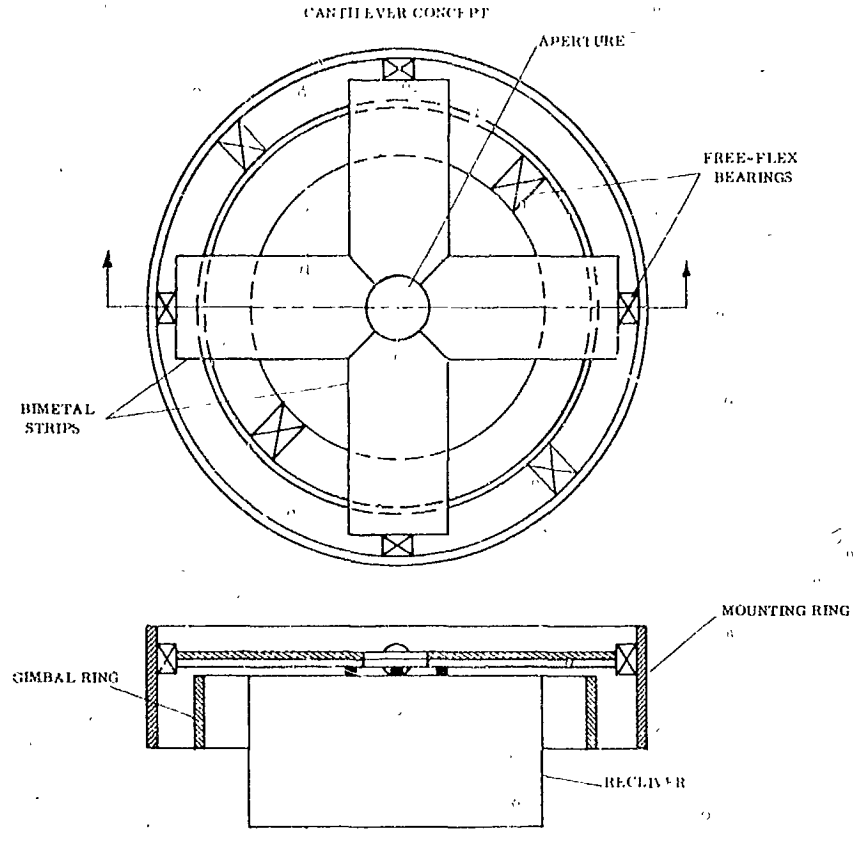

FIGURE 3.2-1a

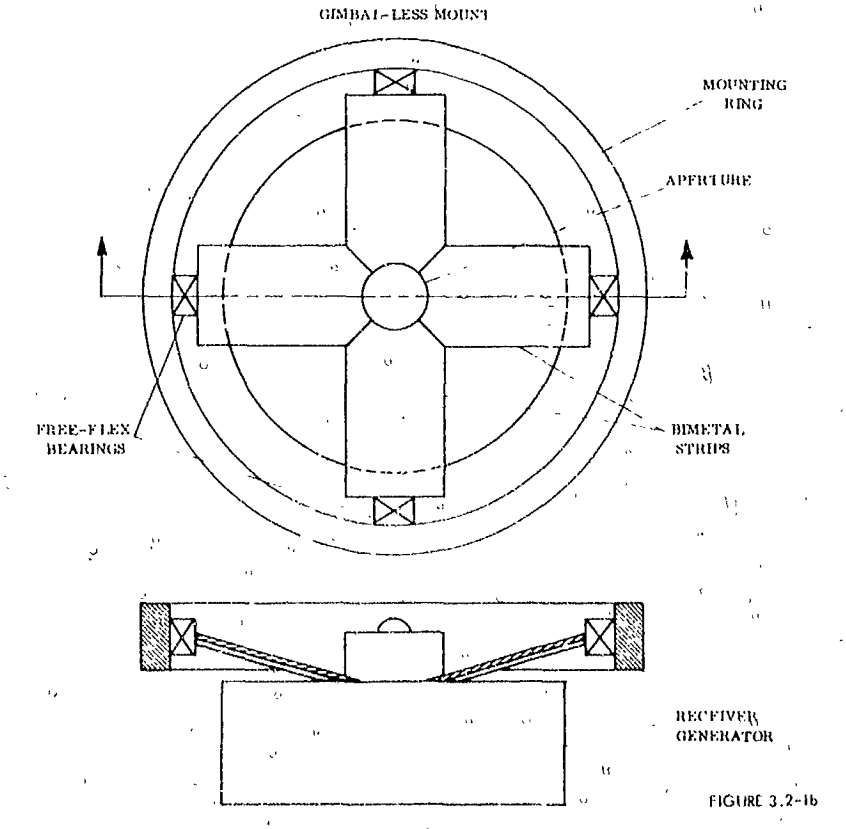

FIGURE 3.2-1b

Advantages	Disadvantages
1. Relatively simple	1. Poor thermal response
2. High gain	2. Poor mechanical strength
3. Easily fabricated	3. Difficult to locate forward bimetal support due to hot cavity
4. Easily assembled	4. Sensitive to overtemperature
	5. Subject to hysteresis
	6. Poor mechanical advantage in support actuator arrangements
	7. Introduces large bearing loads
	8. Suitable forward bearings not available

Gimbal-Less Mount Concept

The concept shown in Figure 3.2-1b is an extension of the cantilever configuration. It introduces some simplification by eliminating the need for gimbal rings and fixing the concentrator rigidly to the generator. Analysis shows this type mount would work only with very thin bimetals and would be very inefficient both thermally and mechanically.

Advantages	Disadvantages
1. Few parts	1. Requires thin weak elements
2. Easy to fabricate and assemble	2. Elements must carry the weight of concentrator-generator
	3. Method of attachment of element tips very poor both thermally and mechanically
	4. Generator moves in and out of focal plane
	5. Low spring rate will reduce response characteristics

Spiral Coil Concept

Figure 3.2-2a shows the spiral concept which permits a large volume of bimetal material to be packaged in a small volume. This dense packaging means a considerable amount of work is made available for a given temperature change. Unfortunately

this dense packaging also complicates heat transfer and heat rejection and greatly increases the thermal response time. This arrangement also suffers the need for a separate probe assembly, and special support or bearing structures, and presents an envelope which is not easily integrated in a thermionic generator.

Advantages	Disadvantages
1. High density packaging of actuator materials	1. Difficult to heat and cool
2. Moderate ease of fabrication	2. Requires probe assembly
	3. Requires complicated support or bearing structures
	4. Not easily integrated in generator structures
	5. Poor thermal response
	6. Possible low mechanical stiffness

Hairpin Configurations

Another arrangement which shows considerable promise involves the use of hairpin or folded bimetal elements. This arrangement, shown in Figure 3.2-2b will double the deflection achieved with the cantilever type and eliminates the need for a forward support or bearing point. The open assembly also provides good heat transfer but the larger mass of the elements is found to result in a longer response time.

Also in order to fully utilize the deflection capabilities and to reduce or eliminate torsional effects at the point the elements are fixed to the generator, a compound type bimetal must be used. This compound type assembly involves the interchange of high and low expansion materials on the same side of the bimetal element to provide control over the deflection mode at critical points. This assembly is of course much more difficult to properly build.

Advantages	Disadvantages
1. Large deflection capability	1. Longer thermal response time
2. Good heat transfer	2. Elements move relative to the focal plane
3. No forward support point required	3. Sensitive to overtemperature
4. Simple to fabricate and assemble	4. Must carry the weight of concentrator and generator
5. Moderate gain	5. Has 1/2 the stiffness of cantilever type for same element cross section
6. No hysteresis expected	

SPIRAL CONCEPT

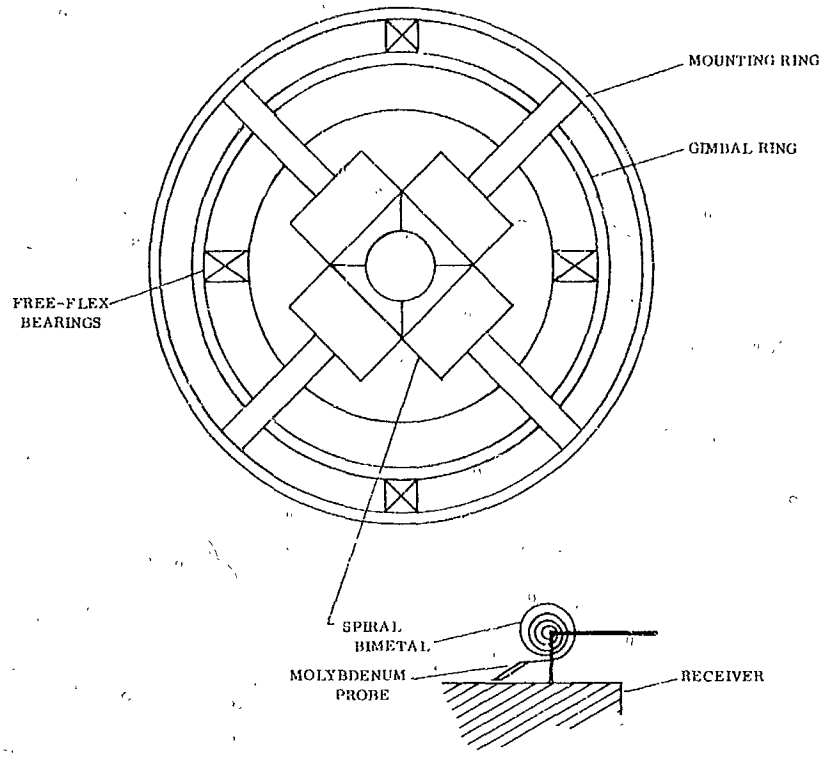

FIGURE 3.2-2a

HAIRPIN CONFIGURATION

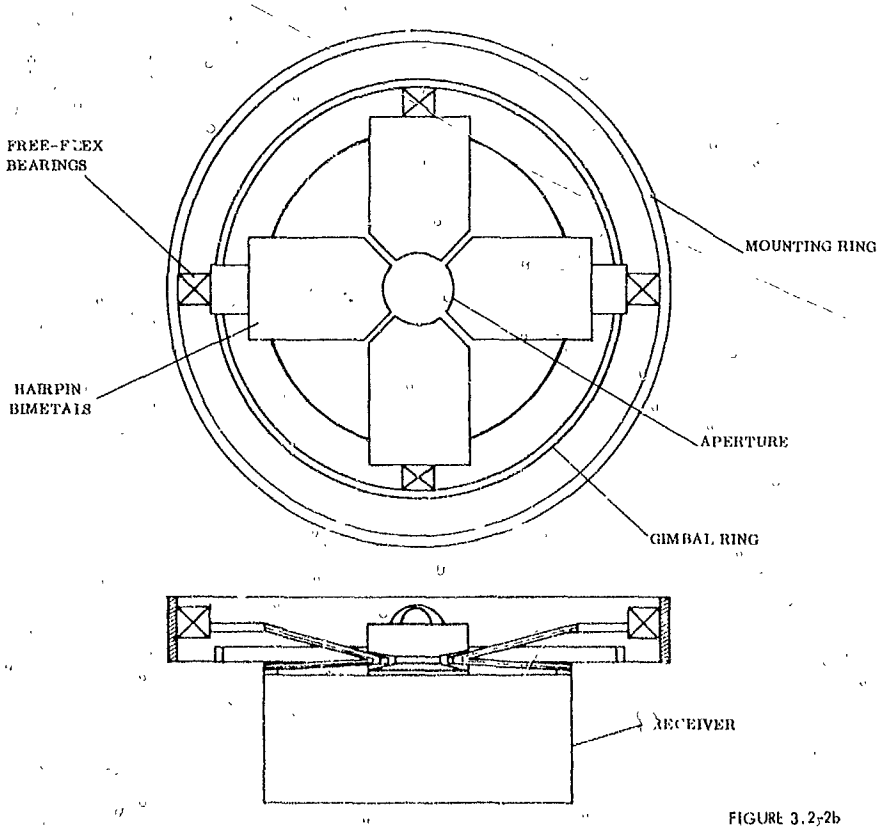

FIGURE 3.2-2b

Disc Configurations

The disc actuator concept is similar in many respects to spiral type and would require similar mounting and sensor probe arrangements. Also because of the ability to package compactly there is a potential for large work outputs. The disc assemblies, as shown in Figure 3.2-3a suffer problems of thermal response and heat transfer and are mechanically very weak. It appears that in order to achieve the large deflections required it is necessary to use very thin disc elements. This aggravates heat transfer and makes the system quite soft with an attendant poor response characteristic. Also, the disc assemblies and the incorporation of a suitable probe is quite difficult.

Advantages	Disadvantages
1. Large deflections	1. Poor thermal transfer
2. Elements removed from high temperature area	2. Difficult to fabricate
3. Large work output possible	3. Not easily integrated in generator
	4. Mechanically soft
	5. Poor response characteristics

Helical Coils

The most satisfactory combination of structural and physical properties is found in the helical type assembly shown in Figure 3.2-3b. The actuating element is protected from overtemperature by the use of an efficient probe. Heat transfer into and away from the actuator element is adequate. The element rotation is applied directly about the bearing axis and the amount of actual element deflection required is held to a minimum. The flexure bearings support all the load of the concentrator and generator and yield only to the torque induced by the elements. The assembly of the mount is also simplified by not requiring the elements to be preloaded under the ambient assembly conditions. Also the assembly is of such a shape as to readily permit its installation in a thermionic generator. The only deficiencies lay in the area of thermal response and mechanical stiffness or spring rate.

Advantages	Disadvantages
1. Relatively simple construction	1. Poor thermal response
2. High gain	2. Mechanically soft
3. Induces rotation directly	3. Difficult to incorporate large volumes of bimetal material
4. Protected from over-temperature	
5. Good thermal transfer	

DISC ACTUATOR

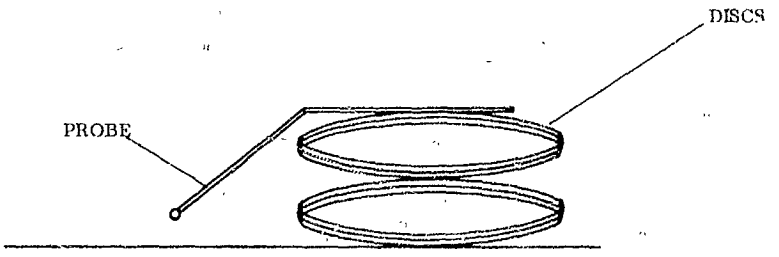

FIGURE 3.2-3a

HELIX CONFIGURATION

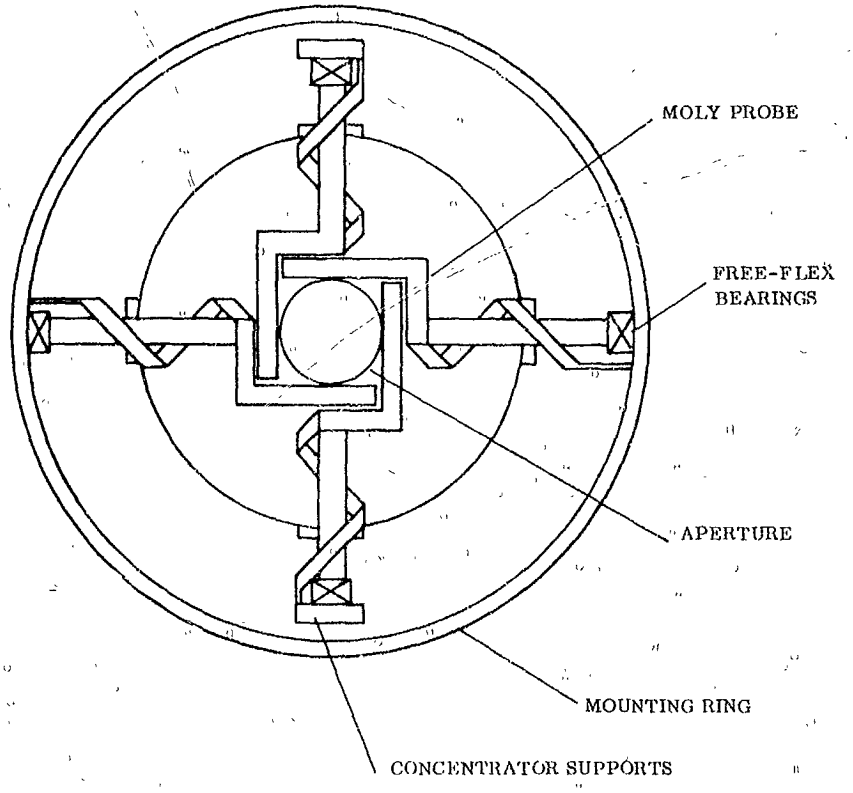

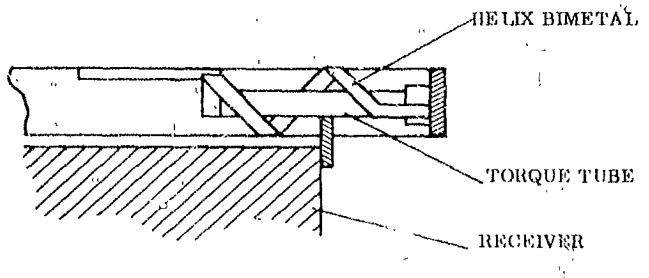

FIGURE 3.2-3b

6. Easily integrated
7. Bearings carry all load
8. No displacement of sensors relative to focal plane
9. Requires no preloading in assembly

Flexure Bearing Configuration

This configuration in Figure 3.2-4 is an attempt to combine the functions of both the frictionless flexure bearing and the bimetal actuator element. The flexible strips used in the bearings are replaced by bimetal elements and the inner sleeve caused to rotate with respect to the outer sleeve by heating or cooling the assembly. When applied in opposing pairs the bearing assemblies could be used to correct for concentrator misorientation. This concept was originally considered for use in mounts powered by either secondary optical systems or auxiliary electrically operated heaters. With the power input derived from sources other than the primary concentrator flux cone such a mechanism may have a potential advantage. Considering only the concentrator flux as a power source, this concept is at a great disadvantage. The assembly cannot be miniaturized sufficiently to permit a close approach to the focal point and probes are not efficient in transferring energy rapidly over the longer path.

Advantages	Disadvantages
1. Large load capacity	1. Poor heat transfer along probe
2. High gain	2. Difficult to fabricate
3. Removes elements from hot environment	3. Assembly must be relatively large
4. Produces rotation directly	4. Poor thermal response
5. Requires no preloading	

3.3 Review of Vapor Pressure Type Mechanisms

Vapor pressure actuated mounts have been tested previously in component stages. The results of these limited tests and some preliminary analysis of potential mount designs have shown this type of mount to have favorable characteristics. Under this program the investigation of the various vapor pressure concepts has been pursued in more detail along with the previously discussed bimetal concepts. In mount configurations designed to restore or control orientation by realigning the concentrator the requirement, design, and protective features of the sensor actuation mechanism is similar to that encountered with the bimetals.

FLEXURE BEARING CONFIGURATION

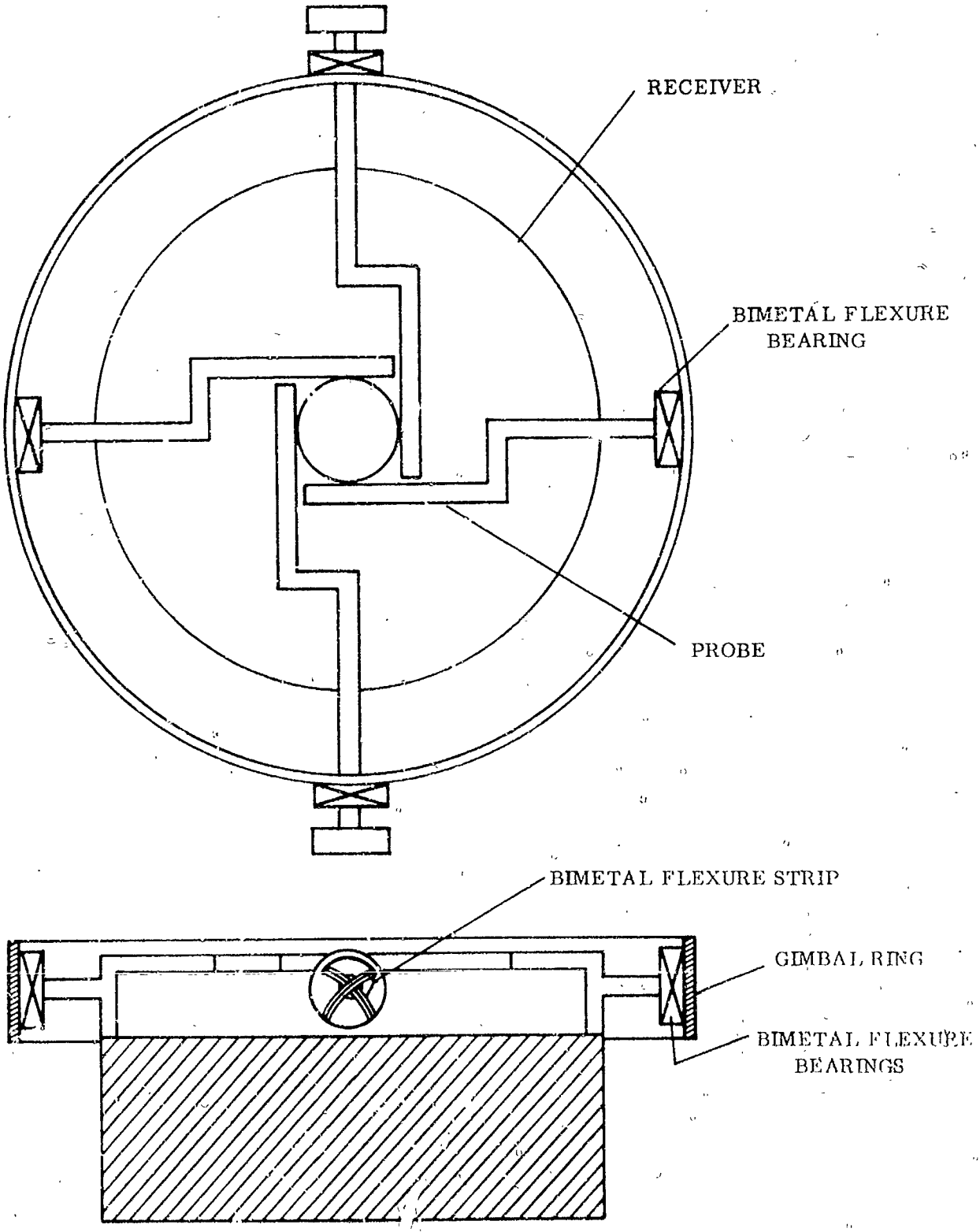

FIGURE 3.2-4

It is necessary to insure against destructive overheating of the sensors, to insure good thermal and mechanical response characteristics, high gain, and general compatibility with the environment and power generating system. In addition the vapor pressure system must be protected against overpressure, charging fluid decomposition, and corrosion. Three basic actuation mechanisms were considered in an effort to select the concept which will offer the best combination of features. These three are described as bellows type, bourdon tube type, and helix type. Many arrangements of each is possible but for the most part the overall characteristics are not appreciably changed by such arrangement changes.

Bellows Actuator Type

Bellows type assemblies are considered to be the easiest and most conventional approach to obtaining actuation. Current technology in the bellows fabrication area has made available a number of small bellows of stainless construction with burst pressures well over 1500 psi and with deflection and spring characteristics which are appropriate for use in a heliotropic mount. A number of arrangements are possible with the compact bellows assemblies most of which are quite suitable for integration with a thermionic generator assembly. Also by varying the bellows size a wide range of motive force or torque and motion can be made available to facilitate the adaptation of the mount to other systems.

The gain of a bellows system is also easily varied with most reasonable working fluids since the rate of change of vapor pressure with temperature increases with an increase in ambient temperature. A typical assembly is shown in Figure 3.3-1.

Advantages

1. Efficient force generation
2. Negligible hysteresis
3. High and easily varied gain
4. Compact and easily adapted
5. Long cycle life
6. Good thermal and mechanical response
7. Can incorporate internal damping for system stability

Disadvantages

1. Moderately expensive
2. Difficult to fill properly
3. Must be protected against gross over pressure
4. Produces rotation indirectly

BELLOWS MOUNT CONCEPT

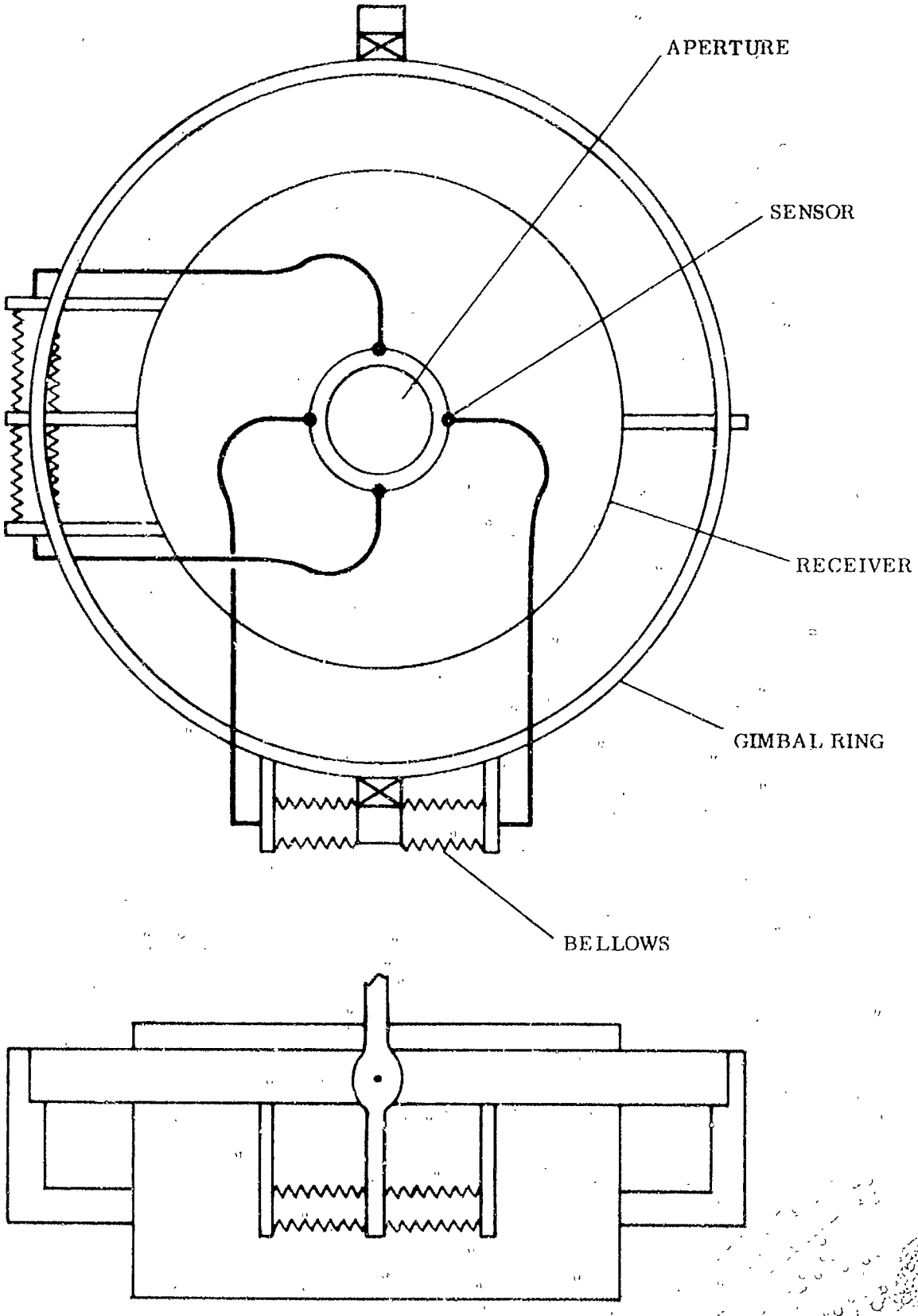

FIGURE 3.3-1

Bourdon Tube Actuators

Assemblies of the type shown in Figure 3.3-2 were considered for mount application. The unit shown was previously tested and found to be relatively inefficient as an actuator mechanism. The assembly does not possess sufficient strength to carry the concentrator generator weight and the amount of torque generated is small compared to the bellows mechanisms. The device has the advantage of eliminating the need for any additional bearings but presents a rather formidable assembly problem and requires a somewhat large and inconvenient shaped assembly.

Advantages	Disadvantages
1. Moderate gain	1. Complicated assembly with many joints
2. Eliminates the need for bearings	2. Large size
3. Good response characteristics	3. Inefficient
4. Produces direct rotation	4. Low strength

Helical Tube Actuator

The use of a pressurized helical tube to produce motion results in a configuration very similar to that shown for the helical bimetal assembly in Figure 3.2-3b. The probe is replaced by a sensor and connecting capillary. This assembly is somewhat more desirable than the bourdon tube configuration in that it is more compact and has the use of external support bearings. Also, the assembly is simpler and perhaps easier to integrate with a generator. Using a sensor probe provides for good thermal response and both this assembly and the bourdon tube assembly require smaller sensor charge inventories because of the way motion is produced in the flattened tube assemblies.

Advantages	Disadvantages
1. Good response characteristics	1. Low efficiency
2. Small sensor inventory	2. Design is not flexible or easily adaptable
3. Produces direct rotation	3. Assembly is difficult
	4. Mount is soft

3.4 Preliminary Design Studies and Analogue Computer Evaluation of Proposed Mount Concept

Based on the review of all bimetal and vapor pressure actuator concepts two mechanisms were selected for a more detailed evaluation. These were of the helical bimetal and the bellows type. The mount designs were developed around state of the art hardware. The

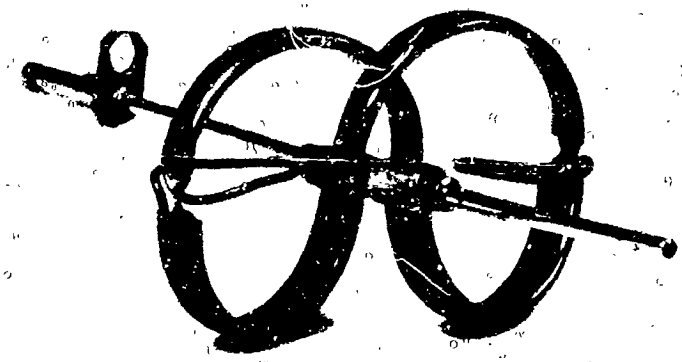

BOURDON TUBE ACTUATOR

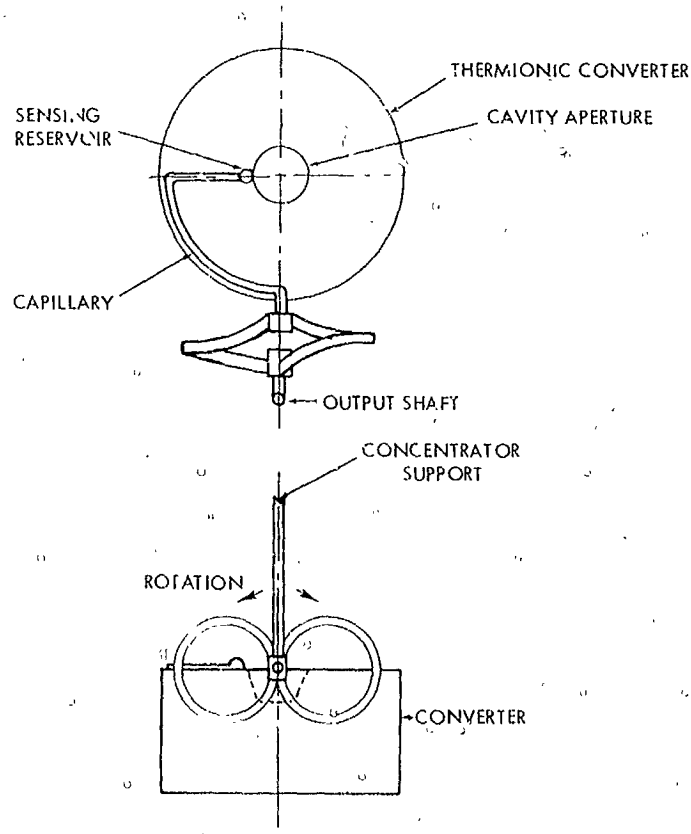

BOURDON TUBE ACTUATOR MECHANISM

FIGURE 3.3-2

designs assume a 60 inch diameter 60 degree rim angle concentrator weighing 10 pounds. This concentrator would represent a moment of inertia of approximately 17.5 lb in. sec.^{2} The generator is assumed to be of the cesium vapor type operating at 2000°K, weighing approximately 5 pounds, and having a 100 watt output capacity.

A parametric study of the helix bimetallic configuration was performed and found to show considerable promise in terms of the resulting element characteristics. In this configuration it appears possible to obtain a reasonably stiff system with a fairly high natural frequency and to get high gains and torques sufficient to move the concentrator.

A summary of these characteristics is shown in Figures 3.4-1, 3.4-2, and 3.4-3. Figure 3.4-1 shows the natural frequency of the concentrator mass-mount spring system. The use of a t/L ratio of 0.01 and a volume of 0.1 in^3 would give a practical bimetal element of 4 x 0.62 x 0.04 inches. The natural frequency would be 1.5 radians per second.

From Figure 3.4-2, it is seen that a 20°F temperature change would produce 1° of mount rotation. Figure 3.4-3 in turn indicates an unbalanced torque of 3.6 in. oz. would be induced by a 20°F temperature unbalance in opposing elements. This typical combination would be satisfactory in most instances although not necessarily optimum.

The inadequacy of the bimetallic concept as determined by analysis and laboratory test lie in its relatively poor thermal response. Tests simulating a helix configuration showed that the thermal time constant of such an assembly is on the order of 6 minutes or greater. This response is consistent with the thermal response achieved with a leaf type heliotropic shown in Figure 1.0-2. It has been concluded therefore, that the conflict between requirements for rapid thermal response and mechanical stiffness can not be completely reconciled.

The concept selected for fabrication and evaluation was therefore the bellows type. A review of the physical and mechanical requirements of an appropriate bellows-sensor-mount configuration was made. It was determined that no insurmountable difficulties would be encountered. A survey of bellows manufacturers was made to select the most appropriate components and characteristics. Sensor sizes were calculated, thermal response times estimated and confirmed satisfactorily by actual laboratory tests of similar sensor configurations. A review of several reasonable charging fluids was made and mercury was selected on the basis of its pressure characteristics, stability at elevated temperatures, and availability in a very pure state.

Based on the various components available, a tentative mount design was developed. From this design and with the particular properties of each key component, an analog computer program was prepared. The complete mount-concentrator assembly was simulated in considerable detail with the only significant linearization being the reduction of the radiant transfer term for the sensor expressed as a direct function of sensor temperature. For a limited range, however, the error here is small.

UNDAMPED NATURAL FREQUENCY VS. (A/L) RATIO

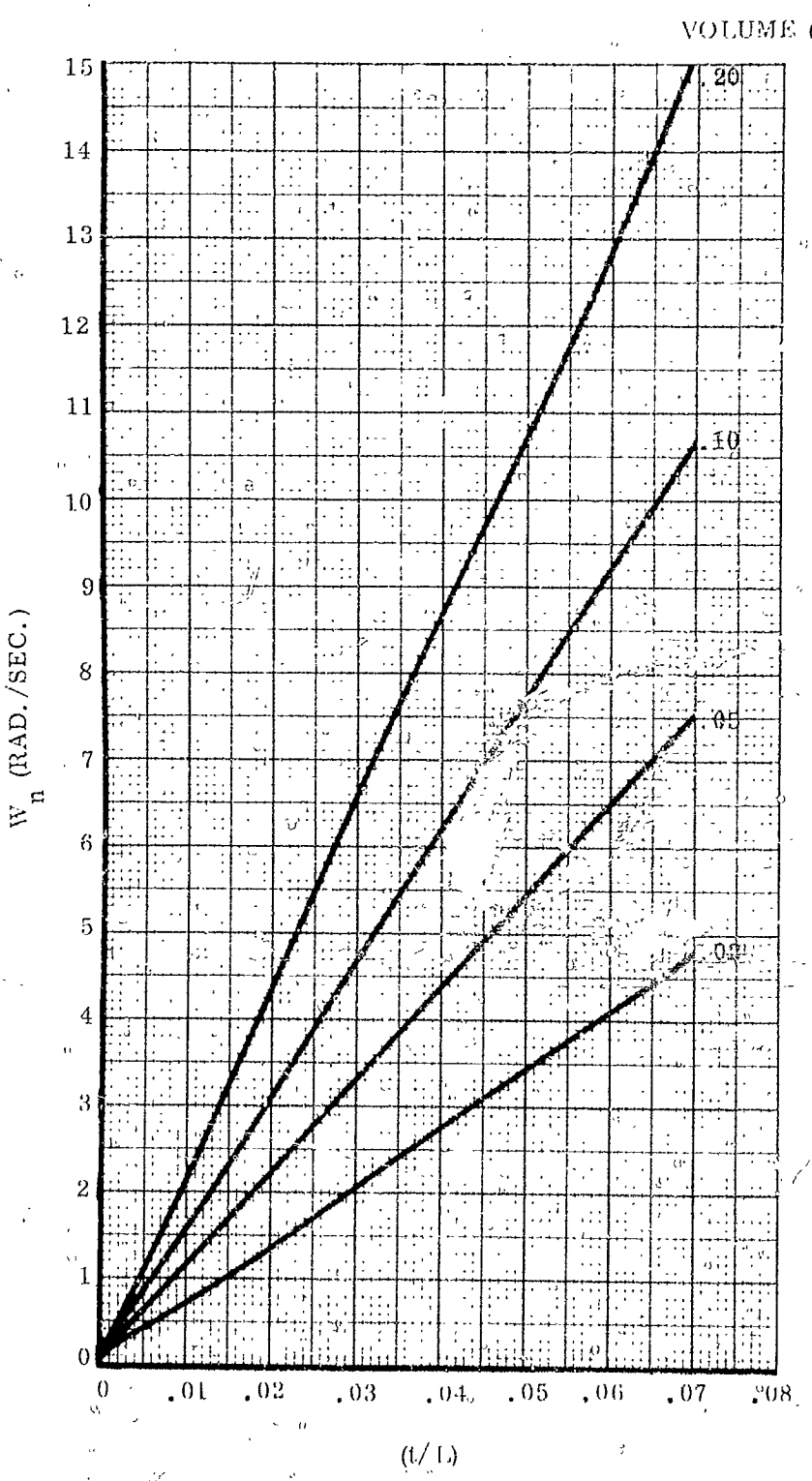

FIGURE 3.4-1

TEMPERATURE DIFFERENCE BETWEEN SENSORS
REQUIRED PER DEGREE ROTATION VS. (t/L) RATIO

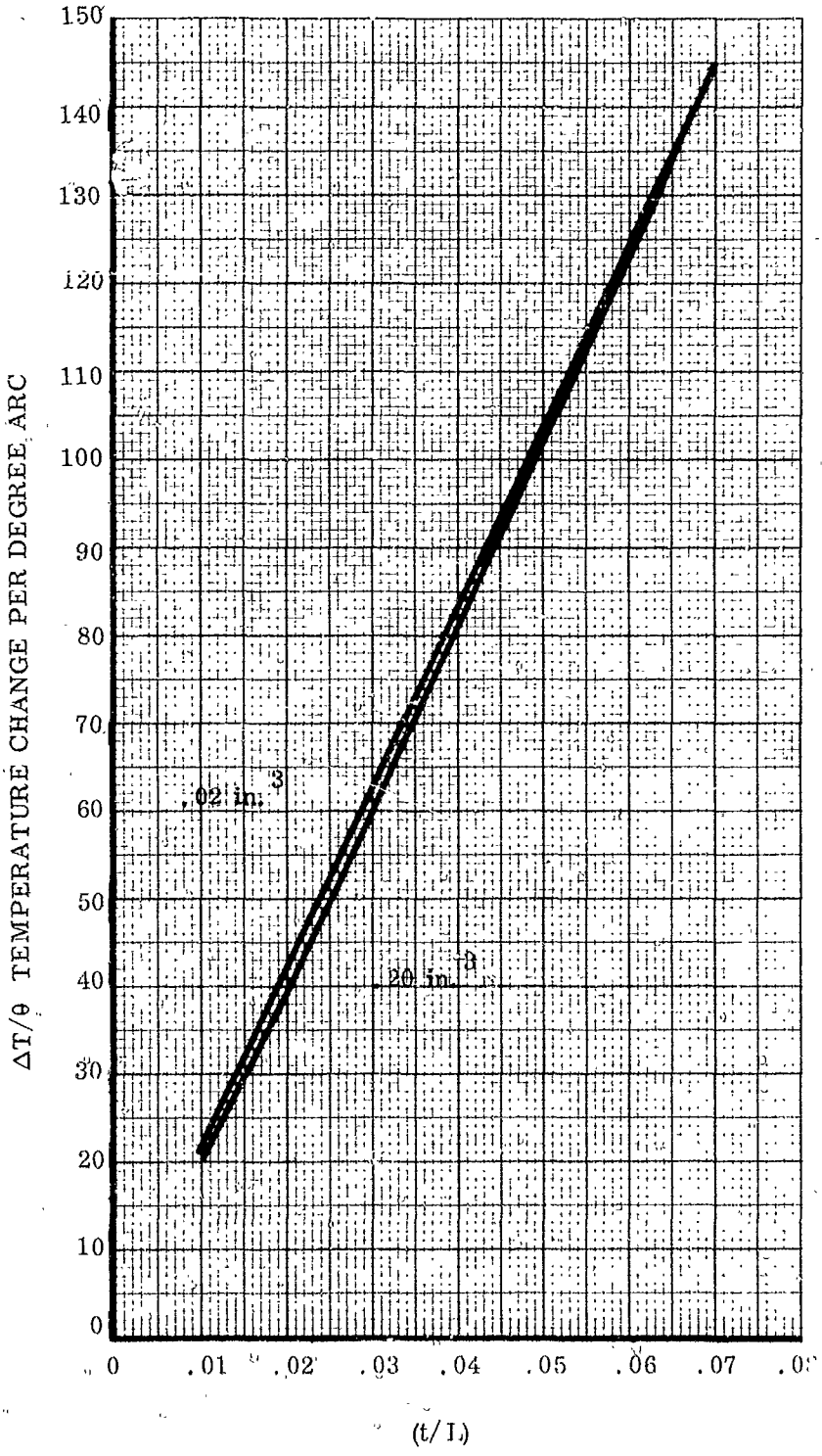

FIGURE 3.4-2

TORQUE PRODUCED PER DEGREE F TEMPERATURE
DIFFERENCE BETWEEN SENSORS VS. (t/L) RATIO

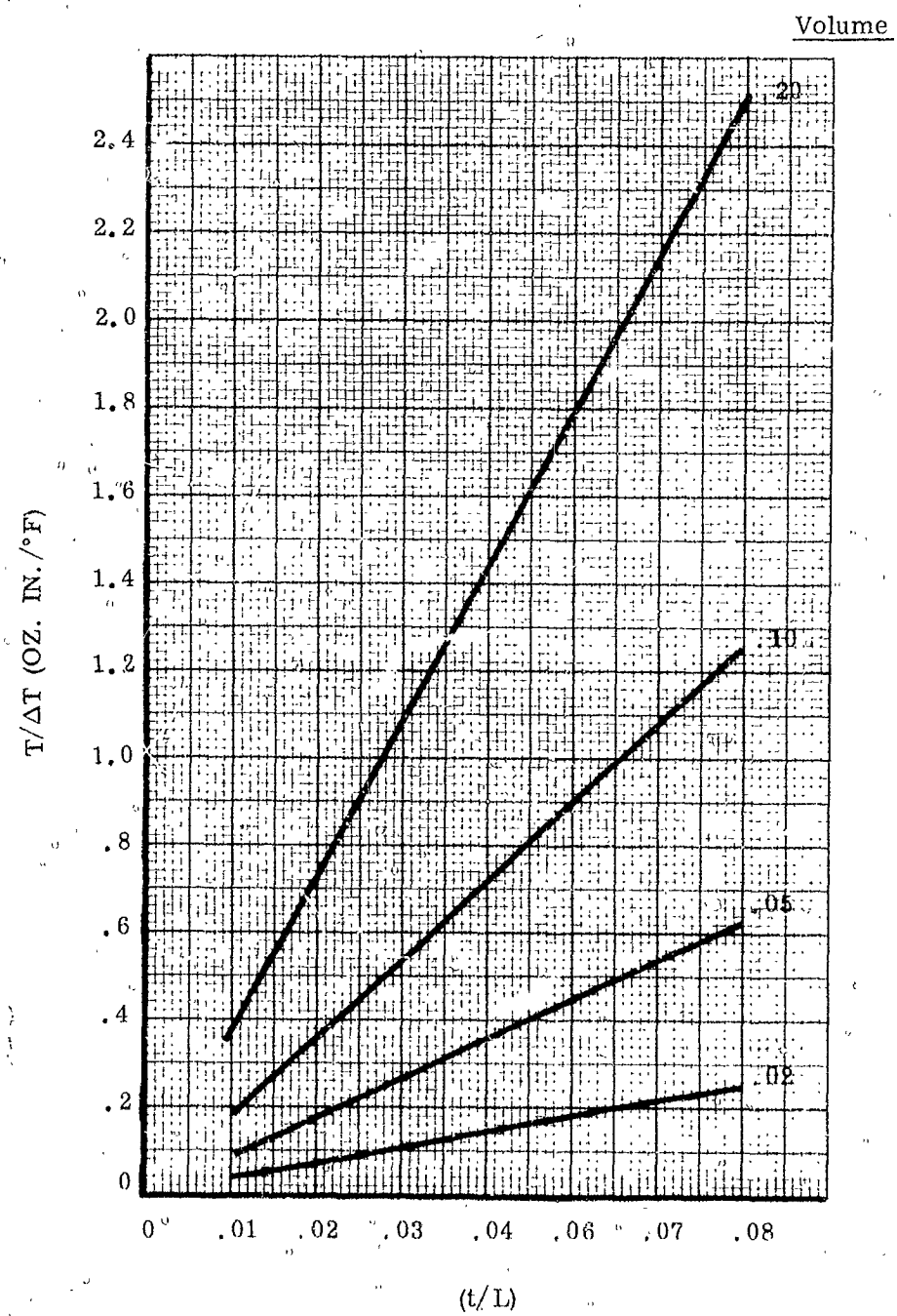

FIGURE 3.4-3

The simulation results confirmed expected dynamic mount characteristics. Of great importance was the clear indication of a need for 10 to 20 times the calculated critical damping based on concentrator inertia and bellows spring rate alone. The system was evaluated on a parametric basis to determine the effect of minor changes in components on system characteristics. This parametric study indicated considerable latitude in several areas and pointed up several ways in which mount performance could be improved. The study also showed that the positioning of the sensor about the cavity aperture will be extremely important in establishing the proper ambient conditions as well as to avoid extremes in temperature or pressure in the sensor-bellows assembly. The general performance characteristics as determined by the computer study are summarized in Figures 3.4-4 and 3.4-5.

Figure 3.4-4 shows the dynamic gain and frequency response characteristics of the mount as determined for the initial design with the addition of a damping factor of 20 times the critical. The system is seen to be stable for frequencies up to at least 0.16 cps. It is of interest to note that a recent NASA space station specification for a 20 to 40 kw power system required a system compatible with a 0.4 radians per second spin. This corresponds to 0.06 cps which is well within the capability of this mount. This mount design is for a zero g environment however, and therefore would not be entirely suitable if the radial location produced large normal accelerations and moments about the mount bearings. The parametric studies are summarized, in part, in Figure 3.4-5 where concentrator alignment error is plotted against the vehicle disturbing frequency assuming a 5 degree vehicle attitude error.

3.5 Mount Test Configuration

Many factors must be considered in the design of a heliotropic mount which will be suitable for a thorough performance evaluation. The mount must be a prototype in the sense that it meets all the requirements in terms of size, response, strength, environment, and practical space and volume limitations. Also the prototype mount must be capable of being tested in a meaningful way to determine its space system capabilities while under the constraints of earth bound test conditions. Finally it is very desirable that as much adjustment as possible be built into the mount to permit changes to be made during the testing without incurring the need for extensive redesign or modification.

The test mount, as previously stated, is designed to operate with a 5 foot diameter 60 degree rim angle concentrator and a 100 watt thermionic generator. The physical properties of these principle components were used to verify favorable mount performance in the computer study. The detailed characteristics attributed to these principle components were derived from actual test results obtained with the solar tracker test facility and experience with several thermionic generators designed for a nominal 100 watt output. The solar test facility is shown in Figure 3.5-1.

BELLOWS ACTUATOR MOUNT GAIN AND
FREQUENCY RESPONSE CHARACTERISTICS

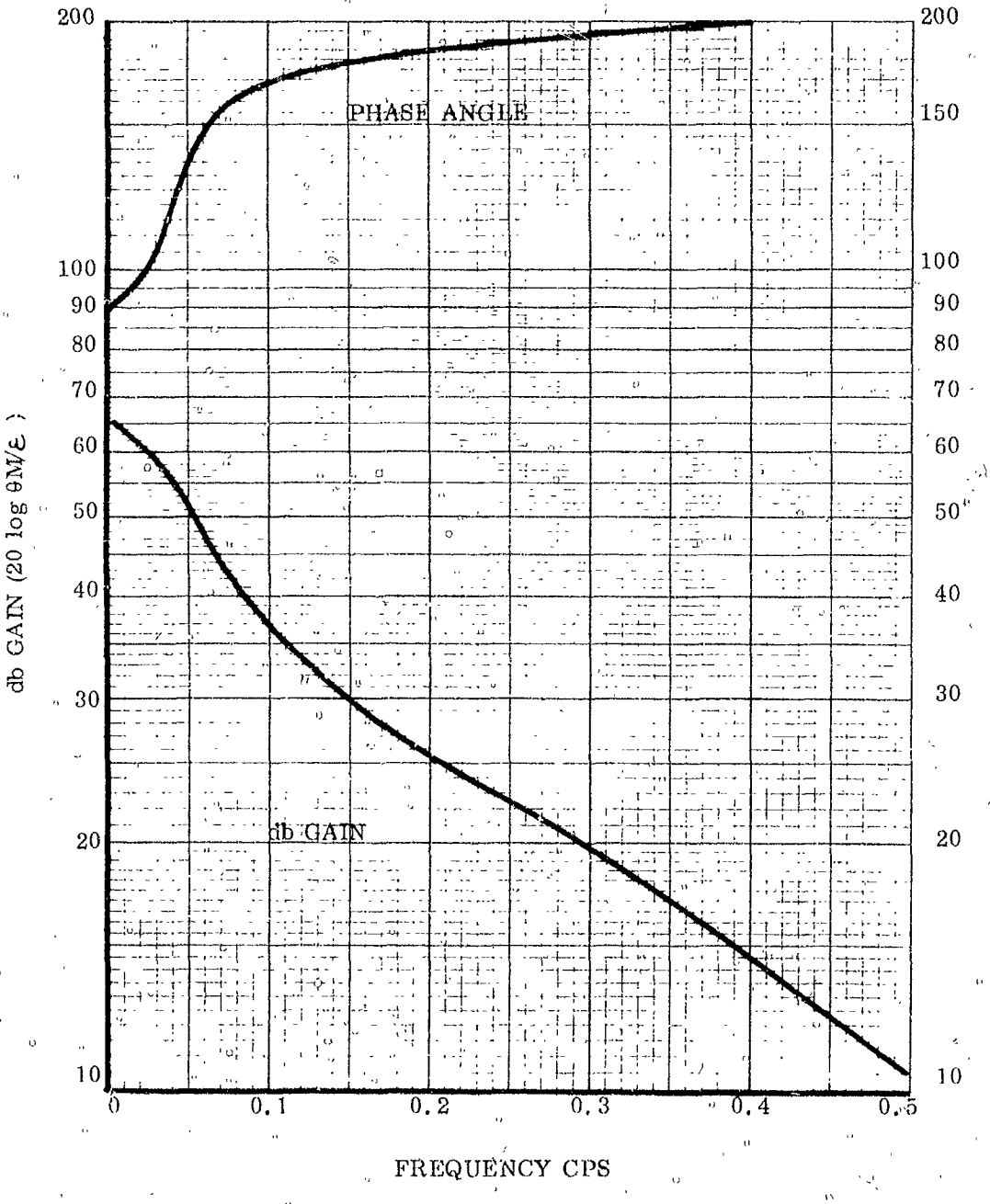

FIGURE 3.4-4

HELIOTROPIC BELLOWS ACTUATOR PARAMETRIC STUDY

ALIGNMENT ERROR VERSUS DISTURBING FREQUENCY WITH $\theta_v = \pm 5°$

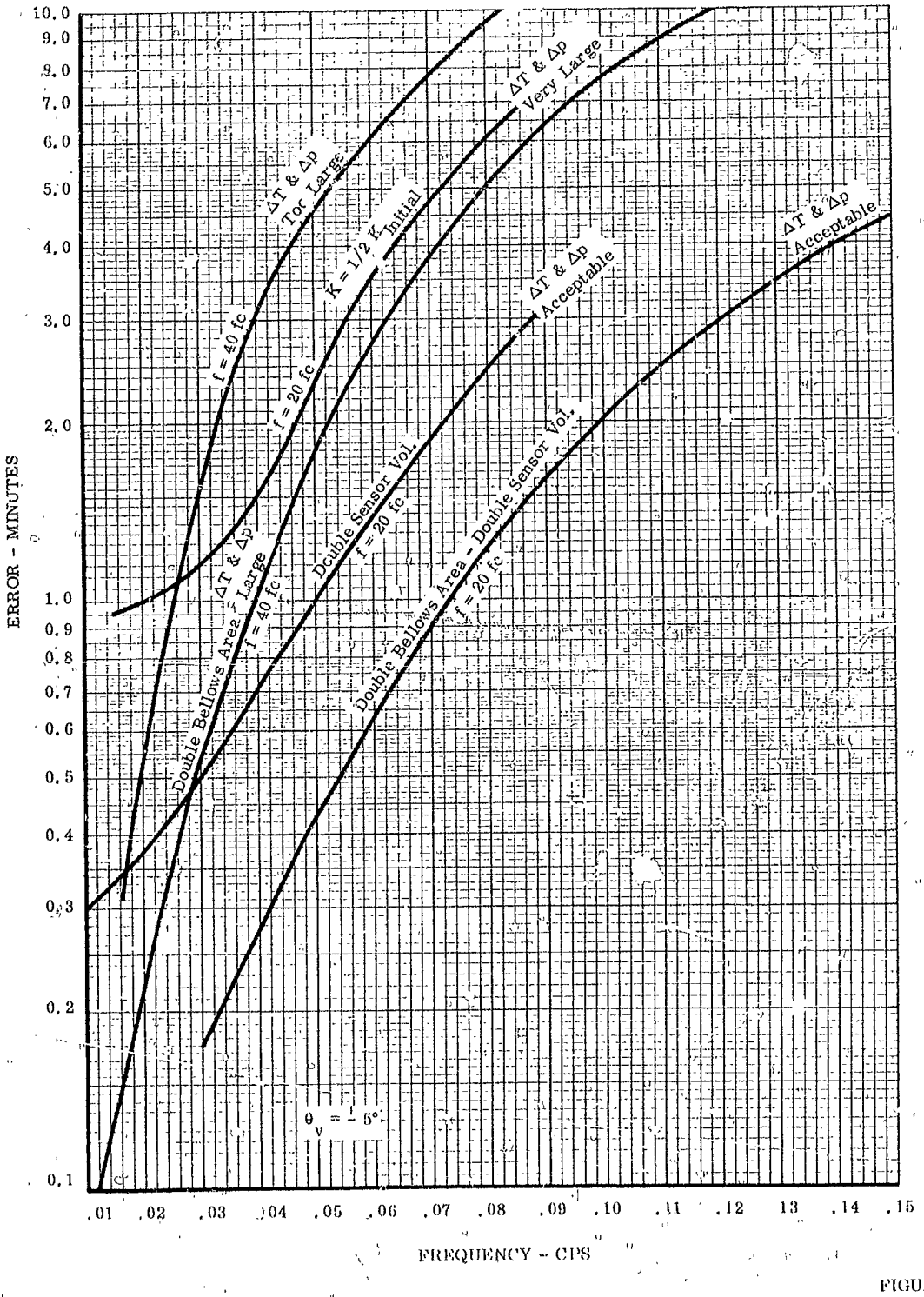

FIGURE 3.4-6

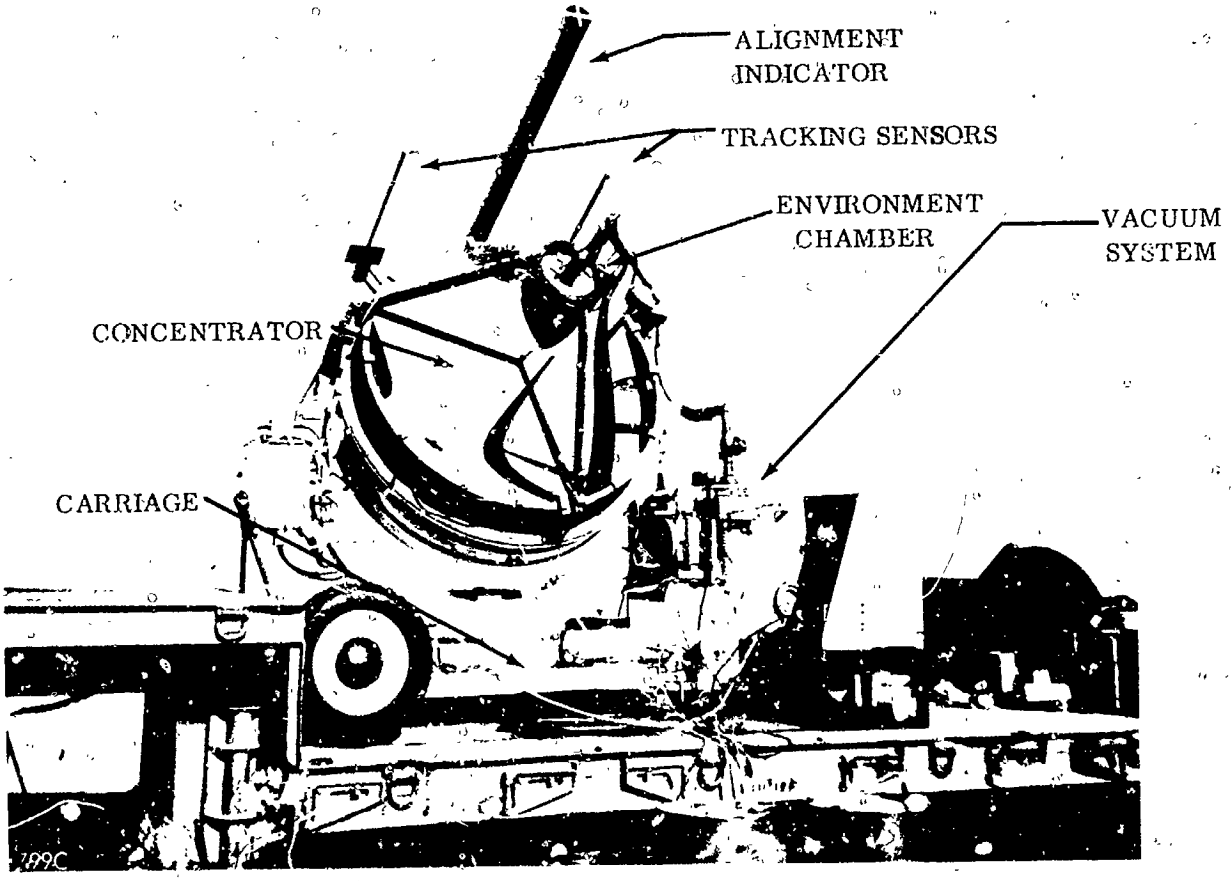

SOLAR TEST RIG

FIGURE 3.5-1

Extensive flux profile measurements have been made for the concentrator. These profiles for some tests include the optical dispersion and attenuation effects of the polished bell jar dome which encloses the environmental chamber. Other measurements of power available for a range of solar constant have also been made and used to determine concentrator reflectivity, bell jar transmission, cavity absorber efficiency (for thermionic generators), and the effects of small orientation errors or displacements from the focal plane. The values derived from these tests and used as the design criteria in this program are listed as follows:

1. Concentrator effective area - 18 ft^2
2. Concentrator reflectivity - 80%
3. Bell jar transmission - 82%
4. Cavity absorptivity (approximate) - 85 to 90%
5. Optimum cavity diameter - 9/16 inch for 2000°K operation - zero misorientation
6. Cavity radiation loss (2000°K) - 82 watts/cm^2

Figure 3.5-2 shows a plot of the flux profile as measured in three planes with a Ruge radiometer. The fringe regions of these flux profile curves were subsequently averaged and used to generate a curve of sensor input power as a function of radial distance from the concentrator axis. This plot of sensor power input is shown in Figure 3.5-3 and served in the computer study using a nominal sensor design point location of 5/16 inch from the concentrator axis.

The thermionic generator configuration used to establish the hot cavity calorimeter design shown in Figure 3.5-4 is for the most recent TRW design executed under contract to the Air Force. It was felt that such a generator is a typical 100 watt unit and therefore was used in defining the working environment and integration requirements for the prototype heliotropic mount. This basic generator design was converted into a calorimeter assembly with several modifications of the body portion made to facilitate mounting of heliotropic hardware.

The calorimeter is of the power distribution type previously built and operated on past TRW solar thermionic test programs. It simulates the temperatures, temperature distributions, approximate geometry, and materials used in an actual generator assembly. Also as a calorimeter device it is able to measure input solar power and power distribution in the event the concentrator is misaligned and the flux transfer is no longer uniform. Such a calorimeter permits a good evaluation of power available for direct conversion by a thermionic device, can be fabricated at a fraction the cost of equivalent generator, and serves admirably in the evaluation of the heliotropic mount in terms of providing a realistic environment and assisting in the evaluation of mount performance under solar test. The design points chosen or calculated for the calorimeter are listed as follows:

FLUX PROFILE DATA FOR FIVE FOOT DIAMETER SOLAR CONCENTRATOR
(DATA WITH PYREX DOME)

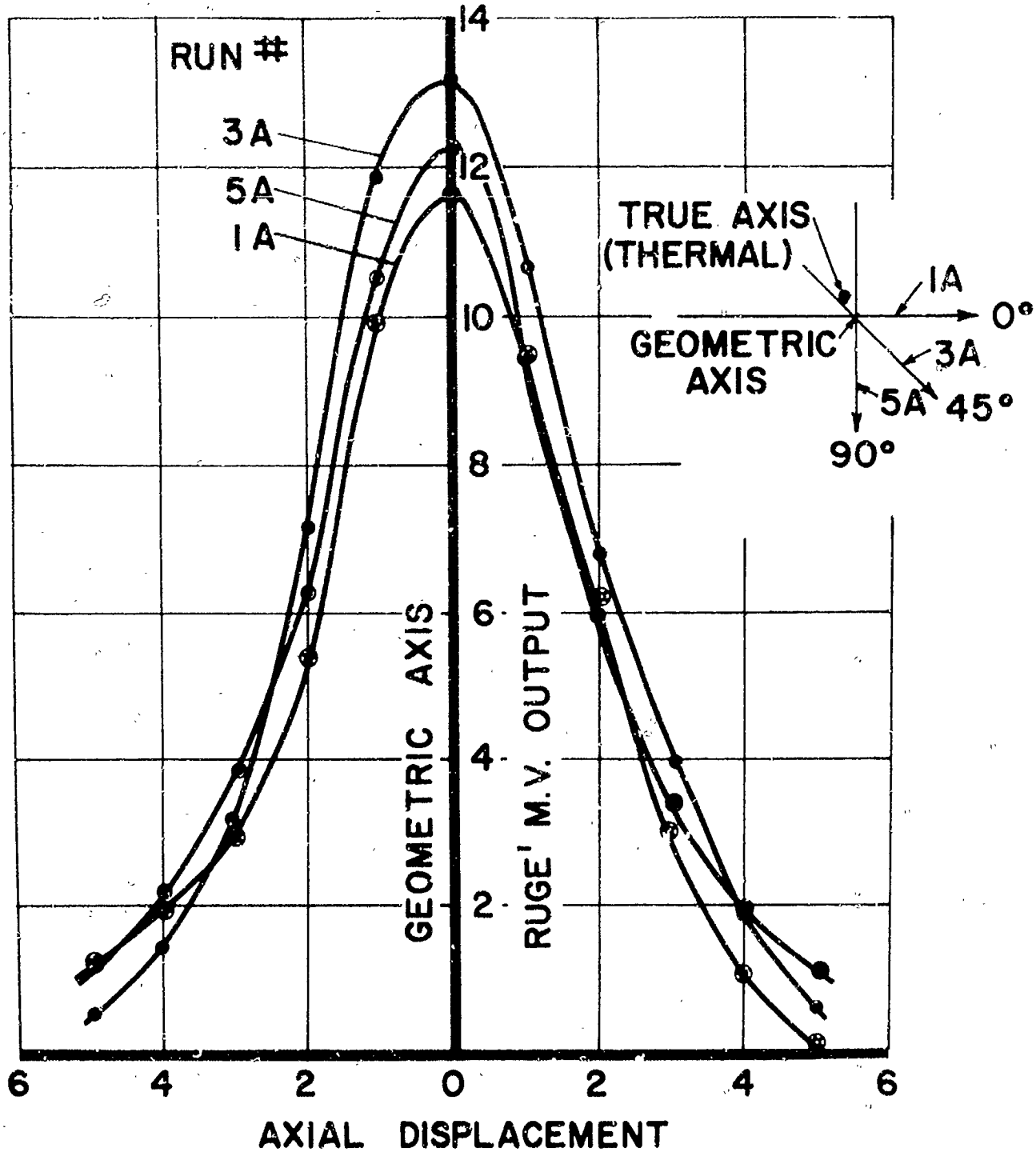

FIGURE 3.5-2

SENSOR INPUT POWER VERSUS LOCATION

(1 BTU/SEC = 1.054 KW)

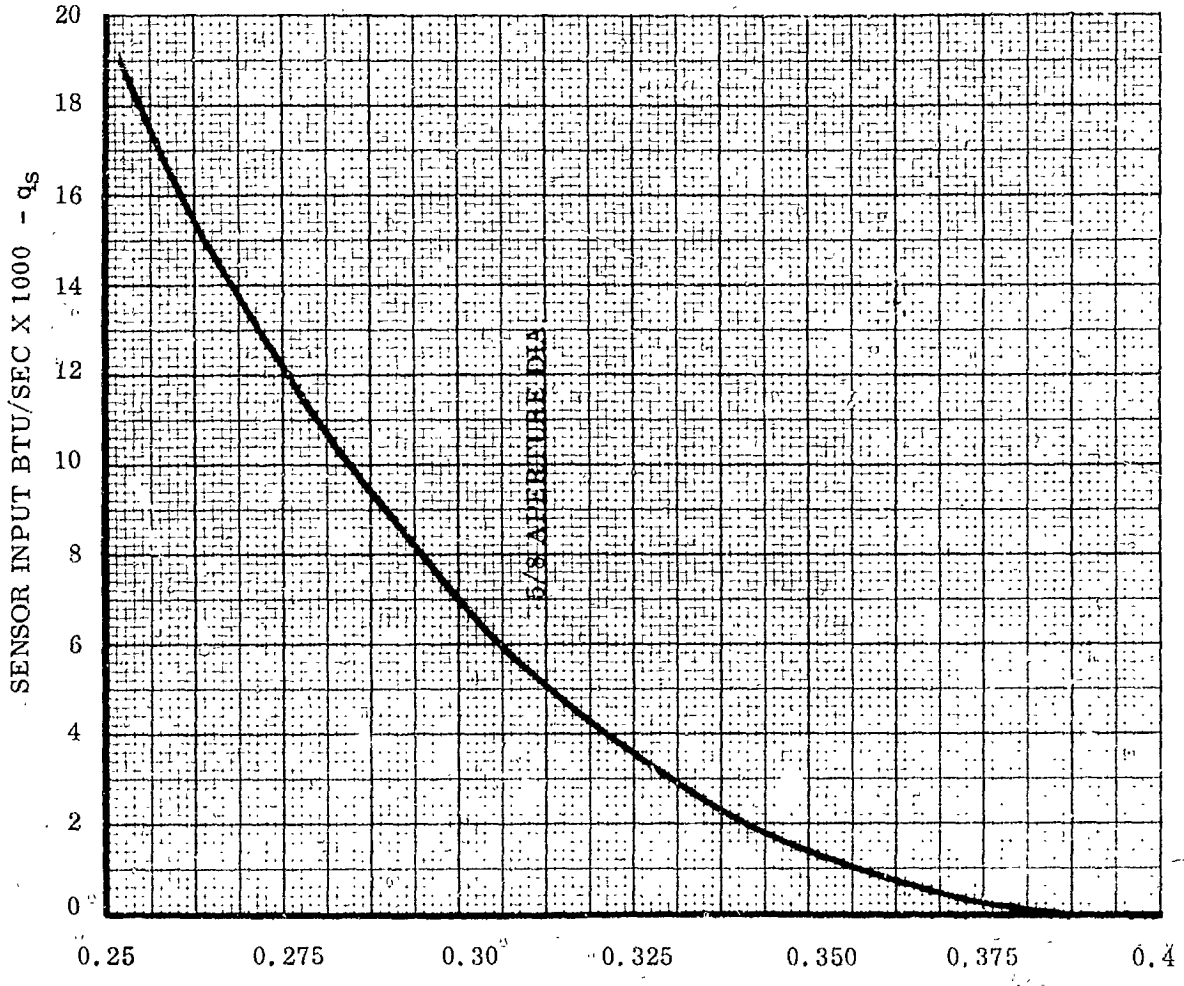

FIGURE 3.5-3

1.	Cavity temperature	1700°C
2.	Cavity design power input (assume a solar constant of 75 watts/ft^2 at the TRW Cleveland test site)	797 watts
3.	Calorimeter body temperature	442°C
4.	Calorimeter element radiator temperature	470°C
5.	Cavity aperture diameter	5/8 inch
6.	Cavity absorptivity	.90
7.	Cavity radiation loss	161 watts
8.	Calorimeter elements heat flux (each)	151 watts
9.	Stray power losses	32 watts
10.	Radiator element emissivity	.85
11.	Effective radiator area (each)	94 cm^2

The power distribution calorimeter operates by measuring the ΔT between two points located on the conductive shaft between the hot cavity and the radiator. By knowing the distance between these points and the area and conductivity of the shaft, the equivalent power transfer can be determined. The actual assembly is also calibrated by electron bombardment techniques which permits an accurate measure of element input power as a function of the measured ΔT. Side losses and support losses are held to minimum by design and efficient multilayer shielding as in the thermionic generator. Small errors which show up during calibration may be corrected to insure nearly identical performance in each calorimeter element.

The body modification to the calorimeter consisted of altering the generator design shown in Figure 3.5-4 to include four flats between the element radiator assembly to facilitate mounting the heliotropic hardware. Also approximately 1/4 inch of space is now available above the calorimeter elements to permit the location of the sensor probes at the edge of the cavity formed by the head pieces of each element. The calorimeter and the mount hardware including the support members and base plate assemblies are designed to be compatible with the existing environmental test chamber. The base plate is designed to mate with the solar test chamber shown in Figure 3.5-5 and with other glass bell jars on laboratory test stands. This plate also includes the receptacle for all power and instrument leads, and special leveling or jack assemblies to permit minor adjustments of the calorimeter relative to the focal plane and axis while solar testing under vacuum.

ADVANCED SOLAR THERMIONIC GENERATOR UTILIZING SERIES 310 CONVERTERS

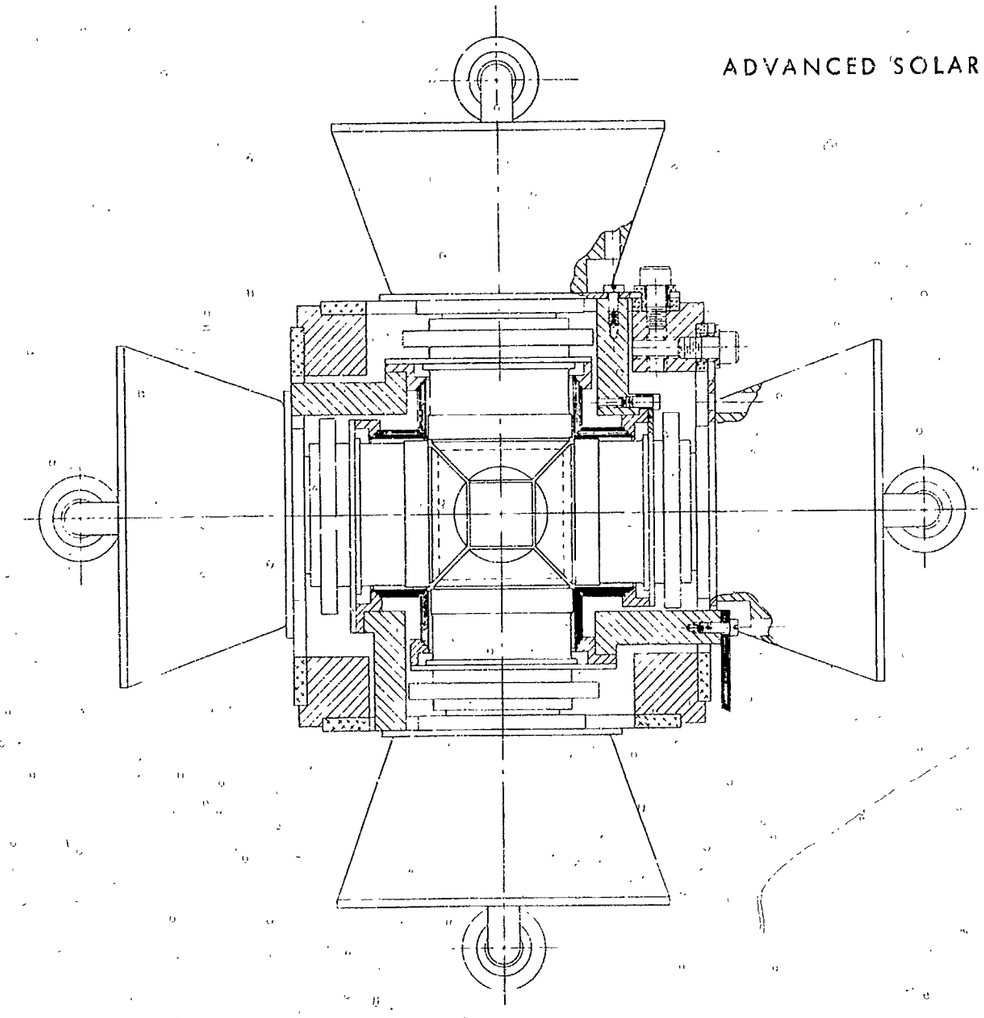

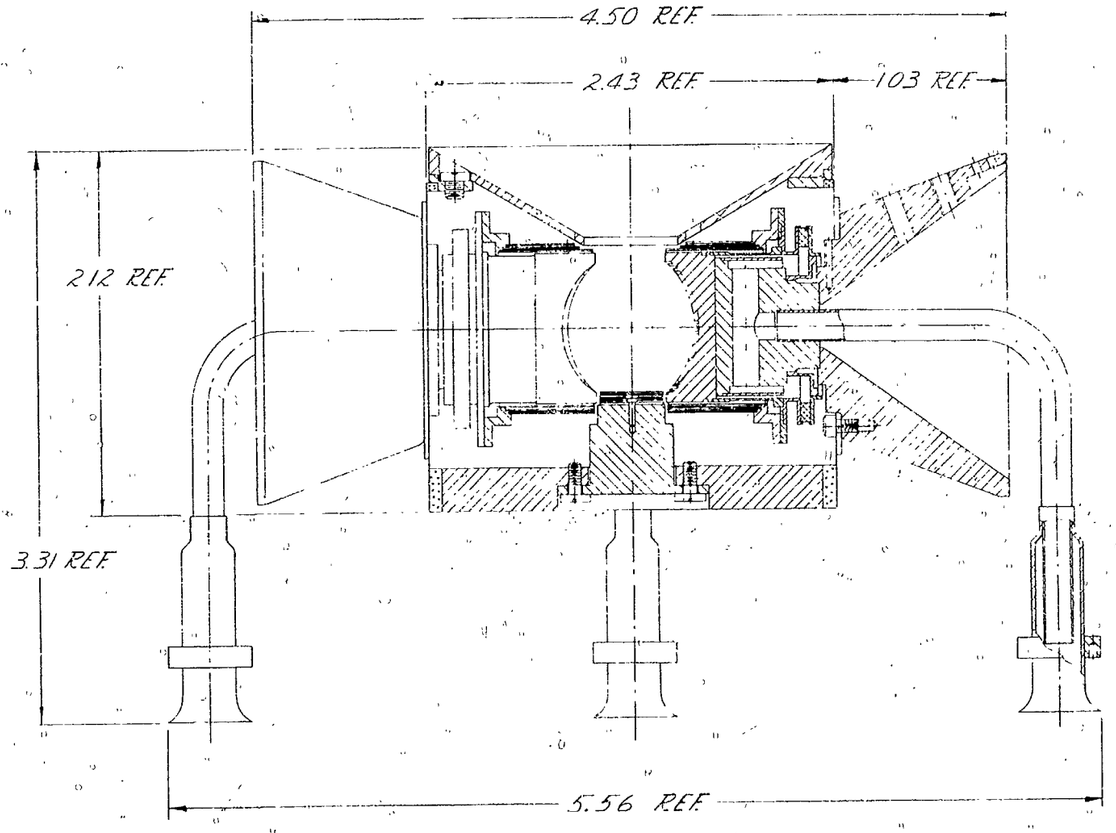

FIGURE 3.5-4

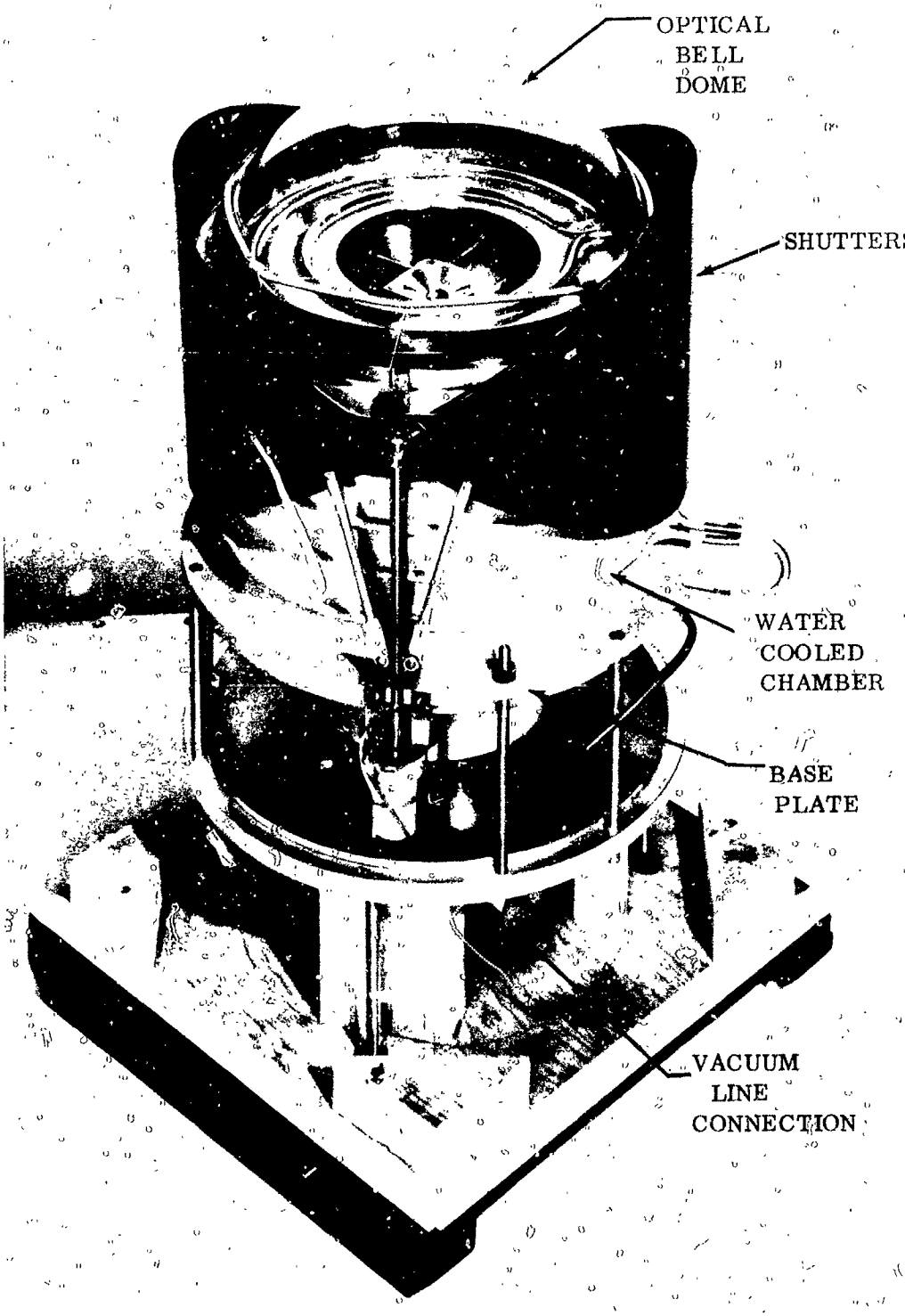

ENVIRONMENTAL TEST CHAMBER

FIGURE 3.5-5

3.6 Mount Assembly

The preliminary design used on the analogue computer was developed by mating the most favorable stainless steel bellows available with the calorimeter assembly. The bellows was chosen based on its burst pressure, spring rate, diameter and length, and stroke. A review of 6 potential bellows lead to the selection of a bellows having 25 convolutions, an effective area of .06 sq. in. a maximum pressure of 1500 psi and a total deflection of approximately .125 inches. The sensor ambient temperature was calculated based on the heat balance attained within the confines of the generator while subject to the solar flux input, radiant transfer from the hot cavity, and reasonable conduction and radiation losses from the sensor body. This temperature was established at 1059°F and was found to correspond to a mercury vapor pressure of 281 psi. Using this pressure, the effective area of the bellows, and selecting a working radius of .8 inches the actuator design torque, sensor inventory and thermal mass were determined. As previously discussed these values were used in the simulation and varied over a small range to obtain parametric type data to determine methods of readily improving the mount characteristics. The computer study indicated a larger bellows area, larger sensor thermal mass, and a softer spring rate would offer even better performance. The computer also indicated a need for an increase in the viscous damping factor of from 10 to 20 times the value calculated based on the concentrator mass and selected bellows spring rate alone. Taking all these factors into account the final design was drawn up.

The possibility of better performance with a larger softer bellows as well as the fact that originally selected bellows required 3 months for delivery, required that another bellows assembly be sought. A most promising welded bellows was located. The bellows was of all welded construction and of nesting ripple diaphragm contour. It was reported to have "excellent long stroke capability and good linearity of stroke with pressure." Its characteristics are an effective area of 0.093 sq. in., a burst pressure of 1500 psi, a spring rate of 60 lbs. per inch and a maximum stroke of 0.225 inches. As well as having a larger area, an almost 100 per cent increase in permissible stroke would allow more latitude in selecting the bellows moment arm. The bellows assembly, as drawn with the new bellows unit, is shown in Figure 3.6-1.

A complete layout of the calorimeter and mount assemblies is shown in Figure 3.6-2. The mount actuator assemblies are shown as four identical attachments which are simply screwed into place on the flats between each radiator assembly. This latter arrangement permits the substitution of mount assemblies at will.

The bellows assembly is fastened into mount brackets by lock screws which facilitate the initial mount adjustments. The elongated slots are provided to permit optimization of the torque - stroke characteristics which would depend upon the nature of the disturbances which must be handled or the concentrator mass. These slots also provide a way of adapting other size bellows assemblies to existing mount and system, or of adapting the present mount and bellows to other generator-concentrator components of different size and mass.

BELLOWS ASSEMBLY

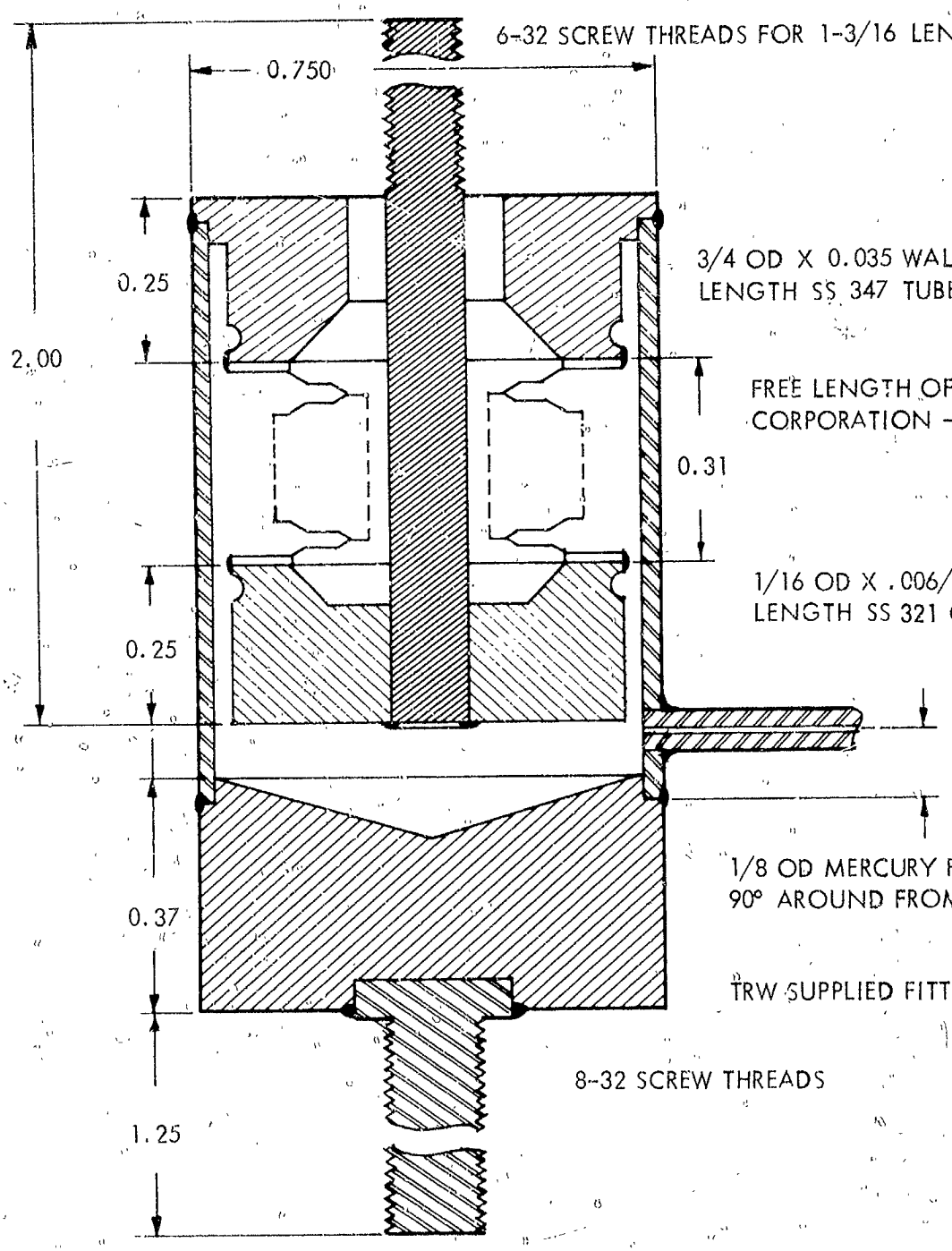

FIGURE 3.6-1

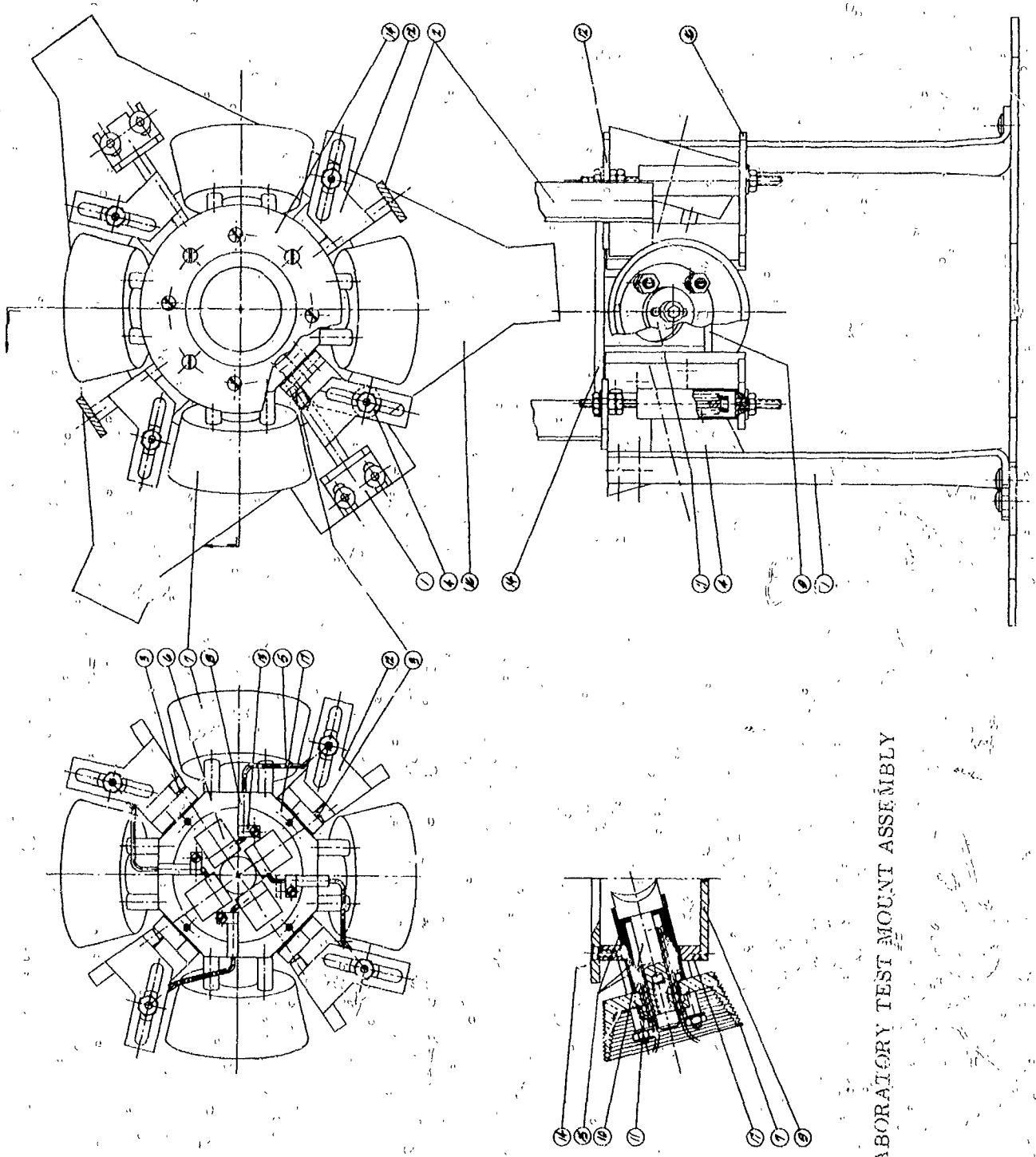

LABORATORY TEST MOUNT ASSEMBLY

FIGURE 3. 6- 2

The sensors are shown as small wedge shaped reservoirs containing mercury sufficient to fill half the sensor volume when the mount is in the balanced position. When the mount rotates the mercury is transferred from the hotter sensor and into its bellows. The opposing bellows forces some of its charge to the cooler sensor. This continues until the mount has rotated at full 5 degrees. At full rotation the heated sensor is deprived of its entire inventory and the mercury recedes into the capillary thereby preventing the overpressure of the bellows assembly.

The damping required for proper system stability is provided by using 10 inches of .006 to .007 diameter capillary tube between the sensor and bellows. Since this bore size is as small as can be found any additional damping would have to be added external to the mount assembly. Calculations indicated however that this capillary size would be sufficient to give the factor of 10 required in the previously calculated critical damping.

The sensors are provided with two adjustment features in addition to the possibility of adding shields or applying emissive coatings to alter the temperature characteristics. A small copper holder is used to thermally ground the sensor capillary to the calorimeter body. The length of the path and the conduction between sensor and body may be varied by adjustment in the placement of this copper holder. Also, by moving the entire holder and sensor assembly in and out, the amount of solar flux intercepted by the sensor at the cavity edge may be controlled to obtain the proper ambient. These features insure the mount will be compatible with the solar concentrator even in the event the concentrator flux profile is not precisely known before hand.

During laboratory tests of the mount head was introduced to the calorimeter element by electron bombadement. A single multi turn tantalum filament is used as the electron gun source. By proper positioning it was possible to obtain uniform power introduction to each of the four calorimeter elements. Each element was monitored for its own fraction of the total bombardment current to permit accurate power measurements to be made for calibration purposes. The sensors include a .110 diameter drilled hole to permit the insertion of a small sheathed heater. These heaters were used to simulate the solar input power and will be arranged through the use of an electrical switching network to allow a variety of misalignment conditions to be simulated.

Photographs of the principle components and assemblies are shown in Figures 3.6-3 and 3.6-4. The parts which make up the calorimeter elements are presented in Figure 3.6-3. The completed mount assembly exclusive of the bellows-sensor subassembly is shown in Figure 3.6-4.

Component Specification

A list of the specifications for, materials used, and other design operating data concerning the mount and the principle components is presented in the following tables.

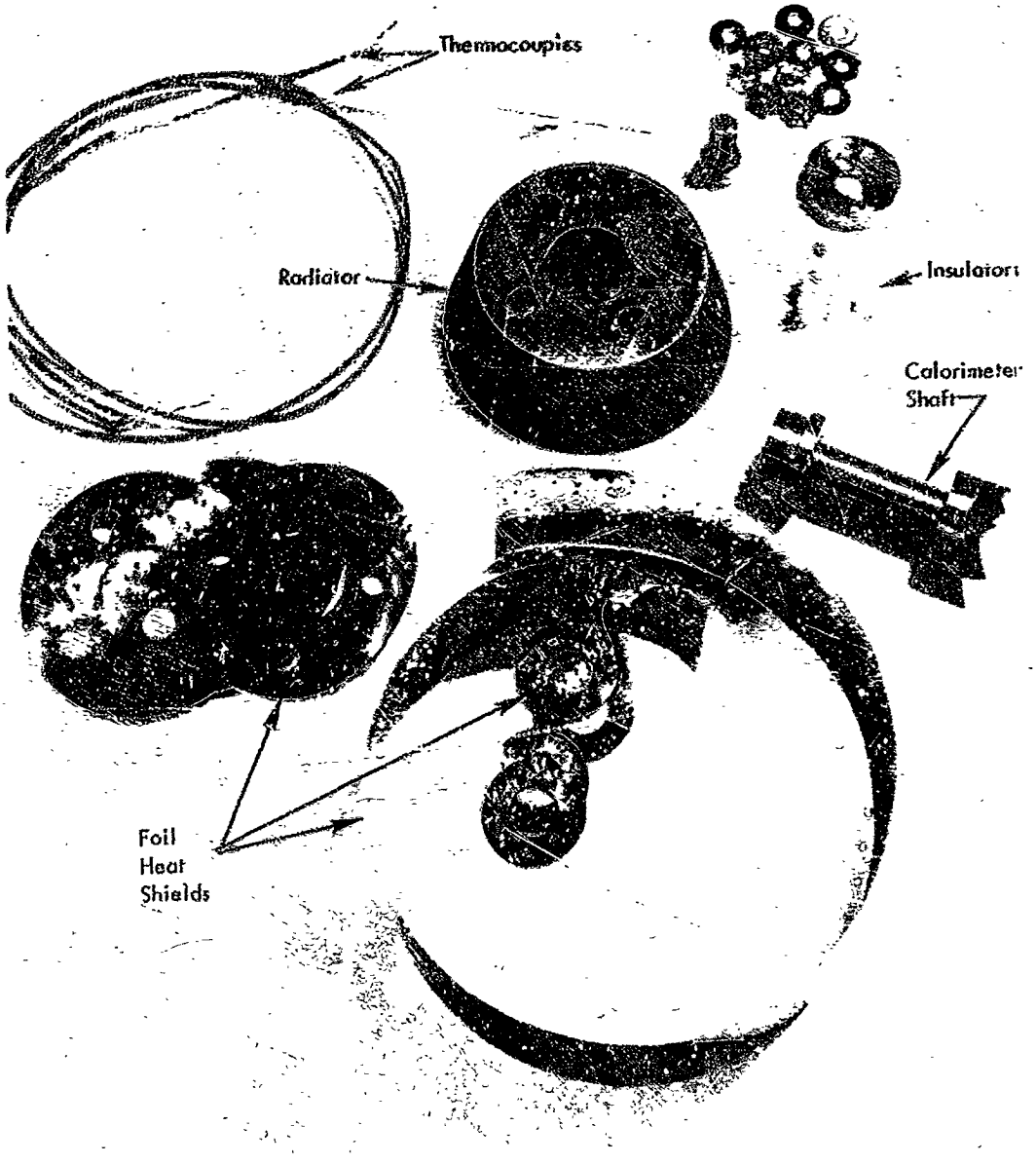

CALORIMETER ELEMENT COMPONENTS

FIGURE 3.6-3

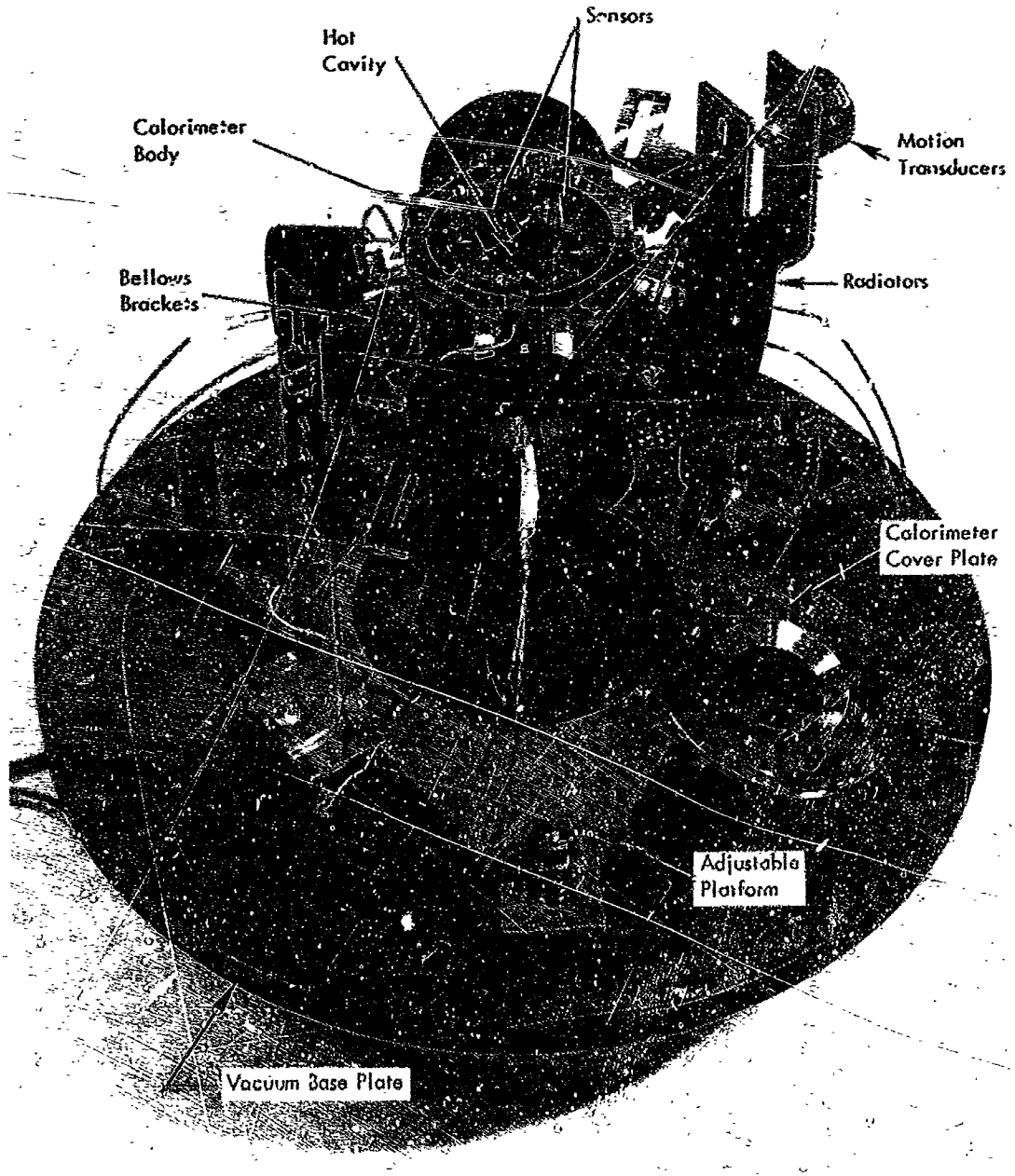

TEST MOUNT ASSEMBLY

FIGURE 3.6-4

TABLE I

DESIGN POINT VALUES

I.	Calorimeter Simulator Assembly	
1.	Cavity temperature	1700°C
2.	Radiator temperature	490°C
3.	Body temperature	442°C
4.	Calculated ΔT values	680°C
5.	Total cavity power	797 watts
6.	Reradiation loss	161 watts
7.	Element conduction power	151 watts
8.	Cavity absorptivity	.90
9.	Radiator emissivity	.85
10.	Body emissivity	.2
II.	Bellows-Sensor Assembly	
1.	Bellows temperature	400°C
2.	Sensor temperature	572°C
3.	Bearing temperature (max)	400°C
4.	Sensor clamp assembly	442°C
5.	Sensor emissivity (selective)	.05 to .8
III.	Heater and E. B. Gun Assemblies	
1.	EB voltage	600 to 800 volts
2.	EB current per element	.251 to .189 amps
3.	Total EB power	604 watts
4.	Sensor heater input power	4.85 watts

TABLE II

MISCELLANEOUS MOUNT PERFORMANCE CHARACTERISTICS AND PROPERTIES

1.	Maximum motion or rotation	± 6 degrees
2.	Design control motion	± 5 degrees
3.	Maximum allowable residual alignment error	± 12 minutes
4.	Anticipated residual alignment error	± 6 minutes
5.	Anticipated steady state gain (min.)	200 degrees/degree
6.	Frequency response	0 to .1 cps
7.	Mount natural frequency	2.2 rad/sec
8.	Critical damping	76 in#/rad/sec
9.	Bearing load capacity	56#
10.	Minimum cycle life	200,000

TABLE III

MATERIALS

I.	Calorimeter Assembly		
	1.	Shaft	Moly
	2.	Cavity	Moly
	3.	Radiator	Copper
	4.	Radiator Coating	Pyromark
	5.	Shields	Moly foil
	6.	Body	316 S.S.
	7.	Cover Plates	316 S.S.
	8.	Insulators	Diamonite
	9.	Thermocouples	C/A
	10.	Studs and nuts	303 S.S.

TABLE III (Cont'd)

II.	Electron Gun Assembly	
	1. Filament	Tantalum
	2. Holder	Moly
	3. Holder support insulator	Lava B
	4. Leads	Copper
III.	Heater Assemblies	
	1. Filament	Tungsten
	2. Insulator	Magnesia
	3. Sheath	Nickel
IV.	Bellows Sensor Assembly	
	1. Bellows	347 S.S.
	2. Capillary	347 S.S.
	3. Sensor	316 S.S.
	4. Bellows Housing	347 S.S.
	5. Charging fluid	Mercury
	6. Bearings	S.S.
	7. Support brackets	316 S.S.
V.	Support structures	
	1. Brackets	316 S.S.
	2. Support Stand	316 S.S.
	3. Misc. Fasteners	Carbon Steel & S.S.

4.0 TEST PLAN AND PROCEDURE

4.1 Test Plan

Four distinct classifications of test must be accomplished to complete the evaluation of the mount design. This requirement arises from the fact that severe complications result from attempting a test of space hardware under earth bound restrictions. In this program both the vacuum environment of space and the mass characteristics of the system hardware must be simulated. Also, the test simulation must exclude or compensate for the effects of gravity to completely qualify the test results. To fulfill all of the requirements the following specific test activities must be included: 1) vacuum system and instrumentation check out, and calibration), 2) tests to determine all thermal equilibrium and dynamic response characteristics, 3) tests to simulate and evaluate the inertial mount-concentrator characteristics and 4) solar tests to confirm mount gain and response characteristics and verify the compatibility of the mount with the solar test environment of a precision concentrator.

Because of the large concentrator inertias it is impossible to include a mass with similar inertial values within the vacuum test chamber walls. Such a mass would weigh 250 pounds to fit within a 12 inch bell jar and would greatly exceed the bearing load capacity and further complicate the effects of g loading on mount performance. The approach therefore becomes one of performing all thermal equilibrium and thermal dynamic measurements under high vacuum and the inertial or dynamic system response tests outside the vacuum. By careful measurements of all temperatures, and rates of change in temperature for various power input with the mount restrained or loaded with simple weighted lever arms, a map of the mount torque and motion is obtained. These characteristics can be compared to the calculated values and computer characteristics to confirm the adequacy of the mount design.

Having obtained the thermal response and torque-motion characteristics under vacuum with the proper temperature environment simulated the mount can be removed from the vacuum for inertial type tests.

Outside the chamber it is possible to apply the weight which simulates the concentrator at a radius of 26 inches. The inertial characteristics are properly simulated and the bearing loads are easily acceptable. The sensors may then be heated to the ambient indicated under vacuum by using oversized electrical heaters and adding more power to overcome the additional heat losses in air. With the sensors forced to the operating temperature in open air the mount torques were exactly the same as were measured under vacuum. The interaction of the mount and concentrator mass simulator were observed and recorded as a function of forced sensor temperature variations. Again the response characteristics can be compared with the computer program results. Having monitored and recorded the relations between sensor excitation and mount movement for various types and frequencies of disturbances the complete mount performance can be determined by combining the results of both vacuum and air tests.

Having obtained all pertinent mount characteristics in the laboratory it will be possible to proceed with the solar test activity. Again because of the need for a vacuum enclosure, the concentrator in the tracker cannot be connected directly with the mount assembly. Also, to do so would be useless since the tracker mirror weighs several hundred pounds. The results of applying flux unevenly to the sensors can be determined indirectly, however. By starting with the concentrator correctly aligned and the mount properly located in the focal plane, the ambient operating conditions can be established. If at this point a known alignment error of several minutes is introduced in the tracker orientation system the sensors will be heated unevenly and a torque developed in the mount actuators. By allowing the mount to rotate until it reaches a new torque equilibrium point at x degrees the mount gain can be calculated. The response was also obtained from recordings of this rotation. By introducing a sinusoidal disturbing signal in the tracker the dynamic response of the mount was obtained for several frequencies and again compared with the previous computer results.

Having completed all three test series all mount characteristics will be known and it will have been demonstrated that the mount is properly designed to respond to an actual solar test environment.

4.2 Summary of Laboratory Test Procedure

The instrumentation available in the calorimeter mount assembly which was used to facilitate the testing is as shown in Figure 4.2-1.

Vacuum System and Instrumentation Checkout

The completed assembly was pumped down and leak checked to insure a tight system. With the pressure below 10^{-5} mm Hg. a high voltage was applied to verify proper insulation of the calorimeter and electron gun assembly. The high voltage was reduced and the bombardment filament heated to produce small emission currents. All thermocouples were noted for proper response, and the bombardment current distribution to each calorimeter element measured, to insure an approximately uniform power distribution throughout the calorimeter. With a checkout of the instrumentation, the preliminary system tests were completed and performance testing of the calorimeter mount assembly began.

Calorimeter Calibration and Thermal Equilibrium

The first tests to determine system characteristics involved the heating of the calorimeter cavity by means of electron bombardment. This was done to determine the operating temperature of various mount components at full power input, and to calibrate the colorimeter elements.

INSTRUMENTATION ARRANGEMENTS

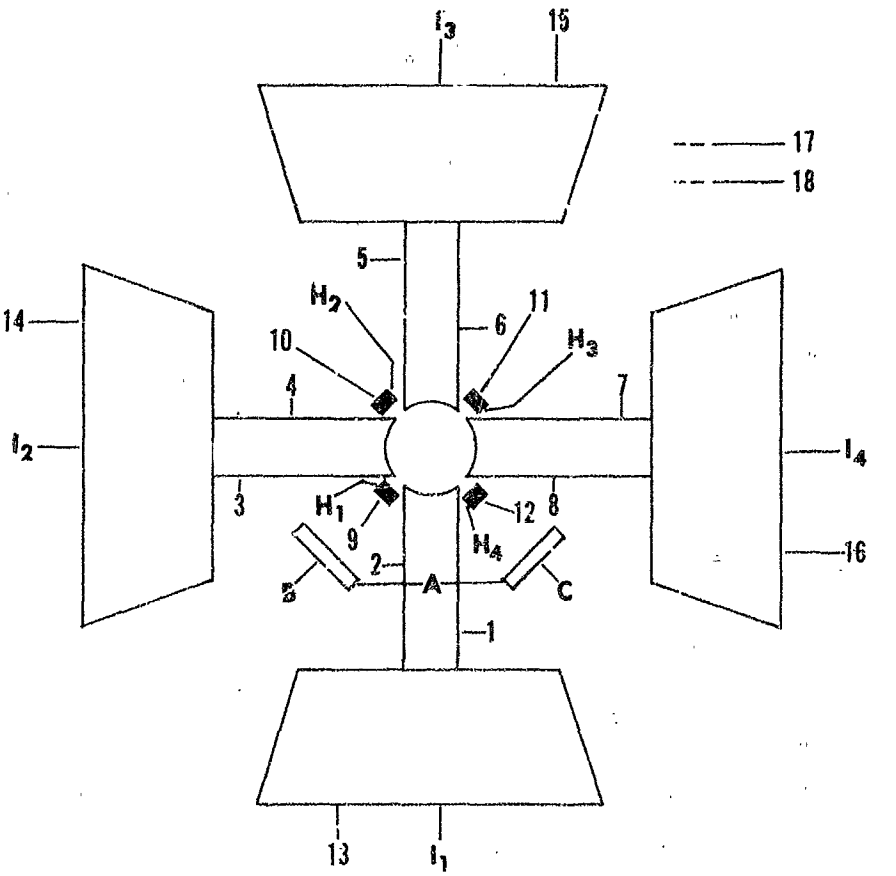

Symbol or Point	Description
1 - 8	thermocouples mounted in diode simulating elements
9 - 12	thermocouples mounted in sensors
13 - 16	thermocouples mounted in radiators
17	thermocouple in calorimeter body
18	thermocouple in base plate
H_1, H_2, H_3, H_4	sensor heaters
I_1, I_2, I_3, I_4	respective EB current leads
A	motion transducer input leads
B	X-axis transducer output
C	Y-axis transducer output

FIGURE 4.2-1

The electron gun assembly was attached to and supported by the calorimeter so that the filament projected well into the cavity formed by the four diode simulating elements. Electron bombardment (EB) of the cavity was achieved by slowly increasing the temperature of the filament and the accelerating potential until the design power level was reached. Tests were conducted using a bombardment current of 1.19 amps with a 512 volt accelerating potential. Approximately 200 watts were used to heat the filament. Making the total power input to the calorimeter 810 watts which is slightly in excess of the 797 watt design level. The exact measurement of total power input under solar test cannot be determined by electron bombardment heating and calibration of the calorimeter. This is true because there is some difference between the losses experienced in the electron gun and from the covered hot cavity and the losses under solar test. Rough estimates of electron gun losses made by noting the difference in calorimeter power with and without the high voltage applied do, however, show a loss of approximately 71 watts from the gun assembly. This loss added to a calculated loss of 11 watts due to radiant transfer from the hot cavity to gun body is reasonably close to the loss expected by reflection during solar operation which is 79 watts assuming a cavity absorptivity of .90. It is therefore reasonable to expect the total power input by bombardment is within a few watts of that which is retained by the cavity under solar energy operation.

Calibration was performed by measuring the ΔT along each calorimeter for various values of EB power. Power input was measured in terms of bombardment current and accelerating potential. From this data characterisitc curves of ΔT vs power input were prepared for each element which permit the determination of total power and power distribution within the cavity during misorientation under solar test.

Rotation vs Sensor Temperature Unbalance

A set of two diametrically opposed sensors were heated to the desired ambient temperature by employing the small electrical heaters. By changing the power input to one sensor its equilibrium temperature was changed while the temperature of the other was kept constant. For various values of temperature, rotation and ΔT were measured, and characteristic curves generated.

Inertial Tests

These tests were performed out of vacuum. Given moments of inertia were simulated by positioning a set of weights at various distances on a yoke arrangement. The sensors were heated to a desired ambient temperature by using electrical heaters. The temperature of one sensor was then made to oscillate about the ambient by varying the power input to its heater, while the other sensor temperature was kept constant. Recordings of rotation and sensor temperature were made. From these recordings phase shift vs. frequency characteristics were determined.

Natural frequency and damping characteristics were also determined during these tests. The mount was given an offset by adding a small weight to one arm of the yoke. When the deflection stabilized the weight was removed and a recording trace of the resulting motion was made as the mount returned to its original position. From these traces the natural frequency and time constants were determined.

Rotation vs. Torque and Stiffness

With the electrical heaters the sensors were heated to a desired ambient temperature. Torques were produced on the mount by adding a small weight at given distances along one arm of the yoke arrangement. For each value of torque the resulting rotation was recorded. From this data a curve of rotation vs torque was generated and spring constants determined. This procedure was repeated for various values of ambient sensor temperature.

Sensor Temperature vs Power Input

With the system under vacuum sensors were heated using a small electrical heaters. After equilibrium was established the temperatures and power inputs were recorded. This procedure was performed for values of sensor input power ranging from 2 to 18 watts. From these tests a curve of sensor temperature vs power was generated which could be used to verify the proper design operating conditions in the mount, and served to indicate the level of flux interception during solar tests.

Attenuation vs Frequency

To determine the thermal response characteristics of the sensors under dynamic conditions the sensors were tested by the application of sinusoidal variations in power input.

This test was performed using differential transformer control circuitry mounted in a relay rack. The sensors were electrically heated to an ambient temperature of 865°F. Using approximately 7 watts of power input. Superimposed upon this power level was an alternating signal of 2.1 watts. This value was chosen because it simulated the sensor input that would result from oscillating concentrator misalignments. The power signal was imposed at various frequencies ranging from 0 to .033 cps, with the upper limit of frequency being determined by the heater response capabilities rather than sensor characteristics. The temperature difference between sensors was measured and a plot of ΔT as a function of excitation frequency generated. Similar dynamic excitations were applied with the concentrator simulating masses in place to determine the inertial response and attenuation characteristics for this portion of the system.

Thermal Response

This test was performed using one sensor only. The sensor was electrically heated to an ambient temperature of 935°F. As various step inputs of power were supplied to this sensor a continuous trace of its temperature was made. From this trace the rate of change of sensor temperature was obtained for each power input. A curve of dT/dt vs. incremental power input was then generated. This procedure was repeated for an ambient temperature of 850°F.

4.3 Summary of Solar Test Procedure

The following procedure was followed for all solar tests. The tracking rig was activated and checked to insure proper alignment and operation. The chamber pressure and instrumentation were also checked. The shutters were opened and solar energy allowed to enter the calorimeter. All pertinent temperature and deflections were monitored continuously throughout the test operation on appropriate meters and recorders.

Static Response Tests

After equilibrium was established and the sensor temperature balanced a given tracker misorientation was imposed. The resulting temperature changes and mount rotations were recorded. This test was repeated with the offset given in azimuth and elevation and then in a direction 45° removed. The test was repeated for several values of misorientation.

Frequency Response Tests

These tests were performed along one axis only. After the sensor temperatures were equalized alternating step changes of misorientation were introduced. These imposed offsets ranged in frequency from .017 to .167 cps and had a magnitude of 3 and 5 minutes. As the rig osciliated sensor temperatures and mount rotation were recorded.

5.0 TEST EQUIPMENT

5.1 Laboratory Apparatus

The major portions of the laboratory test apparatus are shown in Figure 5.1-1 which also shows the calorimeter mount assembly located on the laboratory test stand. The mechanical and diffusion pumps located underneath are coupled to this stand. The two vacuum chambers shown at the left are a 12-1/2" bell jar used for laboratory testing and the precision ground glass dome used during solar tests.

The console shown on the right enclosed all instrumentation used for solar and laboratory tests. Going from top to bottom, the first panel held the ammeter and switches used to measure EB current. It also held the potentiometers used to adjust the motion transducer circuitry. The second panel held two C/A pyrometers and a 16 channel selector switch to monitor the various temperatures. Next are shown two Varian dual channel recorders on top of a 24 point temperature logger. The recorders were used to measure temperature response and mount rotation as a function of time. The logger was used to monitor temperatures during all laboratory and solar tests. The empty panel was later used to contain the sensor heater controls and meters. The bottom panel contained the thermocouple gauge and vacuum ion gauge controller used during the laboratory tests. Other miscellaneous controls, meters, pyrometers etc. are not shown.

The electron bombardment power supply is shown at the lower left side. It has a capacity of 4 amps at 1000 volts D. C.

Calibration of the calorimeter was performed by electron bombardment heating of the cavity. Figure 5.1-2 shows the electron gun assembly used for this activity. It consisted of a tantalum filament mounted in a molybdenum holder. The lead wires were copper and the insulating support block was machined from lava B.

This assembly was attached to and supported by stainless steel studs in the calorimeter cover plate so that the filament projected well into the cavity formed by the four diode simulating elements, as shown in Figure 5.1-3.

A schematic of the electron bombardment circuitry is shown in Figure 5.1.4.

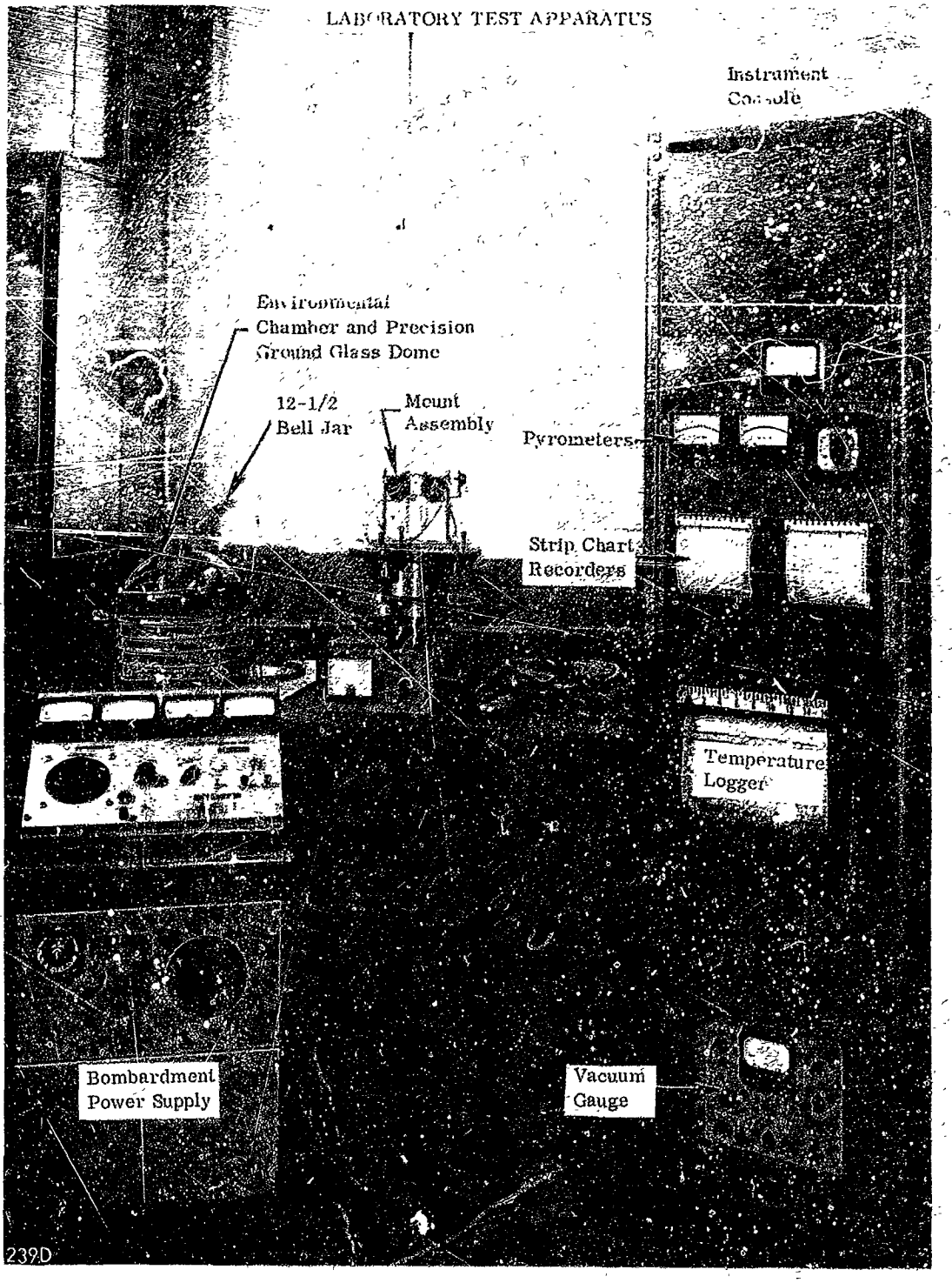
LABORATORY TEST APPARATUS
Instrument Console
Environmental Chamber and Precision Ground Glass Dome
12-1/2 Bell Jar
Mount Assembly
Pyrometers
Strip Chart Recorders
Temperature Logger
Bombardment Power Supply
Vacuum Gauge
239D

FIGURE 5.1-1

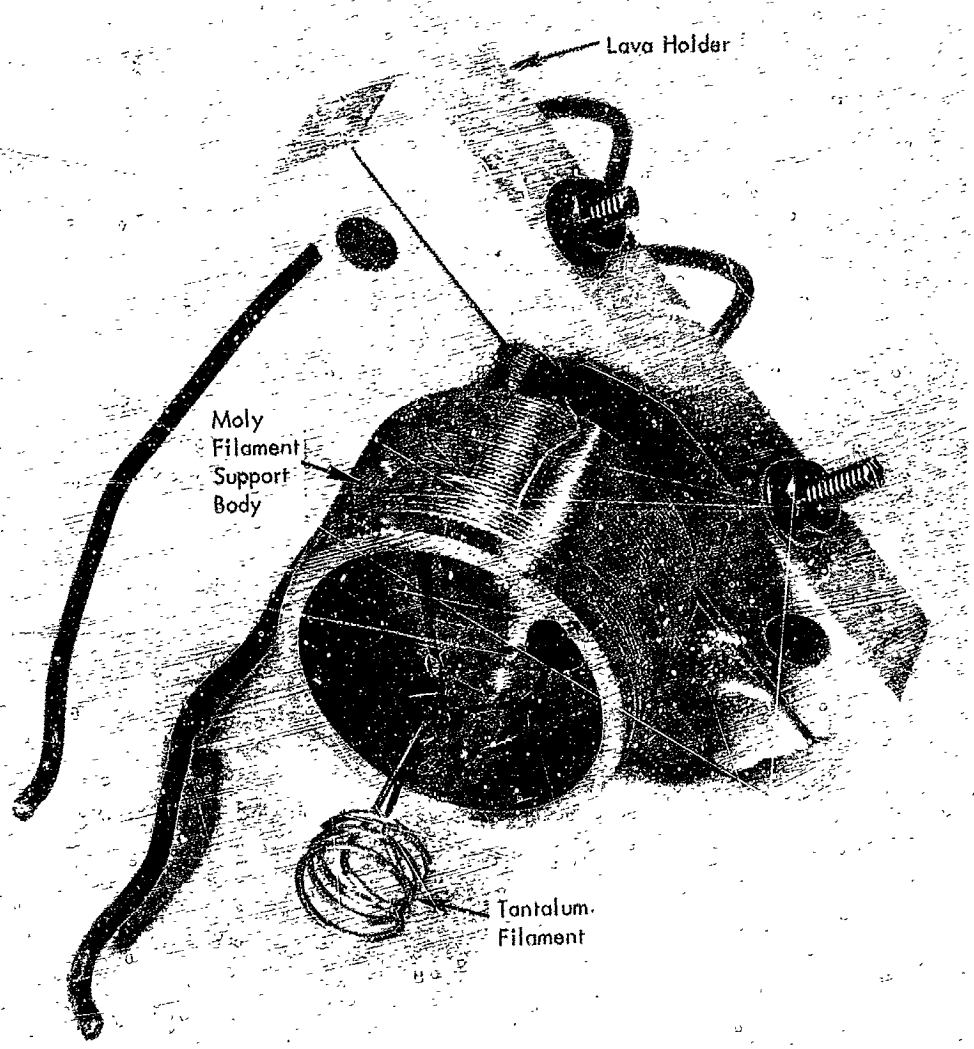

ELECTRON GUN ASSEMBLY

FIGURE 5.1-2

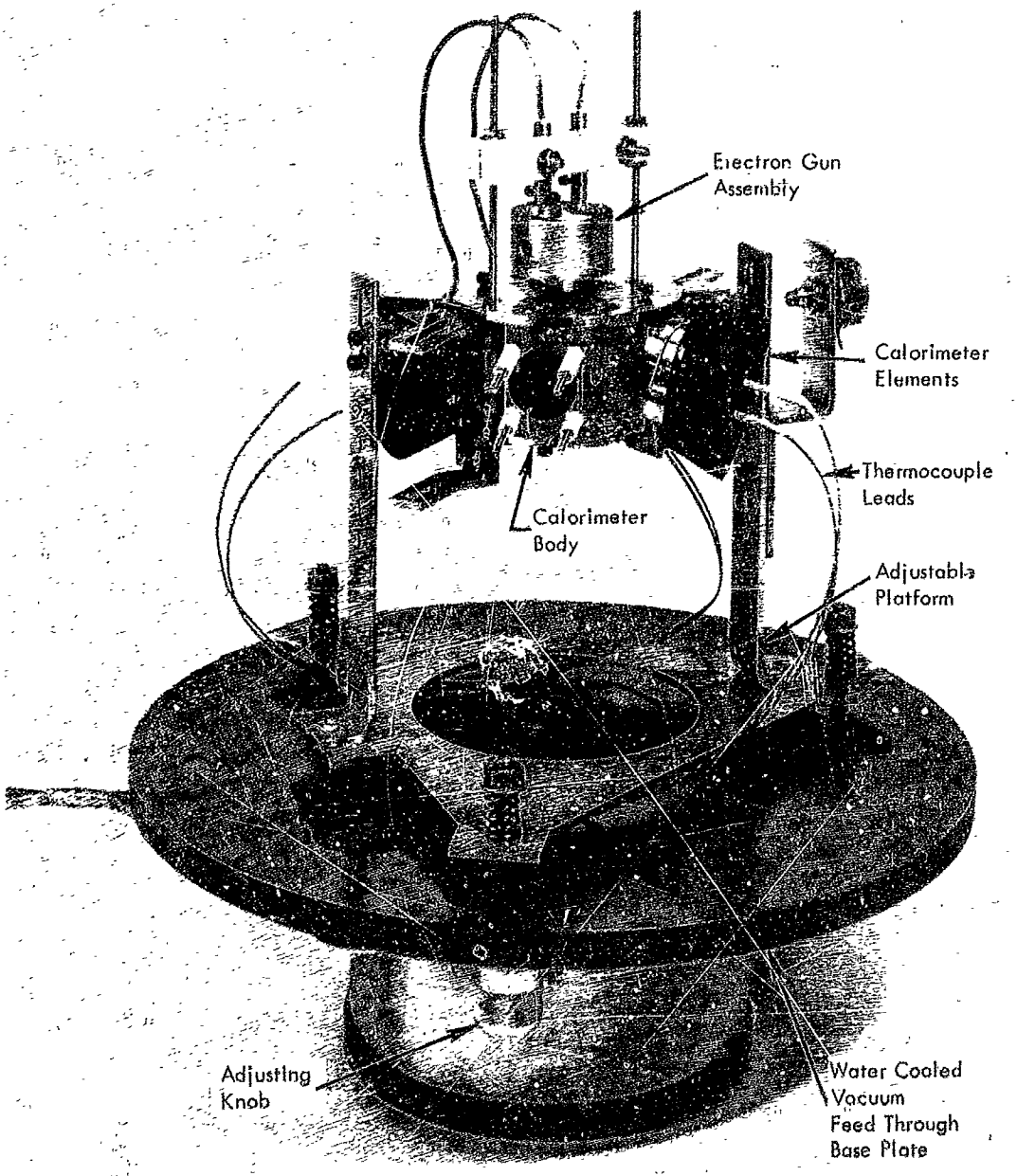

HELIOTROPIC MOUNT ASSEMBLY

FIGURE 5.1-3

Electron Bombardment Circuitry

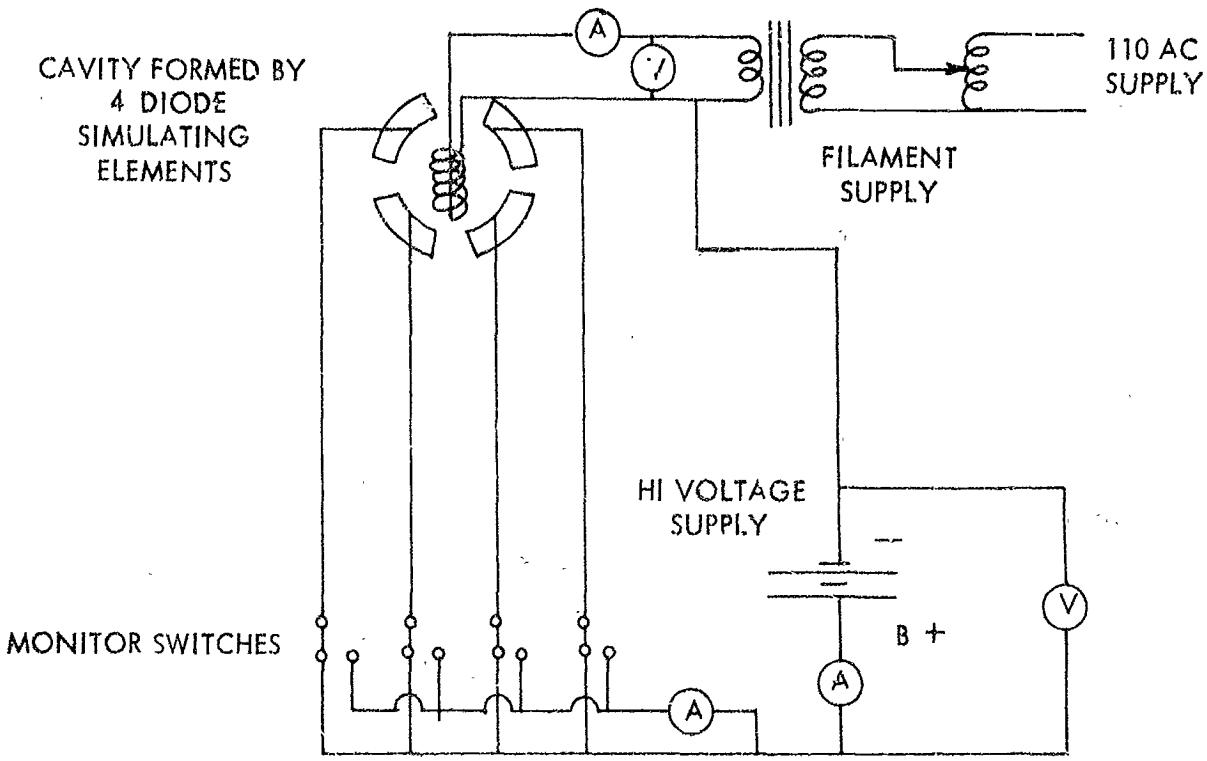

FIGURE 5.1-4

The two transducers used to measure angular displacement were simple carbon film type potentiometers. One was mounted along each axis of rotation so that the motion in both directions could be measured simultaneously and independently. The pots were connected to the movable mounts by a steel support bracket and were free to rotate. The pot stems were not free to rotate being rigidly attached to the calorimeter as shown in Figure 5.1-5. Rotation of the mount would therefore cause relative changes in resistance in the potentiometers producing an unbalance in a bridge circuit which was monitored by the recorders.

Transducer Arrangement

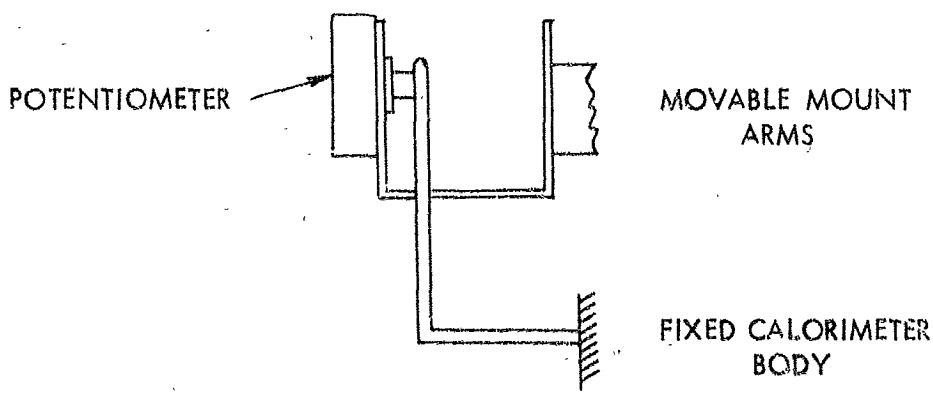

FIGURE 5.1-5

Transducer Bridge Circuitry

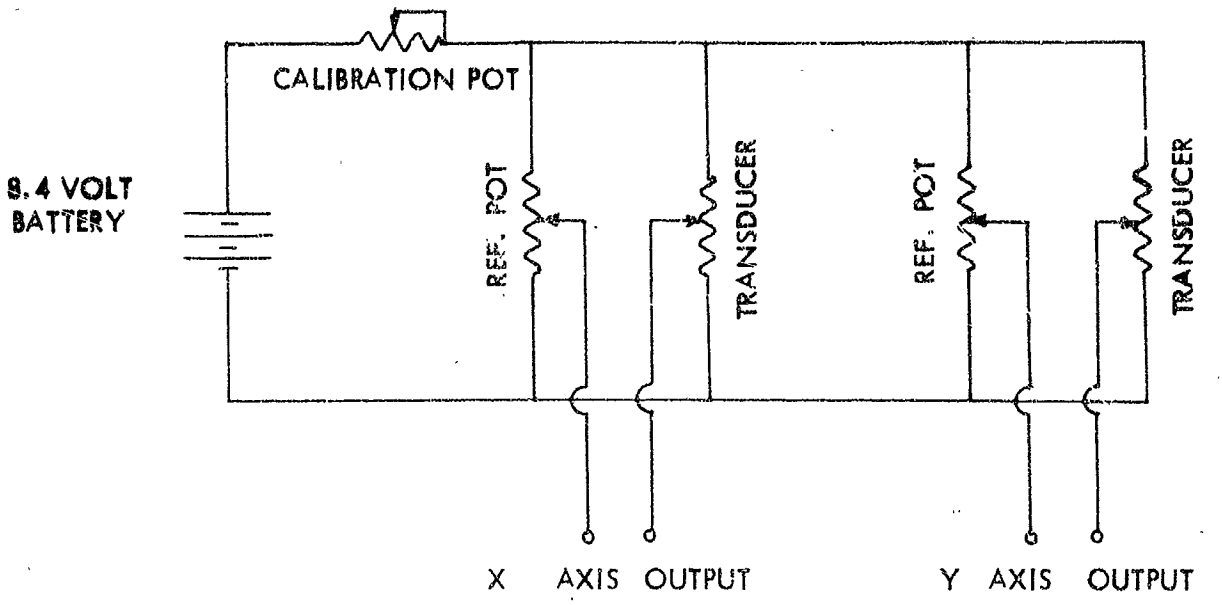

FIGURE 5.1-6

The reference pots were used to reduce the output signal to zero when the mount was in a null or balanced condition. The calibration pot provided a means to adjust the output signal magnitude for a given unbalance. For all tests this was set to yield an output of 20 mv/degree rotation.

Torques were applied to the mount and concentrator inertias simulated without exceeding the bearing load capacity during "in air" tests by employing the yoke arrangement shown in Figure 5.1-7.

Concentrator Simulator

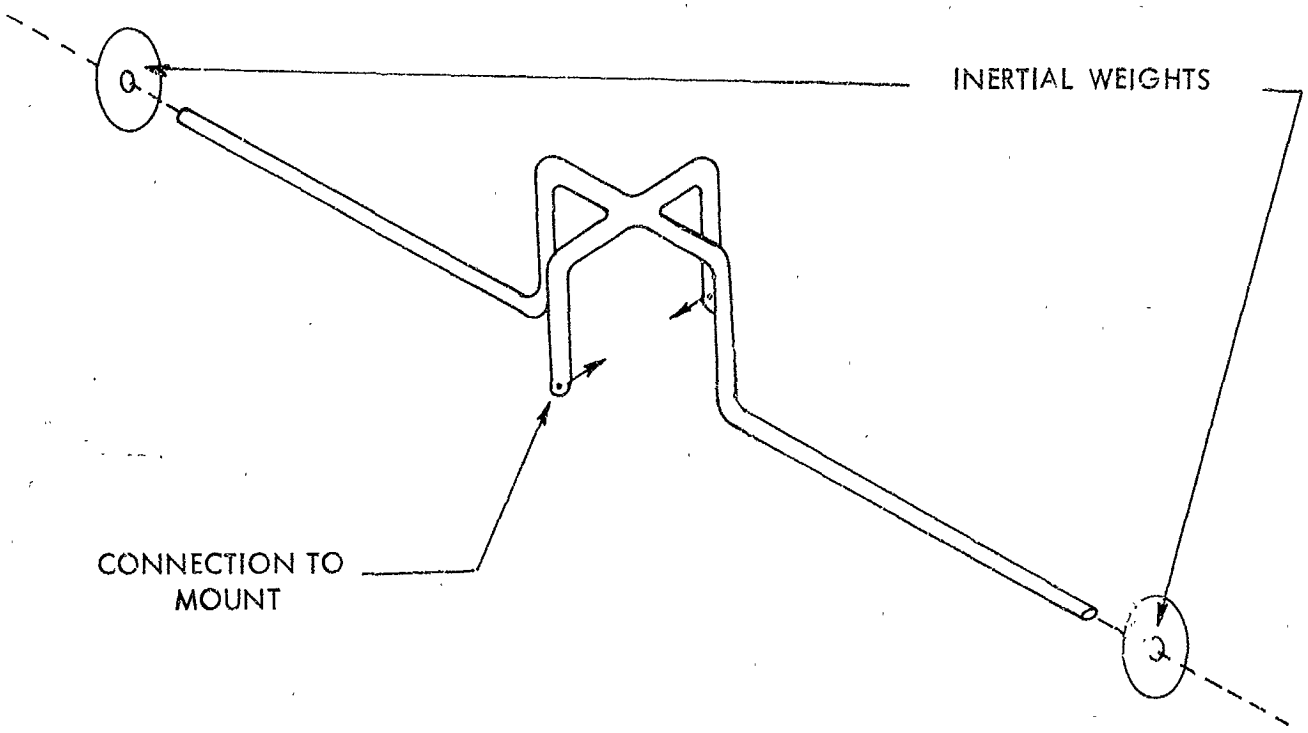

FIGURE 5.1-7

Given torques were produced by applying a small weight at various distances along the arm. To simulate the inertia associated with a concentrator and minimize the effects of gravity a set of 6 pound weights were made which could be positioned anywhere along the arms. By adjusting these two weights to counterbalance each other, dynamic tests of the system were made with moments due to gravitational effects reduced to zero.

The temperature and power inputs to the sensors were simulated in the laboratory using small electrical heaters. The heaters were fastened to the sensors and the whole assembly wrapped in copper foil to insure good thermal conductivity. For the "in air" tests larger heaters were used and insulating material was added. A schematic of the heater circuitry and controls is shown in Figure 5.1-8.

Heater Control Circuitry

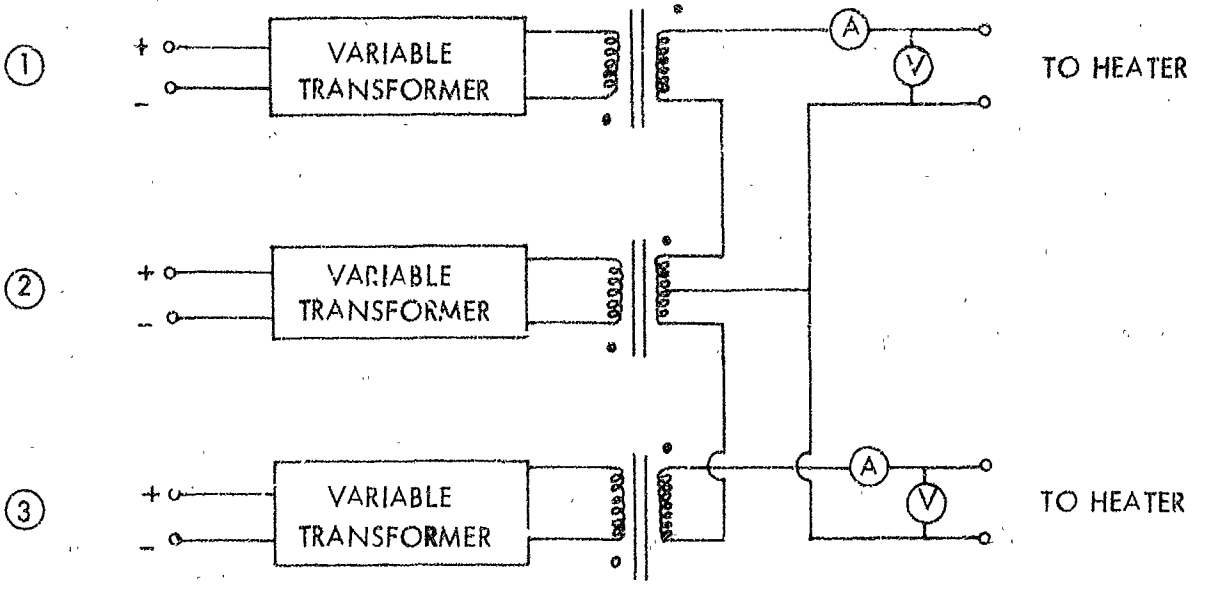

FIGURE 5.1-8

Variable transformers 1 and 3 are used to set the desired temperatures for the two diametrically opposed sensors under test. By regulating the control on variable transformer 2 the power input to one heater increases while it decreases for the other. This heating arrangement simulated the flux unbalance that would be present do to a misaligned concentrator.

5.2 Solar Test Equipment

The tracking rig and instrumentation rack used for the solar tests is shown in Figure 5.2-1. The tracker is a searchlight rig modified to follow the sun and contains a 5 foot diameter precision glass concentrator. The console contained the same components it did during the laboratory tests, except that the vacuum gauge was removed. During operation D.C. servo motors and gear reductions at each pivot axis drive the rig to keep the optic axis of the mirror continually pointed at the sun. The drive motors are controlled by a tracking system which consists of sun sensors, servo amplifiers, and amplidyne generators. With this arrangement the rig will track the sun automatically to within ± 1 minute of error.

A tripod arrangement supported the vacuum chamber so that the calorimeter operture was in the focal plane of the concentrator. A mechanical and a diffusion pump were

mounted on the rig and coupled to the test chamber. The rig also contained a thermocouple gauge and ion gauge controller to measure the operating pressures. Two solar sensors, one each for azimuth and elevation, along with an optical aligning device were mounted on the rig parallel to the concentrator axis as shown in Figure 5.2-2.

The sun sensor each contained two photo resistive cells which formed part of a bridge network. The control box on the rig contained balance pots to null out the bridge when the concentrator was perfectly aligned toward the sun. The rig also contained circuitry so that various offsets could be introduced during the solar tracking. The controls were such that either steady state or sinusoidal varying offsets could be produced independently in both azimuth and elevation.

The optical alignment indicator consisted of a lens system that imaged and projected the solar disk upon a ground glass viewer as shown in Figure 5.2-3. With perfect alignment the solar disk would fall in the center of the grid. For concentrator misalignment this spot becomes displaced from the center of the grid. The graduations on the viewer made it possible to measure the amount of misorientation within a half minute. Each graduation represented one minute of alignment error.

A pyrheliometer was mounted on the rig parallel to the optic axis of the concentrator. Use of this instrument was made during all tests to measure the solar constant.

SOLAR TEST FACILITY

FIGURE 5.2-1

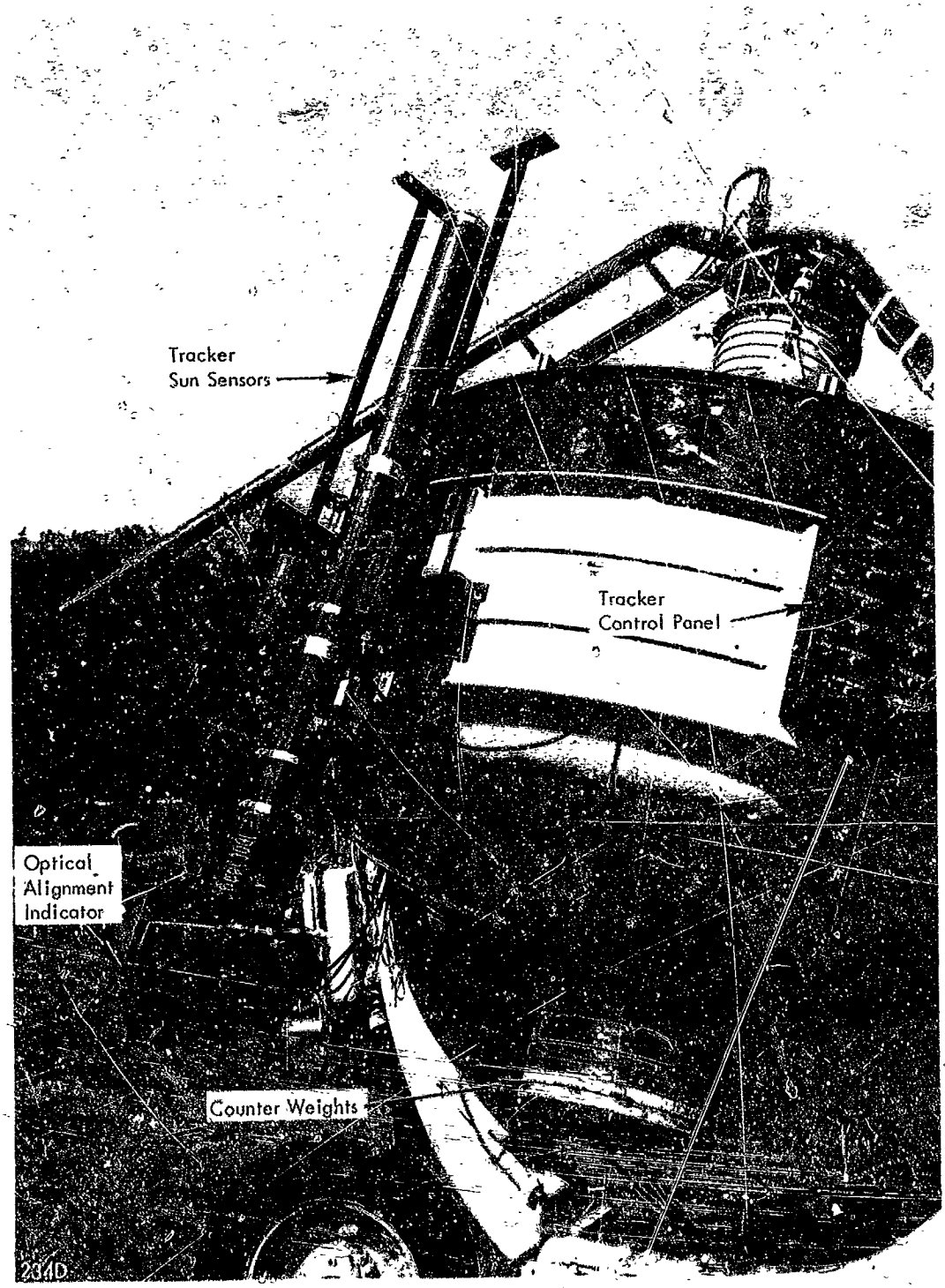

SOLAR TRACKER CONTROLS

FIGURE 5.2-2

OPTICAL ALIGNMENT TUBE

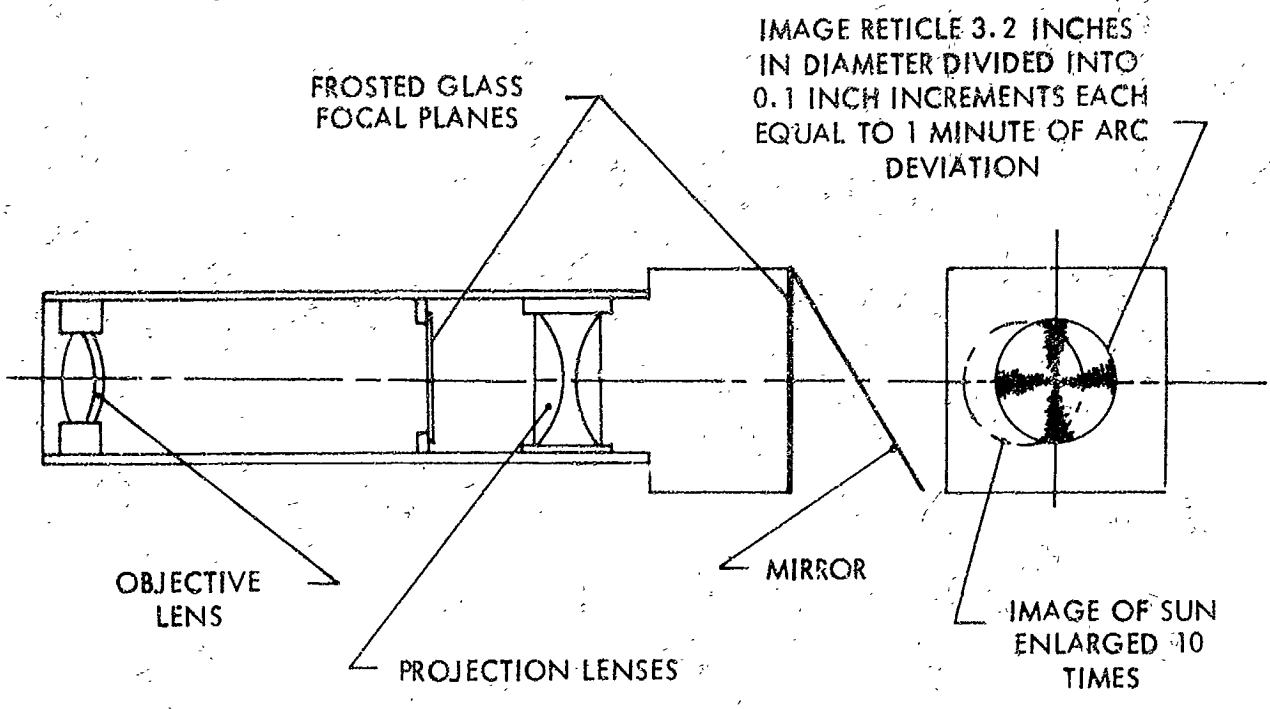

FIGURE 5.2-3

6.0 TEST RESULTS AND CONCLUSIONS

6.1 Preliminary Laboratory Test Results and Mount Modifications

6.1.1 Calorimeter Measurements and Design Changes

The results of the preliminary calibration tests and temperature distribution measurements in the calorimeter simulator assembly showed that the design possessed several minor defects which prevented the calibration of the elements as calorimeter devices.

The two main difficulties encountered with the calorimeter elements were that the thermal contact between the shaft and radiator sections changed as the assembly warmed up, and that the foil shielding which surrounded the shaft section was less effective than the calculations had predicted. The junction between the shaft and radiator was made by clamping the two pieces together with a collar and screw. The arrangement was such that upon heating the clamping action should have tightened due to the relative expansion of molybdenum, copper, and stainless steel. It appeared however that the contact pressure was not increased by heating or at least that this increase was offset by a decrease in contact in the diametral direction between the shaft and radiator.

At about half power the ΔT in the shaft, and the radiator rate of change of temperature with power input was reduced. Also the average shaft temperature appeared higher than it should, and the radiator temperature was somewhat lower than the input power level would indicate as appropriate. The conclusion was that the conduction of heat down the shaft was interrupted by a shifted or a reduction in the contact between the shaft and radiator. This situation was aggravated by the fact that this discontinuity was not consistent or reproducible between elements or test runs.

An attempt at refitting the elements by slightly upsetting the radiator bore to make a press fit with the shaft, and increasing the tension on the clamping screw was only partially successful. The discontinuity occurred at a higher temperature but remained unpredictable. The situation was finally corrected by brazing the two parts together.

The second problem encountered with the calorimeter shielding was not severe but did result in a reduced cavity temperature and a greater percentage of power lost by radiation along the shaft length. The cavity temperature attained at design power input was a hundred degrees below the nominal 1700°C design value. It appeared that the four to five layers of dimpled moly foil were not quite as efficient as calculations based on radiant transfer would indicate. This may in part be due to the existence of pressures as great as 10^{-3} mm hg between foil layers or to more efficient conduction coupling between the dimpled surfaces. A layer of Micro-quartz strip was added at the time the radiator and shaft assemblies were reworked to help improve the insulation characteristics of the foil shields.

6.1.2 Preliminary Mount Tests and Design Changes

Mount rotation as a function of temperature difference between sensors is presented in Figure 6.1.2-1. These vacuum test data were obtained by imposing a temperature gradient and allowing the mount rotate to a new position as required by static torque equilibrium. Mean or ambient temperature of the sensors is 1000°F. The gain or slope of this curve is about 1° rotation per 100°F difference in temperature between the two sensors. This is less than one-fifth that expected based on the manufacturer's stated characteristics for the bellows. Equally unexpected, no improvement in gain was detected with increase in sensor ambient temperature. It was concluded that increasing the test temperature and pressure increases the bellows stiffness thereby nullifying the gain that should result from the pressure-temperature characteristics of mercury.

Upon heating of the calorimeter at the design input power level the sensors which are positioned very close to the cavity were found to reach temperatures of near 1800°F as opposed to the 1059°F design value. The copper heat sink clips which hold the sensor-capillary structure were moved to the closest or most effective position in an effort to reduce sensor ambient temperatures and the test repeated. A slight reduction in sensor temperature was noted. The sensors were then thermally grounded directly to the top plate of the calorimeter assembly by means of supplementary screws which were introduced through slots machined in the top plate. Again a small improvement was noted but the temperatures were still 400 to 500°F too high. Finally the top plate was blackened, stood off from the body block and several foil neat shields arranged between the top plate and sensors and the hot calorimeter elements. Even with these changes the sensors operated over 300°F above design.

It appeared impossible to operate the mercury sensors in close proximity to the focal plane and the hot cavity. After considering other possible modifications to reduce sensor temperature it was decided to locate the sensors farther from the focal plane of the concentrator outside the calorimeter body. This not only reduced the operating temperature of the sensors but could even increase the rate of flux intensity change as a function of misorientation. Near the fringe or tail of the flux distribution curve and at the same radial distance, the rate of change of flux intensity is surely greater for the out of focal plane traverse than for the on focus data. Unfortunately no actual flux profile data is available for the region forward of the focal plane. Estimates were made of the probable flux intensities and sistribution however, and it appeared reasonable that good performance could be expected. These estimates proved to be quite good as indicated by the results of the solar tests that followed.

Moving the sensors on top the cover plate will allow the sensors to be designed to operate more efficiently. With the sensors in the cavity, space limitations alone indicated their shape.

MOUNT ROTATION AS A FUNCTION OF TEMPERATURE GRADIENT BETWEEN SENSORS

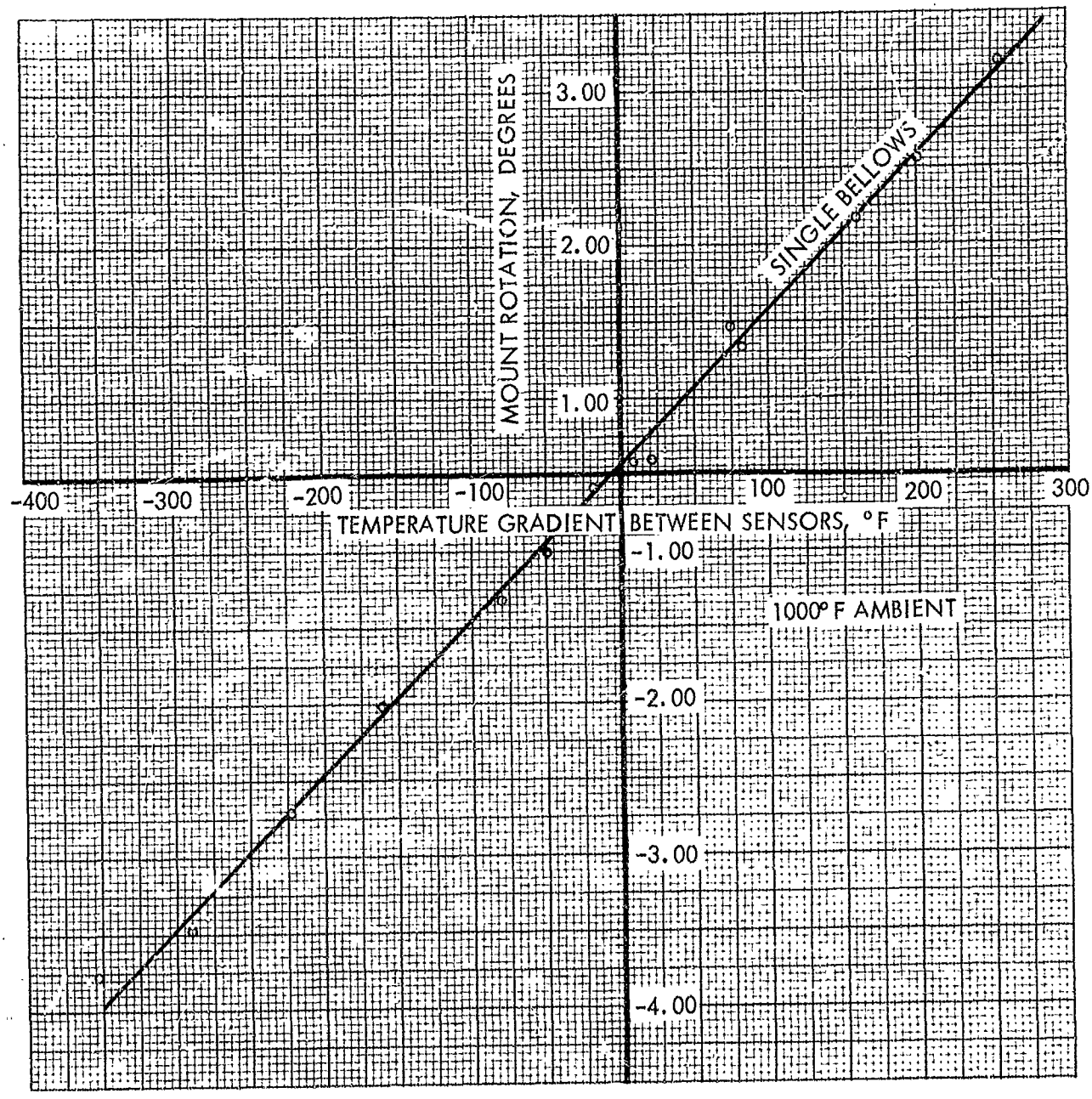

FIGURE 6.1.2-1

In an attempt to upgrade mount performance and establish proper operating conditions a number of changes were incorporated in the mount itself. Doubling the length of the bellows cut the spring rate in half. While the gain was not as high as desired the new unit was able to track or follow through $\pm$ 5° with a persistent error of less than $\pm$ 12'.

The constant gain characteristic was still present in the double assembly and because of this the precise establishment of the sensor temperature was no longer critical. In other words, the mount performed equally well with the sensor ambient temperatures ranging from 850°F to 1250°F. Since the precise control of this ambient had previously been found a problem, this relaxation in operating point control was very fortunate.

With the sensors on top the cover plate, it was appropriate to change the sensor shape. The mass of the wedge shaped sensor could be reduced to improve the time response of the mount. Also, by elongating the sensors so that the four together nearly enclose or surround the cavity, more power change per given misorientation could be expected. Therefore, an elongated tubular sensor was designed and incorporated in the mount.

The new cover plate had been reduced in thickness to reduce the distance from the sensors to the focal plane. In this arrangement, the sensors were shielded by the top plate which cuts off a direct view of the hot cavity. The top plate will itself be better protected by the interposition of several foil heat shields between it and the cavity. In the proposed arrangement the sensors would be entirely exposed. The top of the sensors could be blackened to increase heat rejection and to improve the absorption of solar flux in the reduced intensity region if necessary. Support is provided the sensor-capillary by clamping the capillary with a small bracket to the cover plate which allows the sensor to be positioned radially with respect to the optical axis. The capillary tubes are still carefully shielded by the support structures so that in the case of a gross misorientation the bellows assemblies will not be destroyed by overpressure. A gross misalignment will heat the sensor until the mercury is backed down the capillary tube to a low temperature region where the vapor pressures are tolerable. In this condition the mount is fully actuated and the misalignment is removed by the mount if within $\pm$ 5 degrees, or will require some vehicle correction to establish the 5 degree course orientation.

Figure 6.1.2-2 shows the cover plate and sensor modifications. The new sensors are cylindrical tubes 5/32 O.D. x 1/8 ID x 1.35 inches long. The mass of the sensor has been reduced by more than 50 percent decreasing the response time appreciably. While not a major consideration, the fabrication of the cylindrical sensor is an easier task. Also, the mercury charging of the sensor is easily completed by pinching and welding of the tube itself.

The vacuum and mercury fill arrangement used is shown in Figure 6.1.2-3. The sequence to mercury charge and seal the assembly was as follows:

1. Close valve A and open valve B and C and evacuate the assembly.

COVER PLATE AND SENSOR MODIFICATION

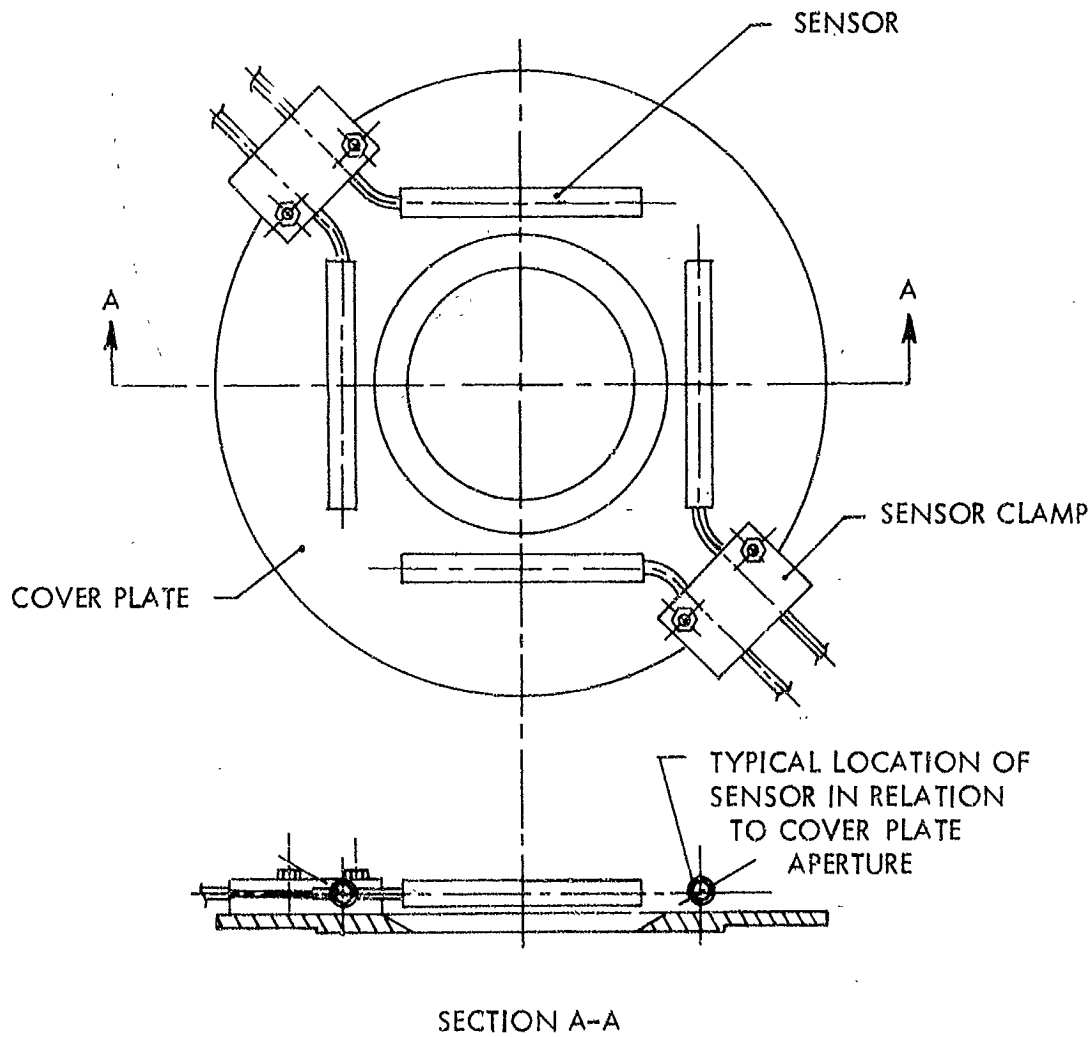

SECTION A-A

FIGURE 6.1.2-2

SCHEMATIC OF BELLOWS-SENSOR ASSEMBLY
CHARGING METHOD

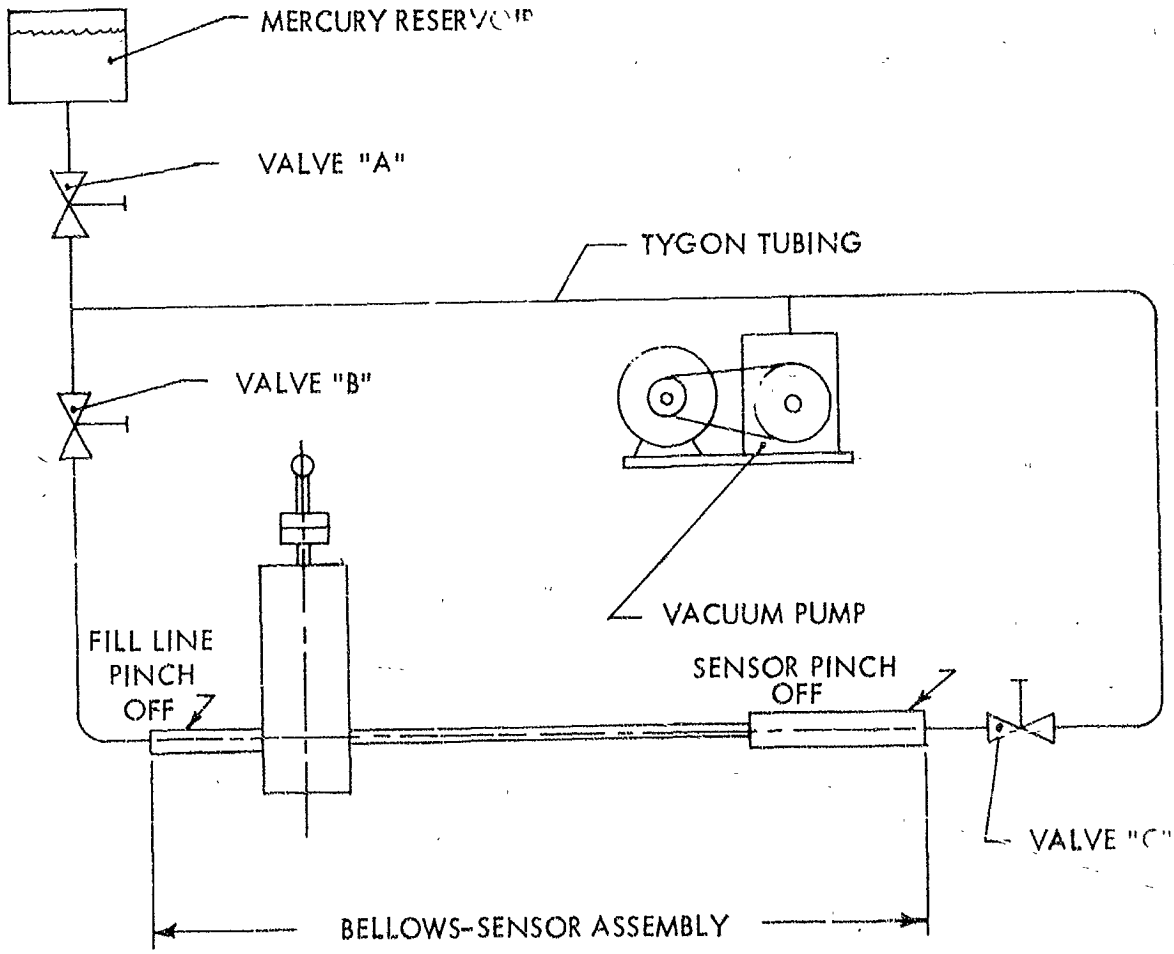

FIGURE 6.1.2-3

2. With a hot air gun, heat the bellows, capillary, and sensor to 200 to 300°F to boil off any residual vapor.

3. Slowly open valve A and bleed mercury into the bellows.

4. Close valve B. Pinch down on the tubing between valve B and the bellows and decrease the bellows volume by stroking the bellows stem, thereby forcing mercury through the capillary and into the sensor.

5. With the assembly full, close valve C and pinch, snip, and fuse tight the bellows fill tube and sensor.

This charging sequence was altogether satisfactory in that seven successive units were filled without incident.

As noted previously, increasing the sensor temperature increased the bellows stiffness and thereby reduced the gain of the mount. To alleviate this problem and to increase stroke, two bellows were welded in series.

This longer bellows assembly required that a ball and socket joint be incorporated into the mount to prevent binding of the bellows fitting within its chamber. The ball and socket joints functioned very well in vacuum with the addition of a dry graphite lubricant, but this is not considered a suitable approach for an extended space application. The use of small flexure bearings would be recommended.

6.2 Laboratory Performance Test

Prior to the presentation of test results, it is worthwhile to examine more closely how the mount is activated as well as the parameters that influence satisfactory operation of the mount.

Figure 6.2-1A shows the bellows assembly in the room temperature condition. The sensor and bellows are almost completely liquid filled. The sockets are backed off from the bellows stems an amount sufficient to allow ± 5° rotation. Additional clearance is provided for the bellows to operate hot. It was calculated and confirmed in the laboratory that disimilar rates of expansion of the mercury and bellow material will account for .025 inch change in stroke per 100°F change in temperature. Since the coefficient of expansion is greater for the mercury than for the stainless steel bellows an increase in bellows temperature extends the bellows stem, thereby requiring additional clearance.

Figure 6.2-1B shows the mount in the balanced position with the socket properly positioned. Increasing the temperature of both sensors at the same rate equally increases the pressure and force on the sockets but the mount remains balanced.

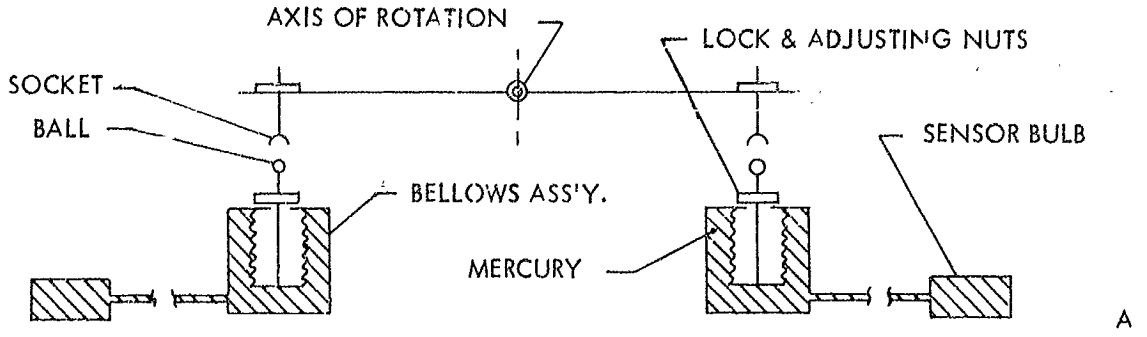

A

SENSORS COLD

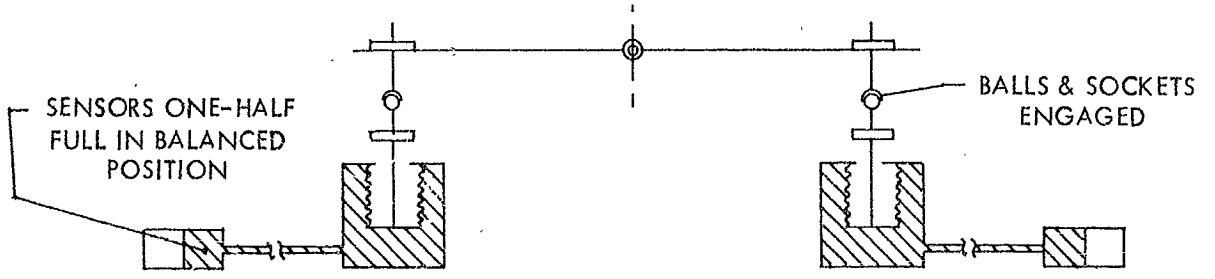

B

SENSORS AT EQUILIBRIUM OPERATING TEMPERATURE
(PROPERLY POSITIONED SOCKETS)

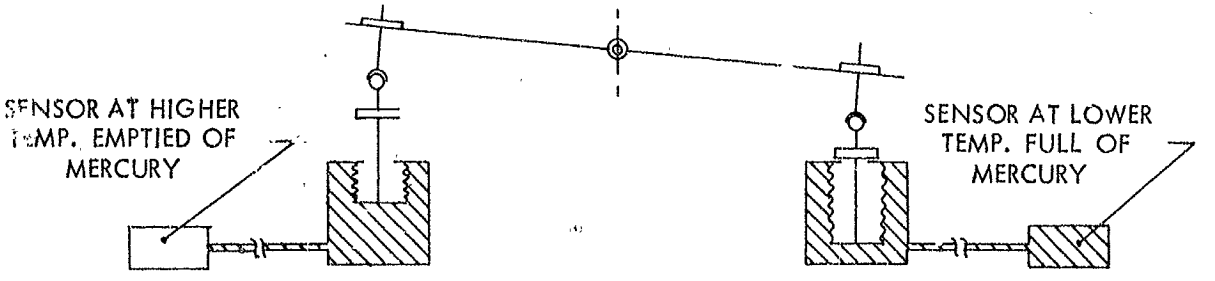

C

MOUNT AT MAXIMUM ROTATION

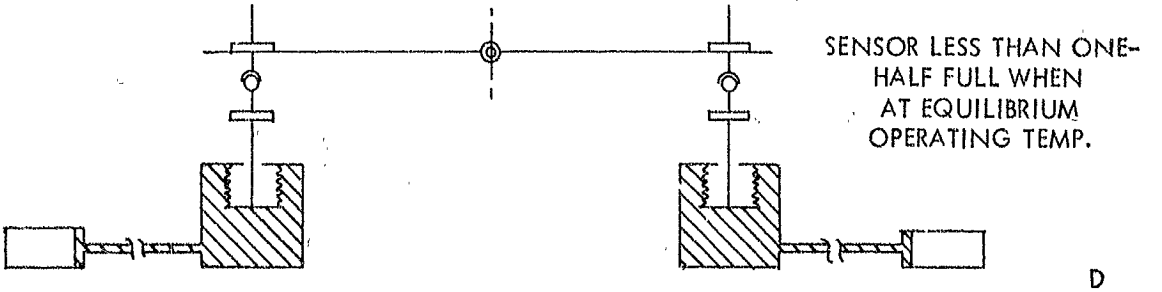

D

IMPROPERLY POSITIONED SOCKETS
(CASE SHOWN-SOCKETS TOO FAR FROM BALLS)

FIGURE 6.2-1

The bellow-sensor inventories at maximum rotation are shown in Figure 6.2-1C. The sensor volume is related to the bellows area and moment arm so that at full rotation ($\pm$ 5°) the one sensor will be depleted of mercury and the other will be full.

Figure 6.2-1D shows what happens if the sockets are improperly positioned. This could result from not accounting properly for the relative expansion of mercury and stainless steel or from the collapse of the bellows under pressure. The mount is shown balanced, but the sensors are not one-half full. At some rotation less than 5° the one sensor will deplete completely, the temperature of the mercury will decrease and the response of the mount will be imparred.

6.2.1 Thermal Response Tests

Static tests of mount rotation as a function of ΔT between sensors were performed for with the double bellows assembly. The results as shown in Figure 6.2.1-1 indicate a gain for all ambient temperatures off 2.2° rotation per 100°F ΔT. This is in agreement with the preliminary tests in that the gain of the new assemblies is about twice that of the single bellows units.

Earlier attempts to obtain the data of Figure 6.2.1-1 with the bellows cold were unsatisfactory. The curves were nonlinear and quite flat or low in gain. This was immediately attributed to lack of mercury inventory in the sensors and the bellows were heated to correct for this deficiency. The calculated relative expansion of mercury and stainless steel was found to be insufficient to completely correct for the low gain and nonlinear characteristics. It was concluded that the bellows convolutions were collapsing under pressure and the void space caused by this partial collapse was consuming an additional volume above what had been made up by the adjustments and expansion compensations. This conclusion was later born out in the determination of a reduced effective bellows area and increased spring rates which are the result of this collapse. The immediate restorations of linearity and gain required only a slight additional volume compensation to overcome the collapse voids. With proper adjustments the mount was found to have reasonable gain and good linearity.

Two of the tests reported in Figure 6.2.1-1 were with the bellows at near 300°F rather than 600°F. These curves flatten or lose their gain more rapidly than the others. This indicates that the mercury volume increase due to the 250°F increase in bellows ambient is not enough to fully compensate for the collapsing phenomenon.

The vacuum thermal response characteristics are shown in Figure 6.2.1-2 which indicates the thermal response of the sensor for a 935°F ambient temperature level. The estimated rate of change under solar test is shown to be almost twice as great since the heaters and a copper foil wrapper material will not be present in the solar

SYMBOL	SENSORS	CONSTANT TEMP. SENSOR		BELLOWS
		SENSOR	TEMPERATURE	TEMP.
o	10 & 12	12	900° F	590° F
×	10 & 12	12	980° F	610° F
△	10 & 12	12	1045° F	570° F
▽	9 & 11	9	930° F	280° F
+	9 & 11	9	850° F	360° F

MOUNT ROTATION AS FUNCTION OF △ T BETWEEN SENSORS

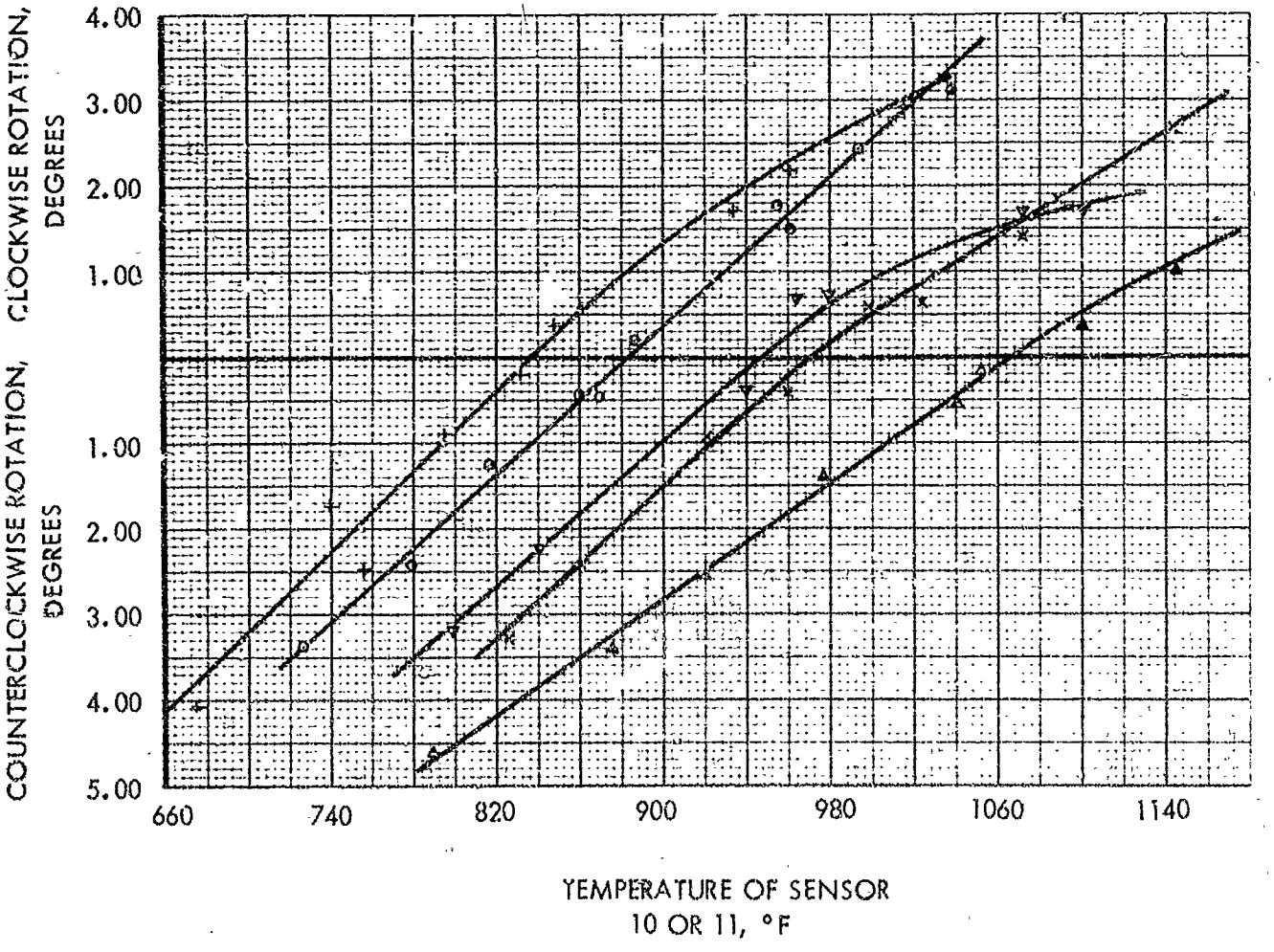

FIGURE 6.2.1-1

SENSOR THERMAL RESPONSE

SENSOR AMBIENT = 935° F

POWER INPUT (NOM.) = 6 WATTS

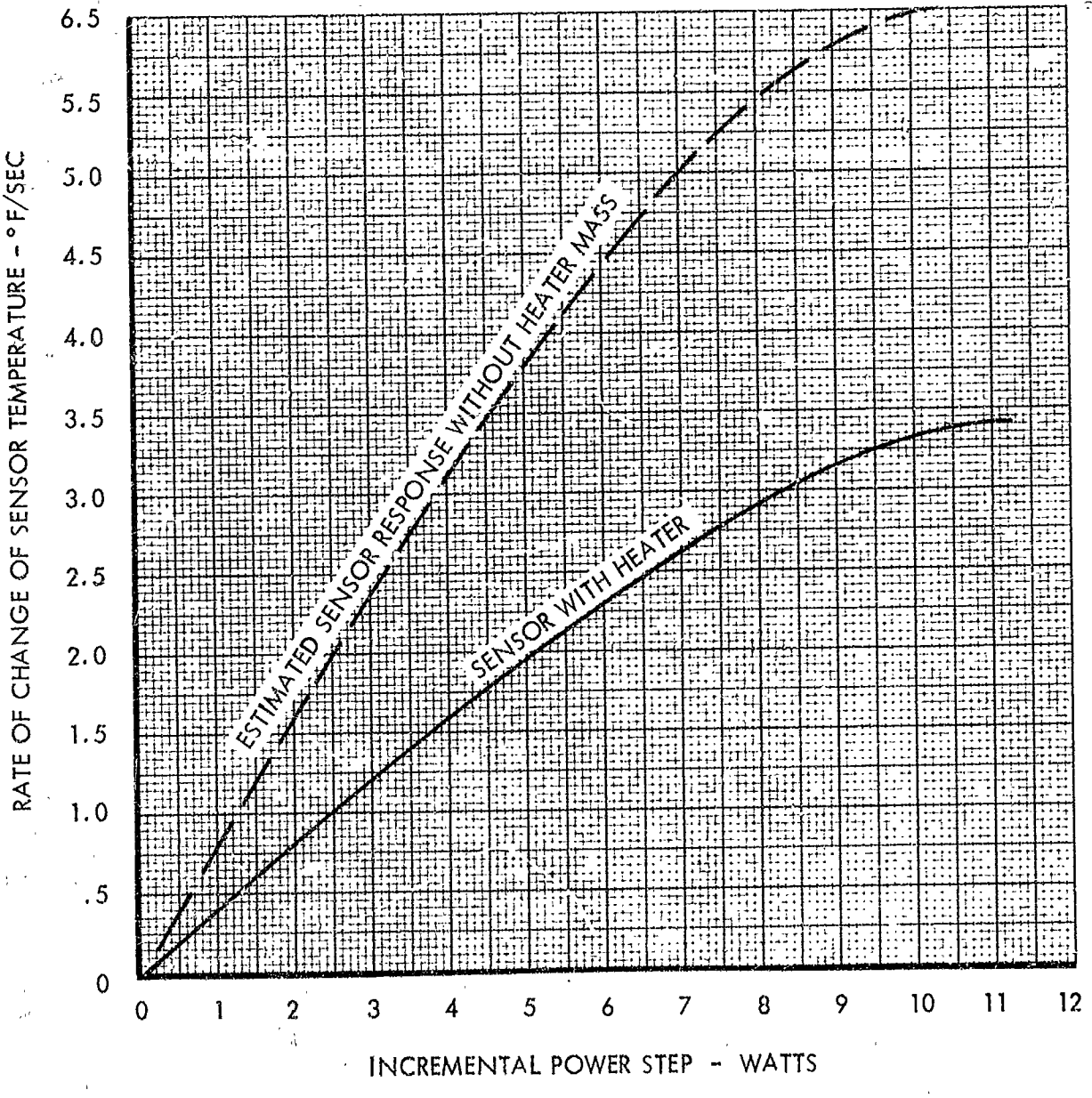

FIGURE 6.2.1-2

test assembly to absorb heat. Based on Figure 6.2.1-2 it is expected that a persistent 5 watt error input to the sensors will produce a full 5 degrees of mount correction in

$$3 \text{ Time Constant} \approx 3 \times \frac{202°F/5° \times 63}{3.8°F/sec} = 100 \text{ seconds}$$

neglecting the inertial lag. This is at least 8 times faster than the bimetallic type mount assembly previously tested by TRW during a corporate research effort.

6.2.2 Inertial Response Tests

The actual spring rate of the bellows was determined by the application of known torques and observing the relative rotation at various sensor ambients. The results of such tests are shown in Figure 6.2.2-1 for four sensor ambients. The decrease in the slope with increasing temperature (and pressure) indicates the increase in bellows stiffness due to the deformation of the convolutions previously reported. The spring constants which are determined from these slopes are also plotted as a function of the sensor ambient temperature in the insert figure. Using this variation in spring constants and the change in mercury vapor pressure with temperature as a function of the sensor ambient, it was possible to determine the optimum operating range for this mount assembly by means of the following relation

$$\Delta p A l = K \theta$$

Substituting $C \Delta T = \Delta p$ where C is the slope of the mercury vapor pressure curve at any given ambient, the curve in Figure 6.2.2-2 was generated. The moment arm (l) equals 0.80 inches; to bring this static torque data into agreement with the output rotation as a function of ΔT data (Figure 6.2.2-1) requires that the effective bellows area be about .045 sq. inches. The value of A is actually about half that quoted by the manufacturer and has been determined as the true effective area which is present under conditions of higher pressure which cause the partial bellows collapse. An examination of Figure 6.2.2-2 shows that for the combination of bellow spring characteristics and mercury pressure characteristics the greatest gain or mount rotation for a given temperature differential in the sensors occurs between 900 and 1000°F, and requires approximately a 202° Δ T. This range was selected for the solar test activities.

From the data obtained under thermal equilibrium conditions in vacuum the 5 degrees of mount rotation will require a plus and minus variation (for opposing sensors) of approximately 3 watts per sensor. This is shown in Figure 6.2.2-3 which indicates a variation of 35 to 40°F per watt at the 950° ambient level for the two sensors plotted.

MOUNT ROTATION AS A FUNCTION OF IMPOSED TORQUE

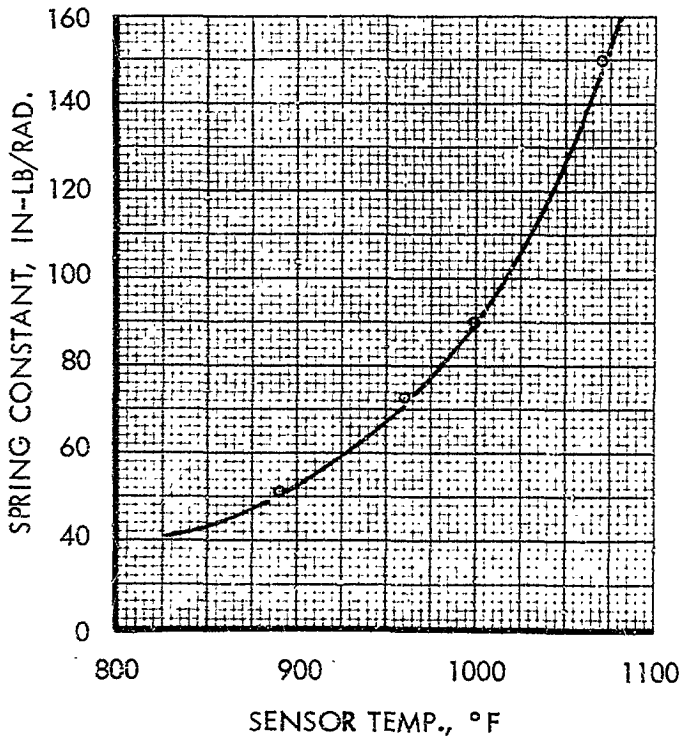

TEST CONDITIONS
DATA ARE FOR SENSORS NO. 10 & 12
BELLOWS ARE HOT (500-600° F)

SYMBOL	SENSOR TEMP.	SPRING IN-LB/DEG.	CONSTANT IN-LB/RAD.
o	960° F	1.27	72.8
x	890° F	0.91	52.0
Δ	1070° F	2.62	150.0
Y	1000° F	1.57	90.0

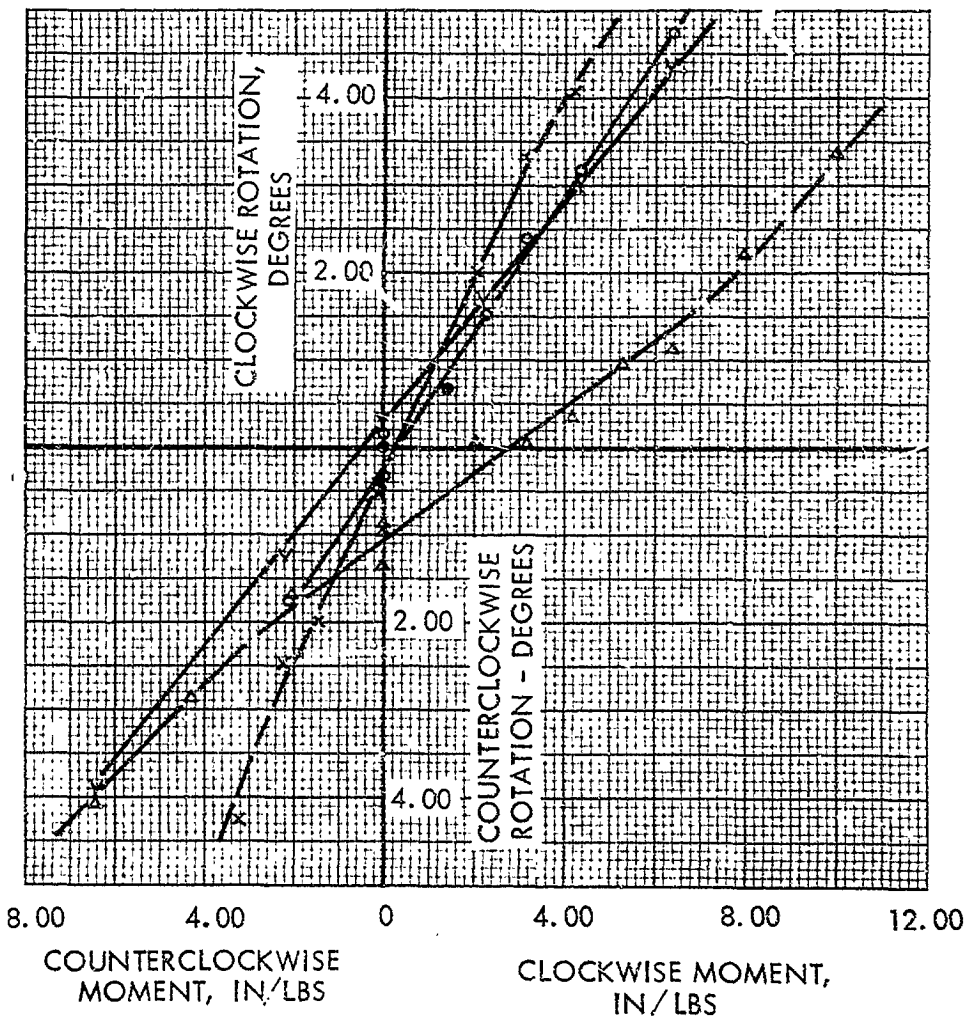

FIGURE 6.2.2-1

Tamb. °F	K IN#/RAD	Δp/ΔT PSI/°F	θ/ΔT DEG/°F	°F/5° 0 °F
890	52	.60	.0237	210
960	72.8	.86	.0246	202
1000	90	1.04	.0237	210
1070	150	1.42	.0195	257

MOUNT GAIN VERSUS SENSOR TEMPERATURE

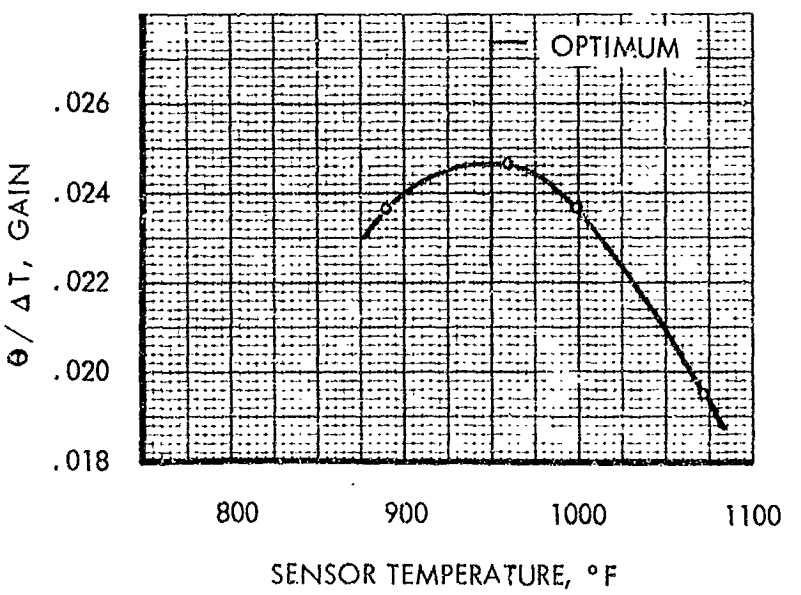

FIGURE 6.2.2-2

RANGE OF MEASURED SENSOR EQUILIBRIUM TEMPERATURE
VERSUS POWER INPUT

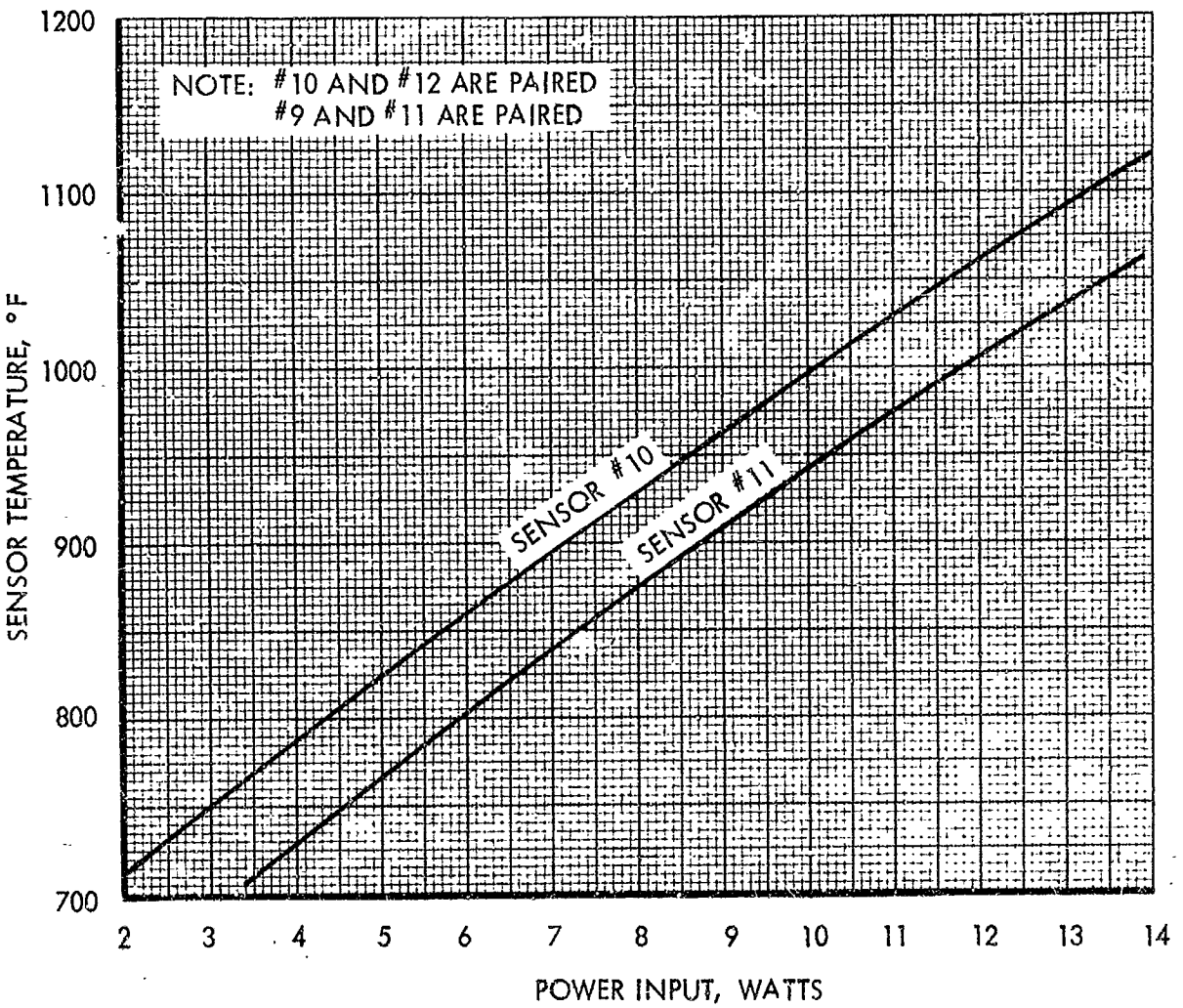

FIGURE 6.2.2-3

INERTIAL TEST RESULTS

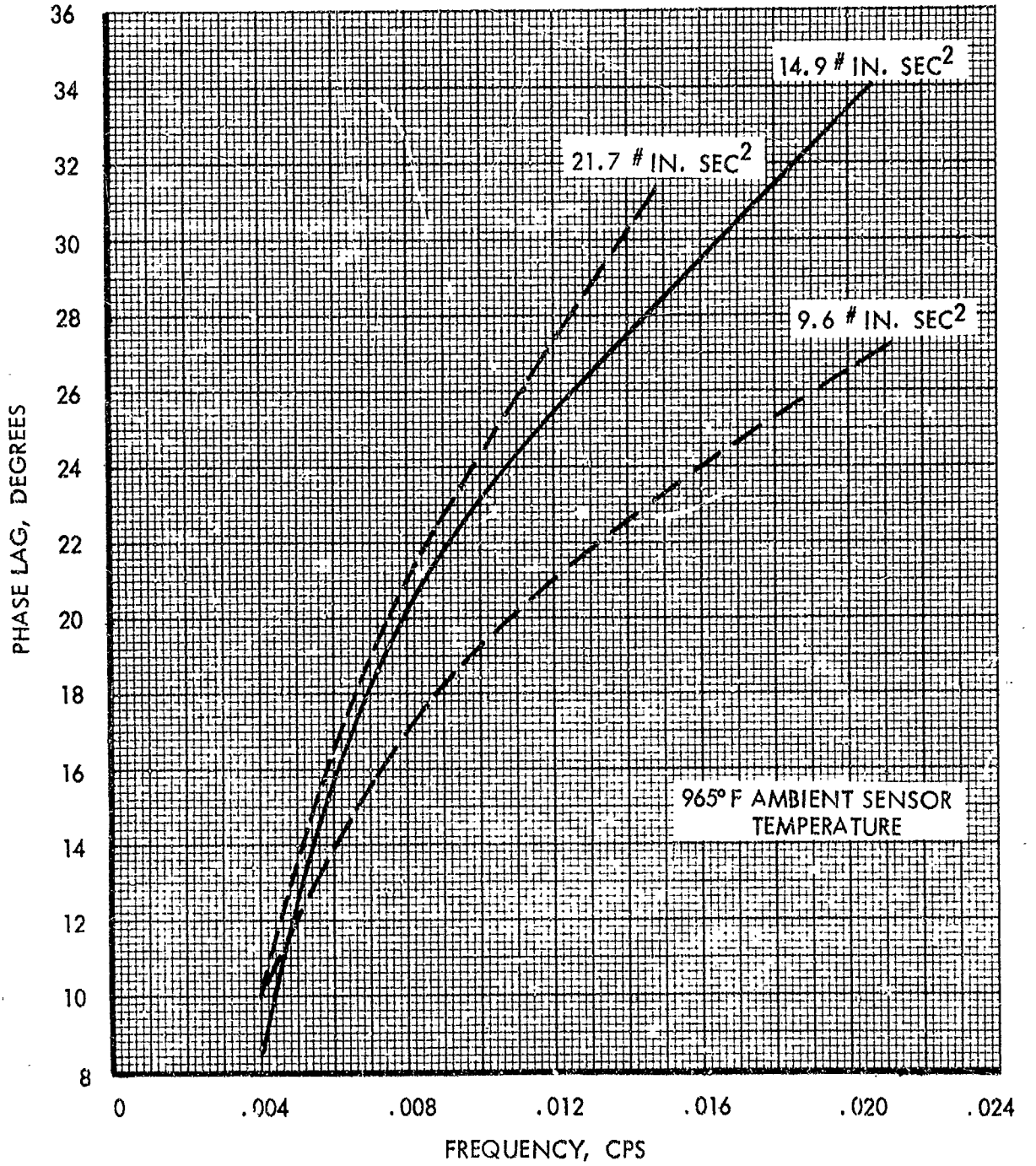

FIGURE 6.2.2-4

Mount responses as a function of frequency was obtained for loads or inertias from 10 to 22 in.-lb sec^2 and for ambient temperatures of 895°F to 1070°F. The results show that the range of excitation is limited to frequencies below .024 cps. The system was stable for all tests; in no case was the phase shift or lag between sensor temperature and mount angular rotation more than about 50°. Typical results are shown in Figure 6.2.2-4. Generally the mount responded as expected in that increasing the inertia increased the lag while increasing the ambient temperature (that is increasing the system stiffness) decreased the lag.

Unbalancing moments were added and removed from the system at each test temperature and inertial load to determine the damping in the system. Figure 6.2.2-5 is an example of these data and shows the rotation of the mount resulting from the unbalance of a function of time. Relating the time constants from these curves to the inertia and stiffness of the mount determines the system damping. A sample of data indicates the energy dissipation capability of the mount is close to that analytically determined. This is quite good correlation considering all the variables involved. For I = 9.6 in. lb. sec^2 and K = 72.8 in. lb. per radian, the system is more than 11 times critically damped as determined by the solution of the equation below which describes the envelope of a transient response in a proportional type servo system.

$$E = e^{(-\delta + \sqrt{\delta^2 - 1})\,\omega_n t}$$

For the 9.6 in. lb. sec^2 concentrator inertia and a bellows spring constant of 72.8 in. lb/rad., as determined for the bellows with a 960°F sensor temperature, critical or natural frequency is:

$$\omega_n = \sqrt{\frac{K}{J}} = 2.75 \text{ rad/sec}$$

Using the 5.5 seconds measured in the recovery trace of figure 6.2.2-5 and setting E = .37 the value of δ which is the ratio of actual damping to critical damping is: δ = f/fc $\approx$ 11. For the system design inertia of 17.5 in. lb. sec^2 which is for a 10 lb. concentrator the critical damping, fc is 71.4 in. lbs/rad. Since f for the 9.6 in. lbs. sec^2 inertia is 11 fc, or 11 x .2 $\sqrt{KJ}$ = 582 in. lb./rad, the value of δ for the design system is:

$$\delta = \frac{582}{71.4} = 8.15 \text{ actual}$$

as compared to the computer determined design value of 10.

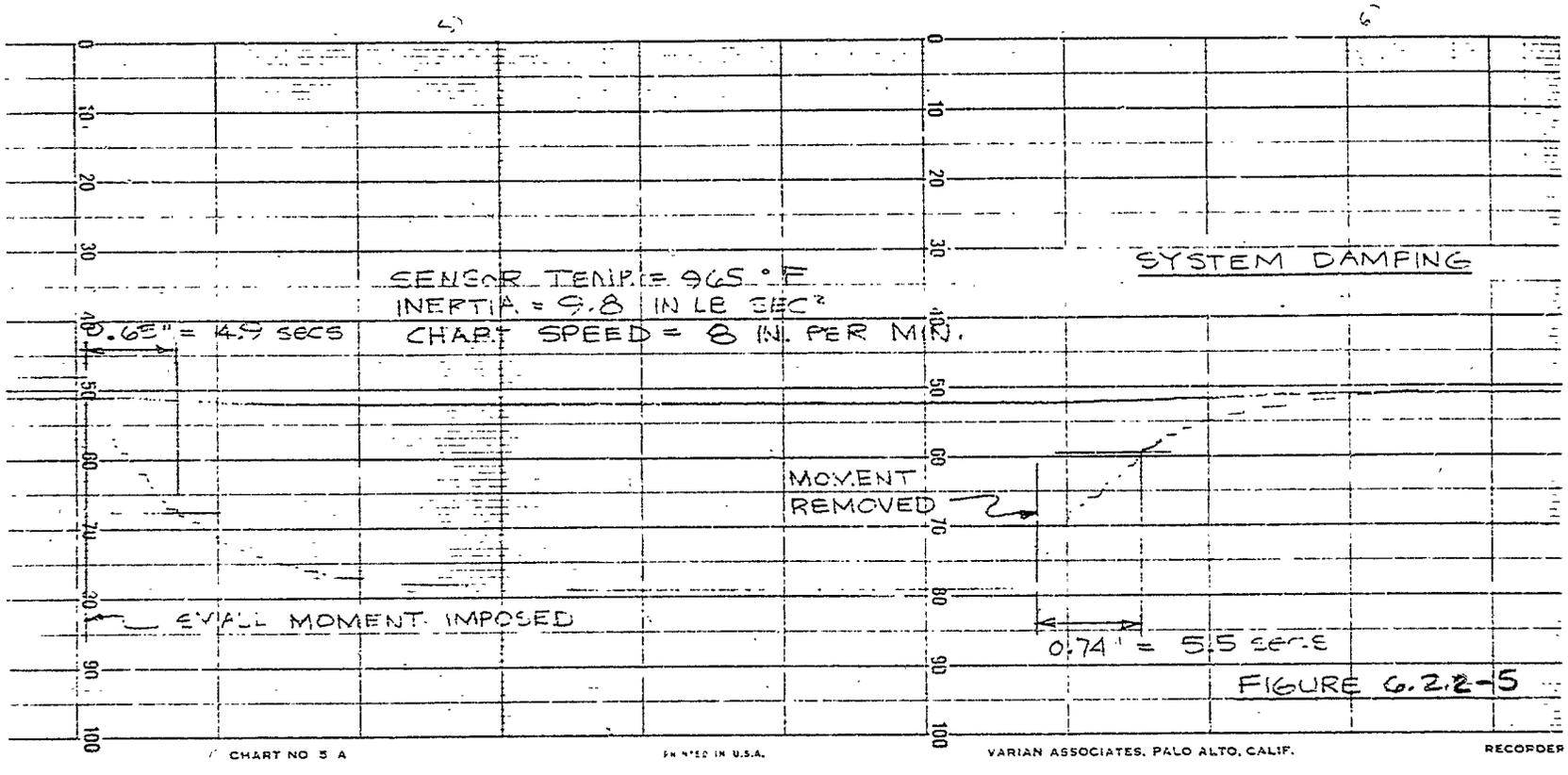
SENSOR TEMP. = 965 °F
INERTIA = 9.8 IN LE SEC²
CHART SPEED = 8 IN. PER MIN.
0.6" = 4.9 secs
SYSTEM DAMPING
MOMENT REMOVED
EVALL MOMENT IMPOSED
0.74" = 5.5 secs
CHART NO 5 A
PRINTED IN U.S.A.
VARIAN ASSOCIATES, PALO ALTO, CALIF.
RECORDER

FIGURE 6.2.2-5

6.2.3 Calorimeter Calibration and Equilibrium

The brazed calorimeter elements with the added micro-quartz insulation were checked individually to insure that the reworking was satisfactory. The elements were placed in a small vacuum chamber and EB heating was supplied. Shaft temperatures were measured and a plot of ΔT vs. power input made. The results showed that the elements were stable and the data continuous and reproducible. The elements were then assembled into the calorimeter body and the final calibration was performed.

The results of the test are shown in Figure 6.2.3-1. These calibration curves present the power input as a function of ΔT for each element.

Equilibrium temperatures were also measured during this test at full power input of 810 watts. The cover plate and body were 970°F and 900°F respectively while the ambient temperature of the bellows was 610°F. Cavity temperature was measured at 1670°C using an optical pyrometer. These temperatures may be compared with design point values of 826 °F for the calorimeter body, 750°F for the bellows, and 1700°C for the calorimeter cavity.

Two sensors were mounted in the assembly during these tests. One sensor was positioned so that its inner edge coincided with the I.D. of the cover plate. The second sensor was positioned .055" further away from the cavity. At full power the operating temperature of the closer sensor was 1186°F while that of the more distant sensor was 1210°F. It was surprising that the second sensor should be hotter since it was further away from the cavity. These excessive temperatures and inconsistencies were attributed to slight leakage currents in the electron bombardment heating circuits. (Later solar test results which showed lower and more uniform sensor temperatures confirmed this conclusion.)

6.3 Solar Test Results

6.3.1 Mount Gain or Static Response

As indicated in Section 6.1.2, the modified sensors were to be mounted on top of the cover plate. Support was provided only by the capillary with about 1/32 inch clearance between the cover plate and the sensor placing the centerline of the sensors in a plane approximately 0.42 inches forward (towards the concentrator) of the focal plane. Radially, the sensors were located so that none of the high intensity solar flux impinged on the sensors with the concentrator in the oriented position. This was established visually and was confirmed by noting that the sensor temperatures were always either equal to, or lower than, the cover plate temperature for zero misorientation. Additionally, within the region indicated, it was established that radial displacements of at least 0.10 inch would neither change the sensor ambient nor the temperature gain for given inputs of misorientation.

MODIFIED CALORIMETER CALIBRATION DATA FOR
FINAL LTM ASSEMBLY

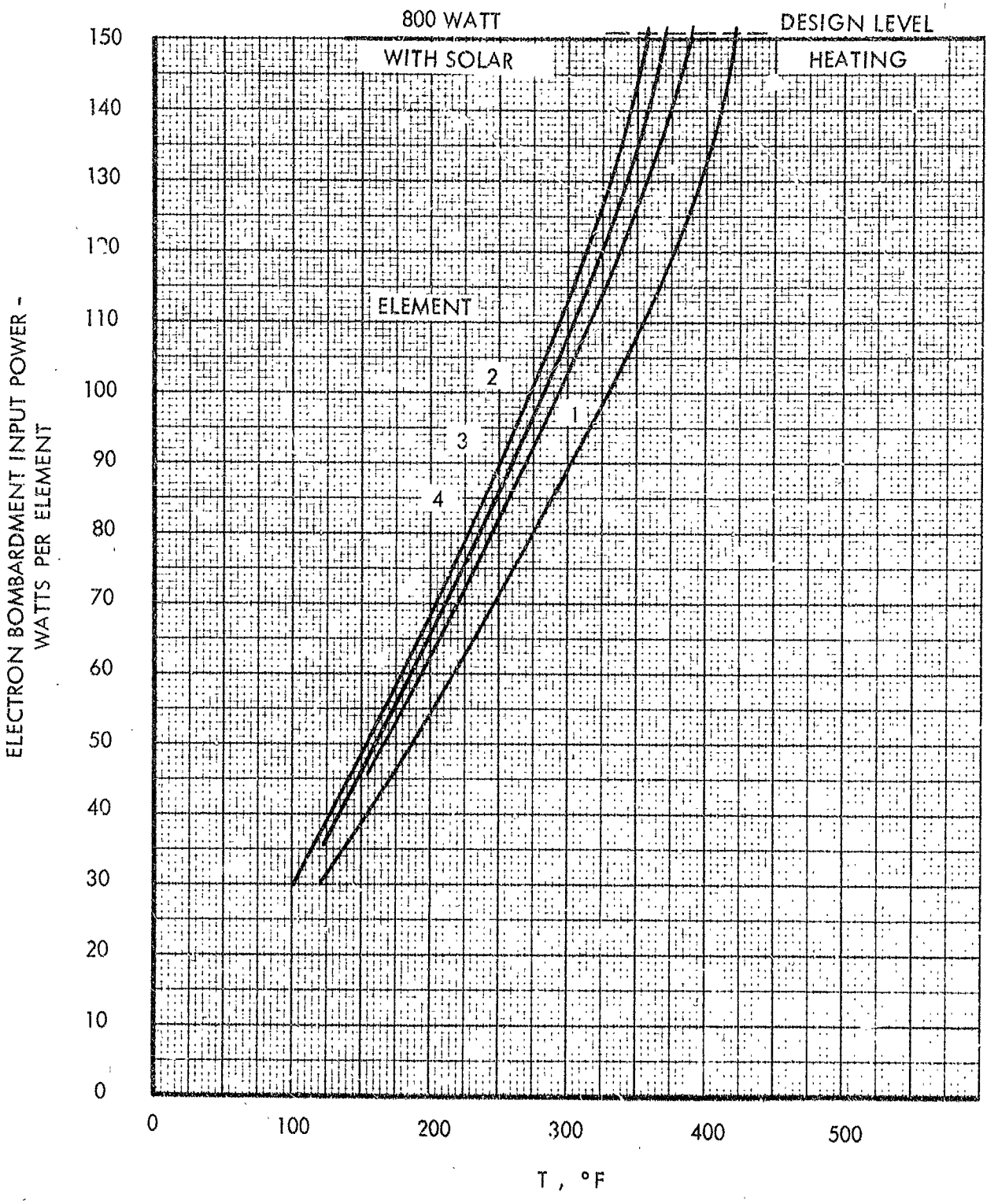

FIGURE 6.2.3-1

The temperature difference between diametrically opposed sensors, based on several misorientations in both directions, was determined to be 35°F per one minute misorientation. This was considered an excellent temperature output since based on the laboratory test results shown in Figure 6.2.2-2, no more than ± 6 minutes of persistent error would be required for the mount to track or follow over ± 5° of misorientation.

Based on the sensor power calibration Figure 6.2.2-3, 1 watt of power input will change the sensor temperature about 33°F. The solar test data indicates, therefore, that there is approximately 1 watt of power interchange between sensors for 1 minute of misorientation.

The mount gain for bellow assemblies No. 10 and 12 is about 2.9° rotation per 100°F ΔT; representing a 25 per cent increase in gain over that established during the laboratory testing for this set of bellows. In terms of misorientation, the output is about 1° rotation per 1 minute misorientation.

Bellow assemblies No. 9 and 11, while indicating the same temperature excursion for a given misorientation, provided substantially less output rotation than bellows No. 10 and 12. The gain was only 0.9° rotation per 100°F ΔT, or about 40 per cent of that established during the laboratory tests. While the exact cause of this reduced output has not been determined, the following events probably relate to this lower output. During the laboratory tests, bellows No. 9 and 11 were never subjected to temperatures above 400°F. At these temperatures, a decrease in gain was detected at the larger mount rotations (see Figure 6.2.1-1). This was attributed to the depletion of mercury from the sensor due to bellows collapse. As with the other set of bellows, this could be corrected by adjusting the bellow stem sockets for higher bellow temperatures expected during the solar tests. The volume gained through relative expansions of the mercury and the stainless steel would then keep some mercury in the sensor through 5° rotation. Conceivably, an overcorrection was affected in that the bellows temperature during solar test activity was near 700°F rather than 600°F as expected from laboratory test results. This would cause the bellows and sensor to completely fill during the first solar cycles. The bellow convolutions would then deform into some new, and possibly stiffer, configuration thereby reducing the gain of the assembly.

Examples of static response during the solar tests are indicated in Figures 6.3.1-1 through Figure 6.3.1-3. Figure 6.3.1-1 shows the temperature excursions for sensors No. 10 and 12 during ± 3 minutes of misorientation and the accompanying rotations. Figure 6.3.1-2 is the same kine of data for bellows No. 9 and 11. Figure 6.3.1-3 indicates the mount response for simultaneous misorientation in both directions; the output for both assemblies is indicated; temperatures were traced continuously only for sensors No. 10 and 12, however. In all these tests, ambient sensor temperatures are near 925°F, the bellows are at 700°F, the cover plate temperature is 950°F, and the solar flux is 75 watts per sq. ft.

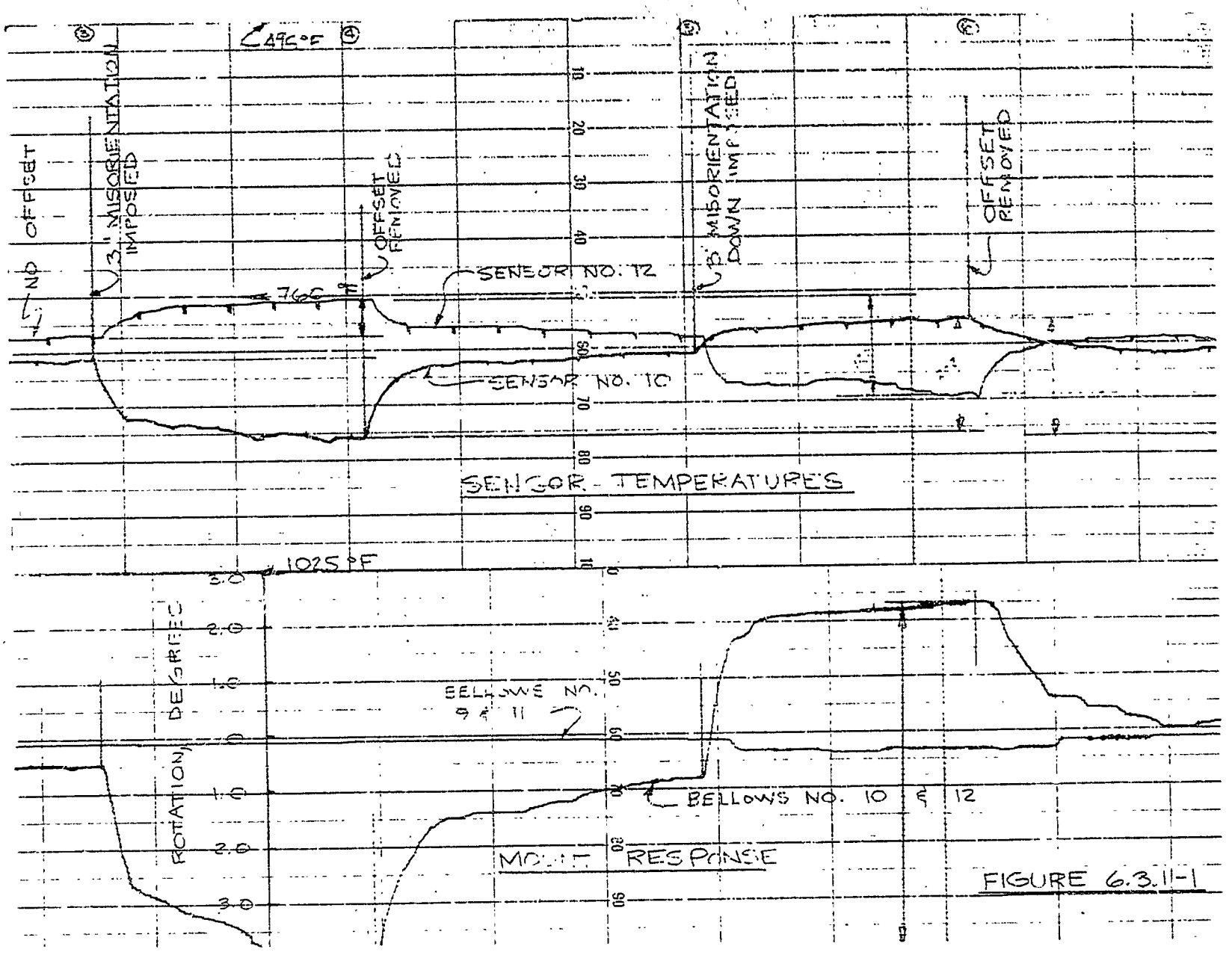

FIGURE 6.3.11-1

OFFSET REMOVED
3" OFFSET LEFT
OFFSET REMOVED
SENSOR NO. 11
SENSOR NO. 9
SENSOR TEMPERATURES
3" SIGNAL RT
OFFSET REMOVED
3" SIGNAL RT
BELLOWS NO. 9 & 11
NOMINAL PIESPHICE
ROTATION
10
20
30
40
50
60
70
80
90
100
2.0

FIGURE 6.3.1-2

SENSOR TEMPERATURES
MOUNT RESPONSE
BELLOWS 9 # 11
BELLOWS 10 # 12
SENSOR 12
SENSOR 10
MISORIENTATION DOWN 21°
OFFSETS REMOVED
OFFSETS REMOVED
MISORIENTATION DOWN 4°
760 °F
495 °F
105 °F
ROTATION DEGREES
2.0
1.0
0
1.0
2.0
3.0

FIGURE 6.3.1-3

6.3.2 Mount Frequency Response

Solar testing was highly successful in that the frequency range was extended several times beyond that possible in the laboratory. Without difficulty, response through 0.16 cps was obtained. Examples of data are included as Figures 6.3.2-1 and 6.3.2-2.

The frequency response results are presented in Figures 6.3.2-3 and 6.3.2-4. The first of these figures is phase shift as a function of frequency. Thermal lag is related to the time delay between the change in orientation signal and the time the sensor thermocouple senses such a signal. Physically it is related to the time involved to transfer heat from one part of the sensor to another in that at any one point in the body, a change in heat input instantaneously changes the temperature. Thermal plus mechanical lag is the lag between signal and temperature response plus the real mechanical lag associated with the inertia, stiffness, and damping of the mount. It was not possible to simulate, during the solar tests, the large concentrator inertia. Nevertheless, based on the low phase shifts reco. d during the laboratory tests plus those reported here, it is expected that a fully loaded mount will remain stable and perform satisfactory for frequencies through 0.10 cps.

Figure 6.3.2-4 presents attenuation of output as a function of frequency. Statically and at low frequencies, the solar test gain is lower than that indicated by the computer program and it attenuates more rapidly. The differences can be explained by the actual bellows characteristics compared to those used for the computer simulation.

6.3.3 Calorimetric Measurements

Calorimetric measurements were made to determine the loss of cavity power as a function of concentrator misorientation. All measurements were taken for offsets in line with diode simulators 2 and 4 to simplify data taki .g, and control of the tracker orientation. The resulting curves are normalized so as to make them independent of concentrator size and relative solar intensity. Figure 6.3.3-1 shows the percent of energy absorbed for individual elements as a function of misorientation. These curves were combined or summed to form the curve in Figure 6.3.3-2 which shows the total percent energy absorbed for the entire calorimeter. It is shown that total cavity power loss can be held to approximately 1.5 to 2 per cent despite a $\pm$ 5 degree alignment error in a space vehicle solar power system by using a mount possessing the characteristics demonstrated in these tests.

6.4 C neral Performance and Material Compatibility

One failure was experenced during solar test activity. As a result of cloud cover that caused the solar tracker to hunt or track momentarily over $\pm$ 2 or 3 degrees, solar inputs of 10 to 15 times design values were imparted to sensor No. 9. This resulted in a burn-out of the sensor. Inspection of the bellows assembly indicated deformation but not complete failure. The burst pressure of the bellows is 1500 psi which is equivalent to a mercury temperature of less than 1500°F. This attests to the ability

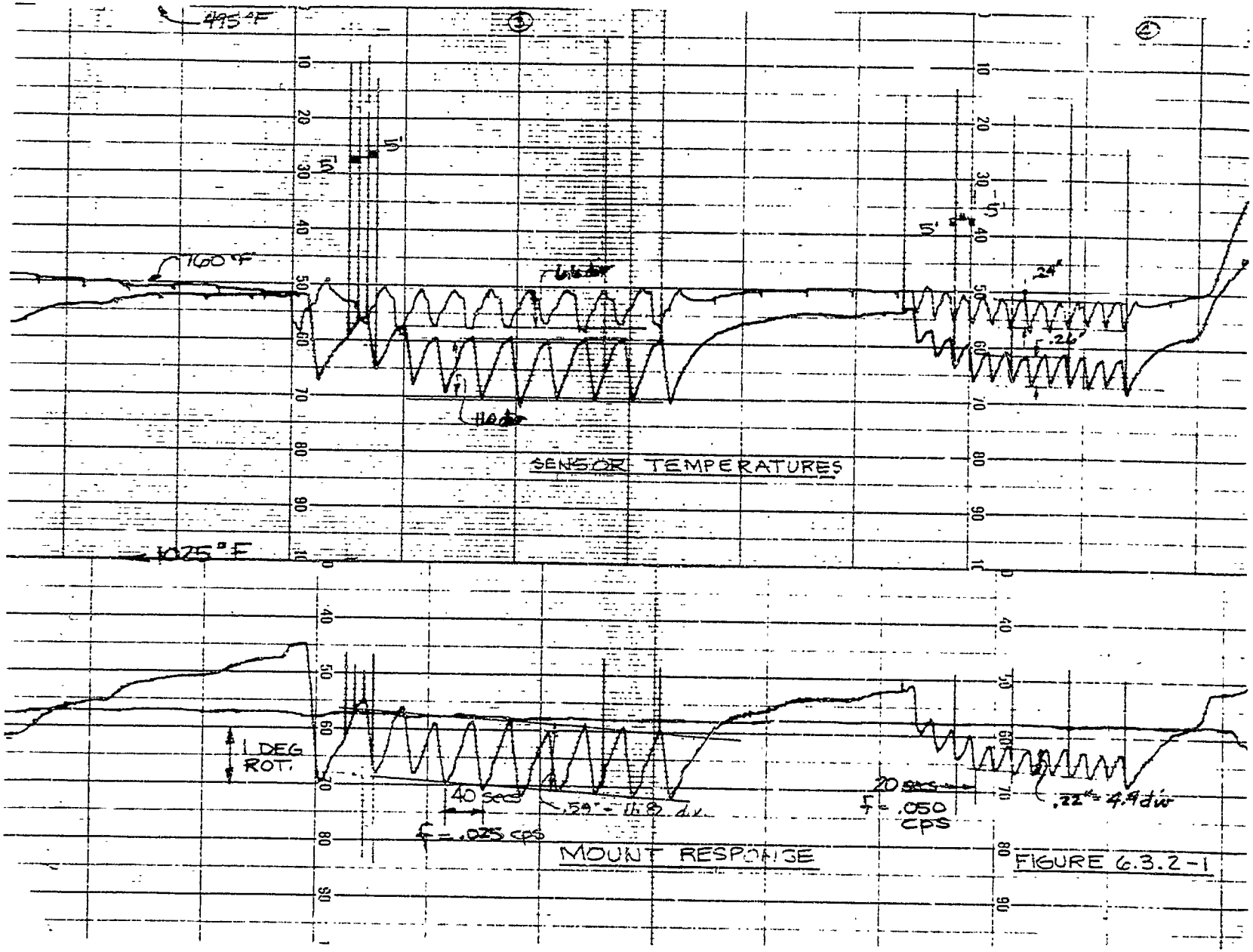
495°F
160°F
SENSOR TEMPERATURES
1025°F
1 DEG ROT.
40 secs
.59" = 11.8 div.
f = .025 cps
20 secs
f = .050 cps
.22" = 4.4 div
MOUNT RESPONSE

FIGURE 6.3.2-1

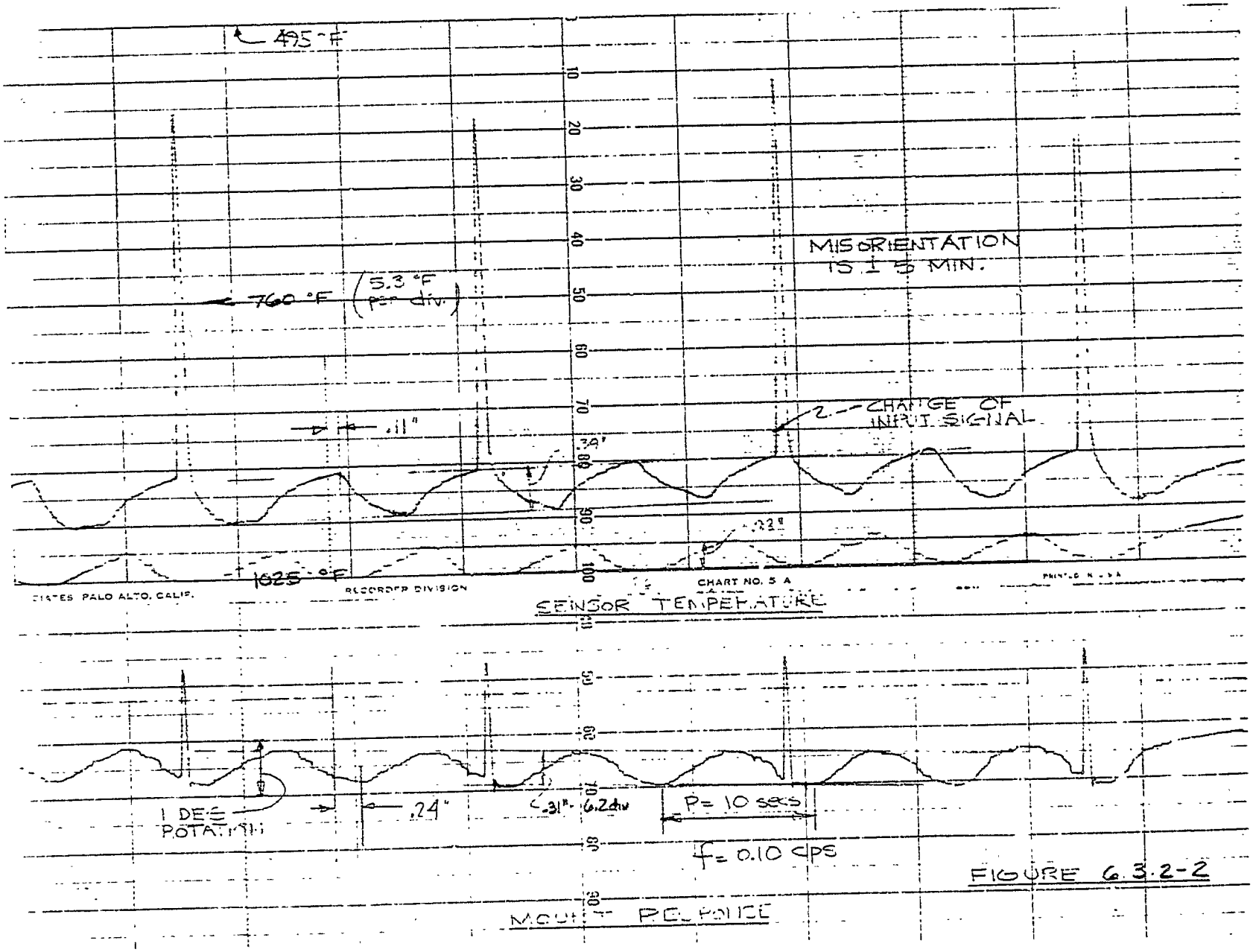
495 °F
760 °F
5.3 °F per div.
1025 °F
.11"
.24"
MISORIENTATION IS 1 5 MIN.
2 -- CHANGE OF INPUT SIGNAL
CHART NO. 5 A
RECORDER DIVISION
SENSOR TEMPERATURE
1 DEG ROTATION
.24"
.31" - 6.2 div
P = 10 secs
f = 0.10 cps
MOUTH PRESSURE

FIGURE 6.3.2-2

PHASE SHIFT AS A FUNCTION OF FREQUENCY

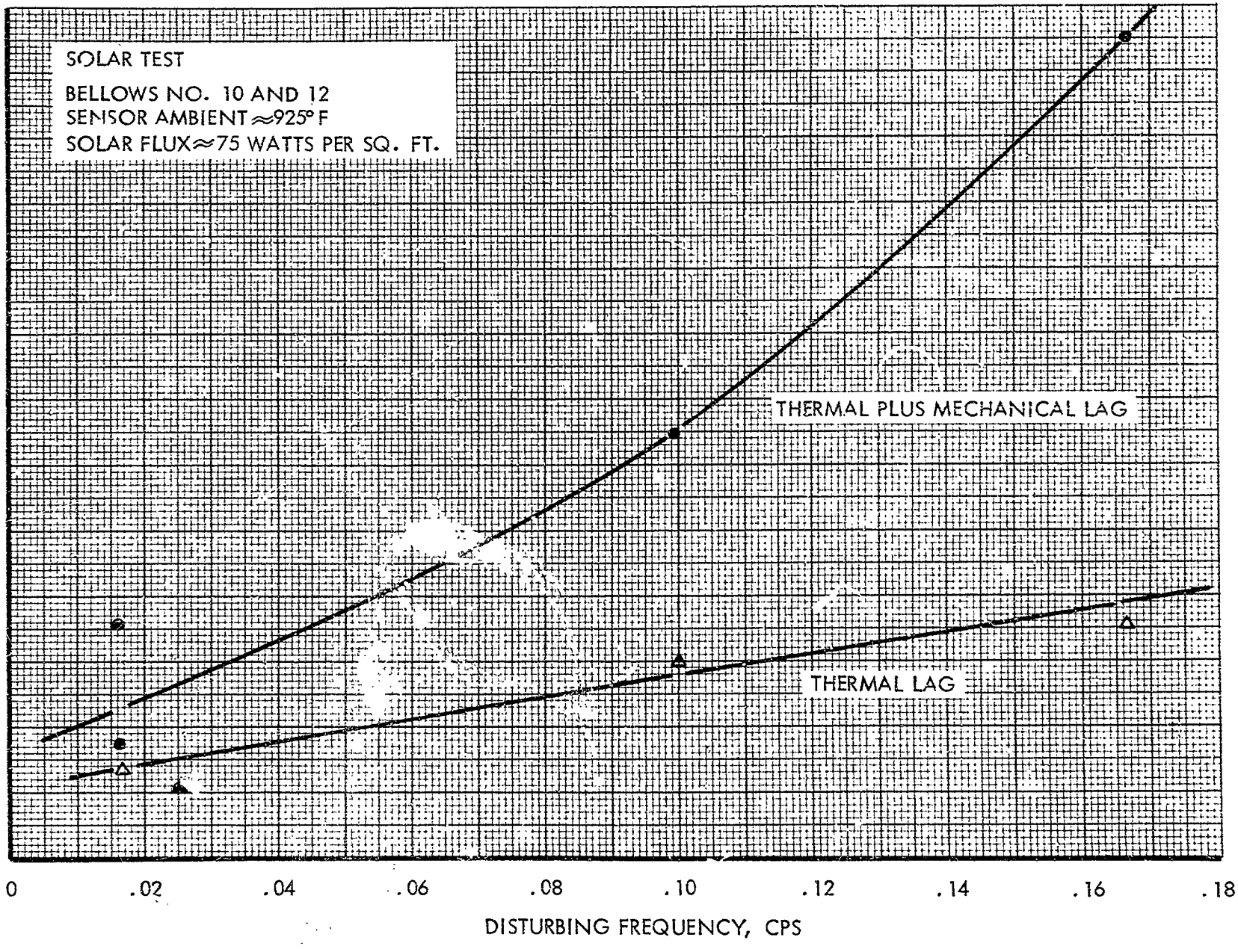

FIGURE 9.3.2-3

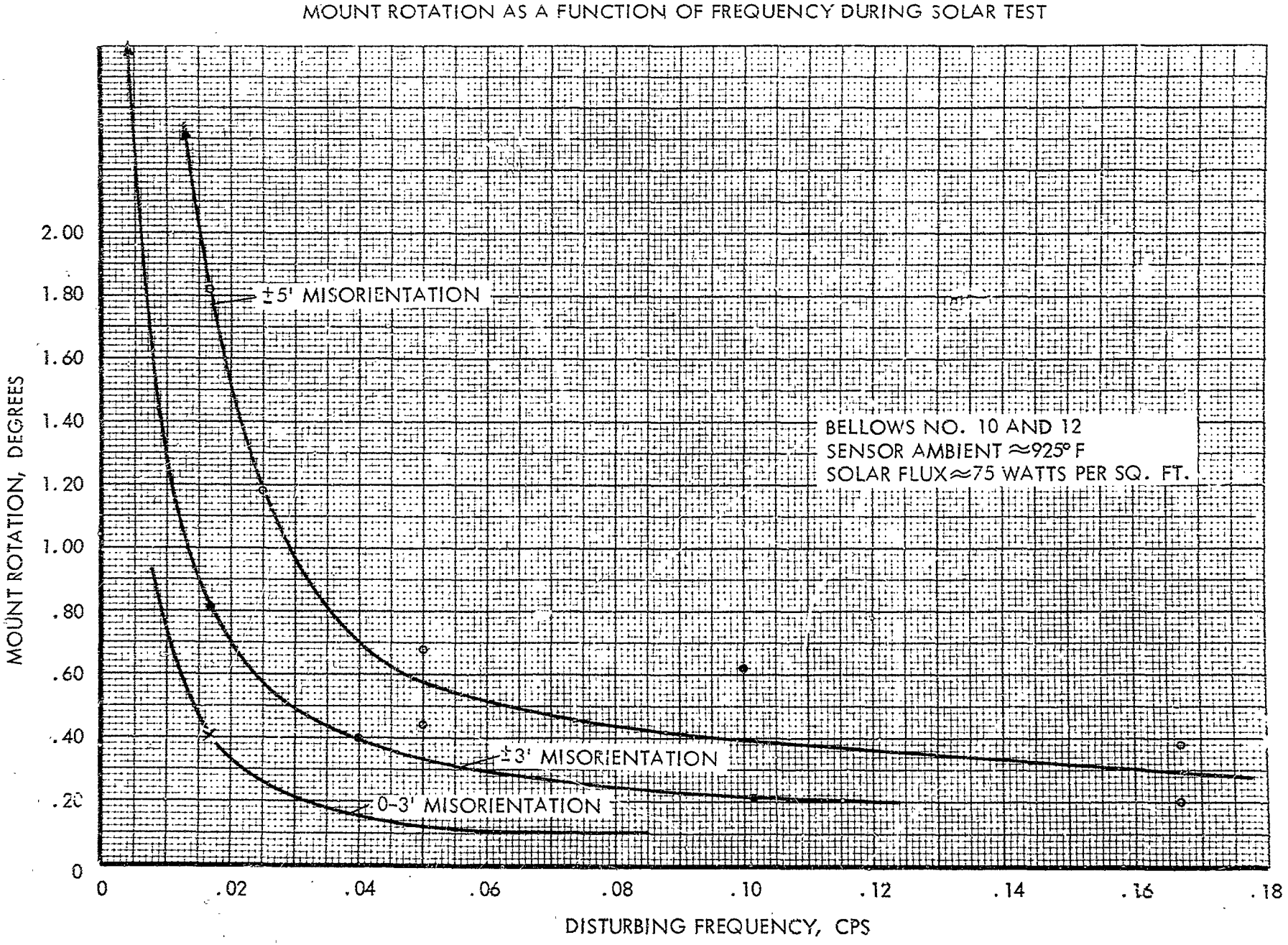
MOUNT ROTATION AS A FUNCTION OF FREQUENCY DURING SOLAR TEST
MOUNT ROTATION, DEGREES
2.00
1.80
1.60
1.40
1.20
1.00
.80
.60
.40
.20
0
±5' MISORIENTATION
±3' MISORIENTATION
0-3' MISORIENTATION
BELLOWS NO. 10 AND 12
SENSOR AMBIENT ≈925° F
SOLAR FLUX≈75 WATTS PER SQ. FT.
0
.02
.04
.06
.08
.10
.12
.14
.16
.18
DISTURBING FREQUENCY, CPS

FIGURE 6.3.2-4

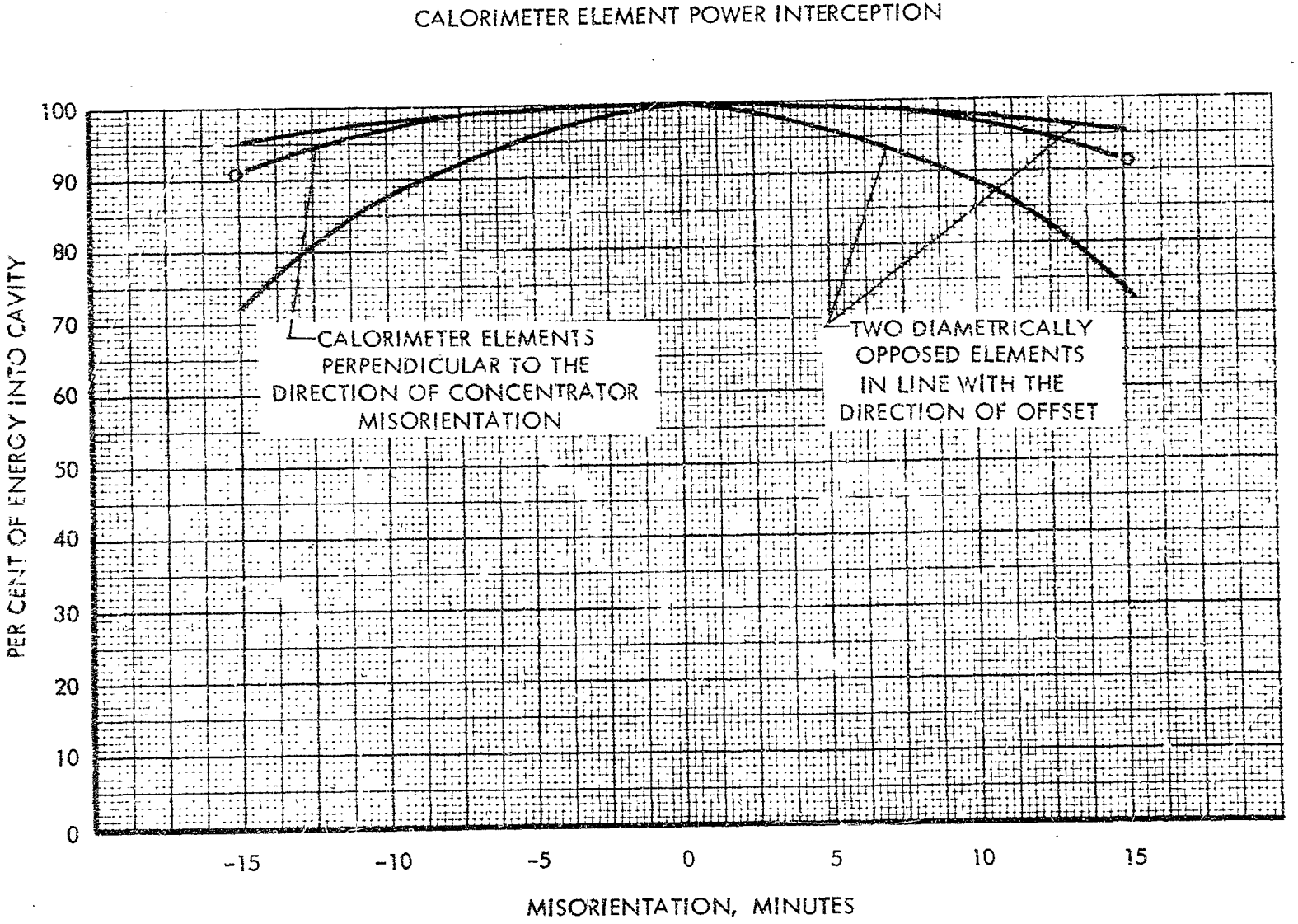
CALORIMETER ELEMENT POWER INTERCEPTION
PER CENT OF ENERGY INTO CAVITY
100
90
80
70
60
50
40
30
20
10
0
-15
-10
-5
0
5
10
15
MISORIENTATION, MINUTES
CALORIMETER ELEMENTS PERPENDICULAR TO THE DIRECTION OF CONCENTRATOR MISORIENTATION
TWO DIAMETRICALLY OPPOSED ELEMENTS IN LINE WITH THE DIRECTION OF OFFSET

FIGURE 6.3.3-1

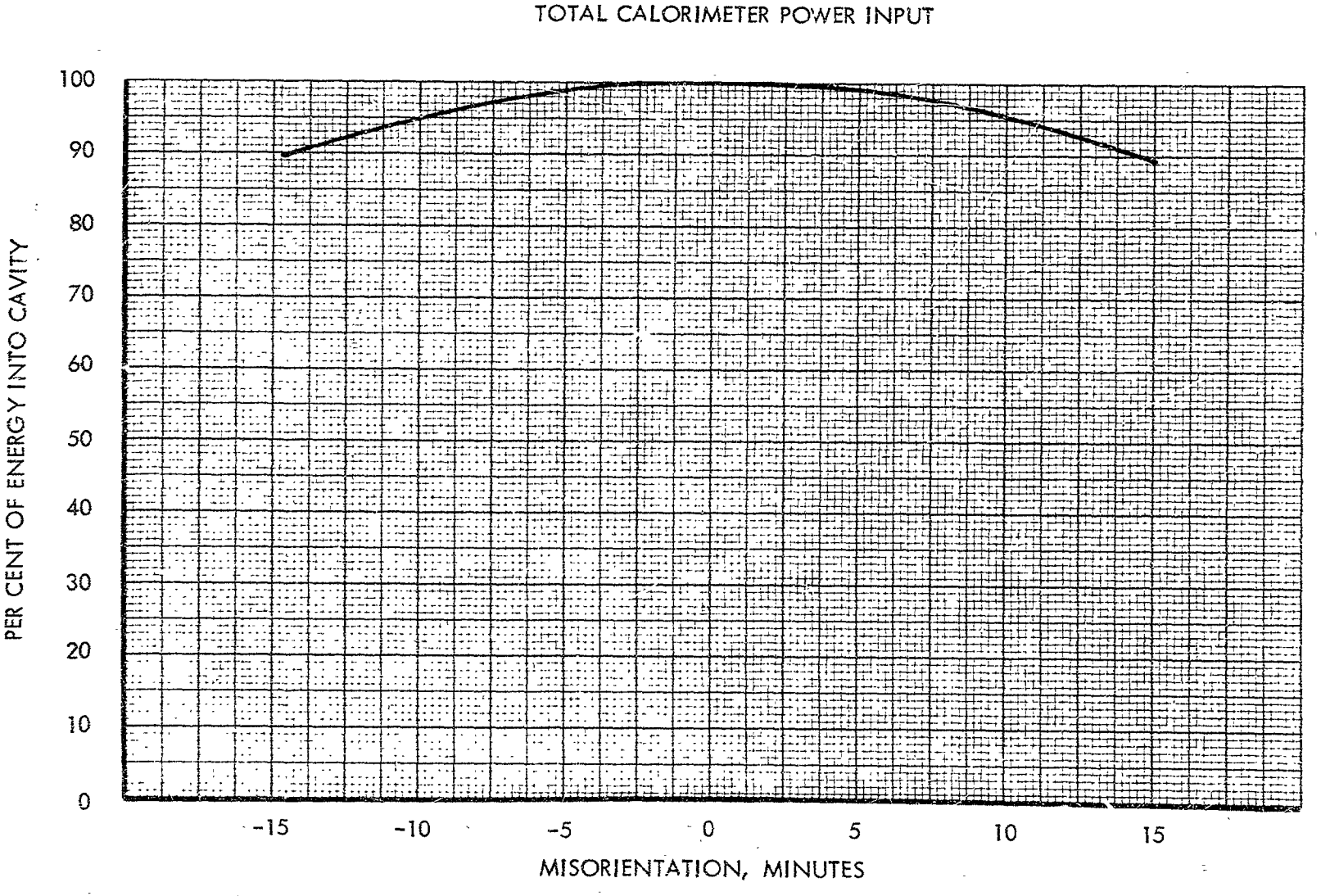
TOTAL CALORIMETER POWER INPUT
PER CENT OF ENERGY INTO CAVITY
100
90
80
70
60
50
40
30
20
10
0
-15
-10
-5
0
5
10
15
MISORIENTATION, MINUTES

FIGURE 6.3.3-2

of the mercury to drain out of the sensor and remain at a lower temperature should a malfunction or human error result in excessively high solar input.

The mount has been restored to its original condition by replacing the damaged sensor. In any further development however, a sensor material able to withstand higher temperatures should be considered.

By pressurizing the inside of the bellows (the area normally open to vacuum) it was returned, as best could be determined, to its original configuration. Yielding was initiated at a pressure of 150 psi. This corresponds to a mercury temperature of 970°F and substantiates our observations about deficiencies of this particular bellows. The burst pressure of the bellows may be 1500 psi, but it begins to exhibit nonlinear characteristics at 150 psi.

As indicated earlier, the deficiencies that are known to exist in the bellows should not detract from the favorable features of the mount concept since bellows can be designed to attain the desired characteristics.

Except for the bellows, the rigidity or stiffness of the mount is completely satisfactory. Each pair of bearings supported 15 lbs of load repeatedly during laboratory tests without bad effects. The operating bearing temperatures were higher than recommended by the manufacturer but no difficulties were encountered because of this. It seems certain that other materials could be used in the bearings to eliminate the marginal status of this component.

Some static change in null or balance position of the mount was detected during the tests. This has been attributed to transducer frictional resistance. With the pots out of the system, the mount would oscillate about a unique balance position.

All materials used were found compatible with the operating environment. No indication of failure or short lived operation was noted for any component. The ball and socket joints used in the bellows assemblies are not considered suitable but were adopted only as an expedient and could easily be replaced with a flexure bearing in future mounts. Similarly, the sensors and capillary and aperture plate materials were made of stainless steel to expedite fabrication of the mount. Other materials such as tantalum or molybdenum would be much more suitable and would preclude burnouts in an improved mount design.

7.0 CONCLUSIONS

In spite of the numerous difficulties encountered in the testing of the present mount configuration, all the objectives of the program have been met. Most of the problems center around the deficiencies of the bellows. The bellows selection, which was forced by virtue of availability, delivery schedule, cost resulted in a system with nonlinearities, and gross losses in performance due to reductions in effective area and increased in spring rate at the design operating pressures. Other lesser complications such as the introduction of additional and unpredictable volume changes in the system due to partial collapse of the bellows convolutions were also aggravating though not insurmountable. It has been definitely established in the program that mount mechanisms of the type reported can be built, integrated with compact high temperature thermionic generator hardware, and made to operate in the total environment of such a system in space.

The mount has demonstrated steady state gains which are more than twice as great as specified for the program. The bellows concept chosen for development is flexible in design and has shown its adaptability in handling the inertial loads associated with a wide range of concentrator sizes or weights. Of more importance, the mount has shown that it is possible to make use of the stray flux at the edge of the focal plane to permit accurate sensing of concentrator alignment and to provide the power necessary to operate the actuator mechanisms in restoring or reducing alignment errors. The small sensor mass used in the present design produces very commendable response characteristics and at the same time provides inherent safety features which limit mount operation and possible destruction under conditions of excessive or initial misorientation.

There remains several areas in which improvements must be made before the present concept can be fully qualified for space use. The improvement of the bellows design, substitution of refractory materials for use in the sensor assemblies, the elimination of ball and socket joints, would all be areas in which improvement can certainly be expected. Also before a true prototype mount can be developed a definite mission and concentrator-generator module must be specified. Each mount, in spite of inherent flexibilities, should be designed and qualified for a specific application. There is no reason to believe the present configuration represents the ultimate in attainable characteristics. This fact is illustrated by a comparison between the mount performance data and the characteristics which were predicted in the computer study using idealized component data. This comparison is best made on the basis of the response characteristics relating gain and phase shift to a mount disturbance or excitation frequency. Such a comparison is shown in Figure 7.0-1 where the solar and laboratory test data for a concentrator inertia similar to that used in the computer study is plotted along with the original computer result curves. The test results are quickly seen to be inferior to the ideal or maximum obtainable characteristics but are nonetheless achieving twice the design of objectives of this program and responsive enough to qualify this present mount for many anticipated system applications.

BELLOWS ACTUATOR MOUNT GAIN AND FREQUENCY
RESPONSE CHARACTERISTICS

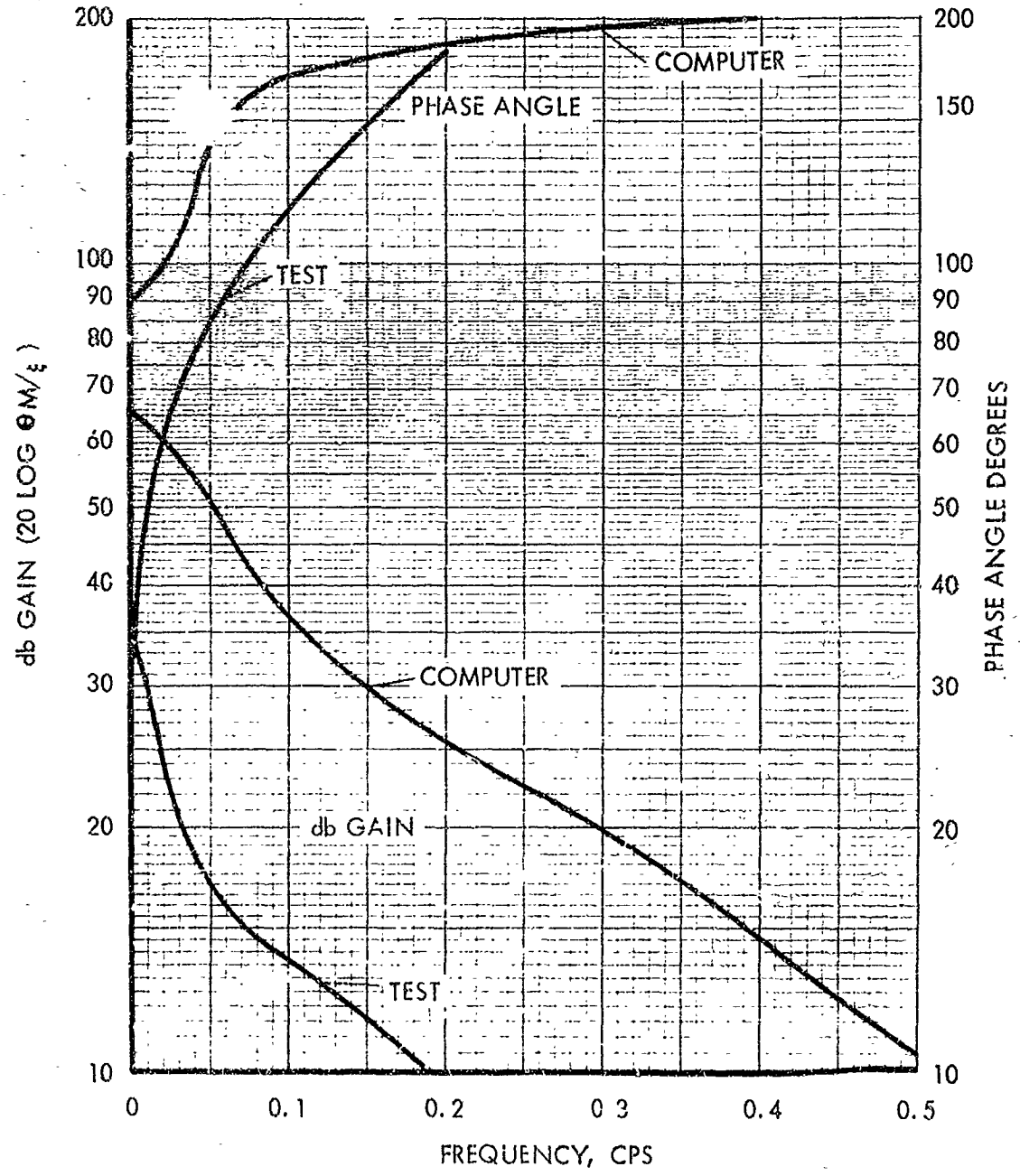

FIGURE 7.0-1

APPENDIX I

CALORIMETER DESIGN CALCULATIONS

The Calorimeter design incorporates the features of the most recent thermionic generator concepts. The environment in the region of the operational calorimeter is made identical with that of the generator. The calorimeter structures also offer similar areas for mounting attachments and the placement of proposed heliotropic devices. The calorimeter will be subject to modification to permit integration of the mount as would a generator of prototype design to accommodate system integration. No compromise of the generator or calorimeter function will be permitted however.

The calorimeter will consist of four elements simulating four diodes of a generator. The following calculations will size these elements appropriately.

Assumptions and Design Values

1. Solar Const. SC = 75 W/ft^2 (for Cleve.)
2. Conc. Area = A_{Con} = 18 ft^2 (with shadowing)
3. Bell Trans. = η_J = 82 per cent
4. Moly Surface Absorptivity ϵ_S = 0.5 (with machining)
5. Aperture Dia. = 5/8 inch
6. Element Face Dia. = DE = 0.8 inch
7. Cavity Radius = R_C = 0.5 inch
8. Concentrator Reflectivity η_R = 0.8

Cavity

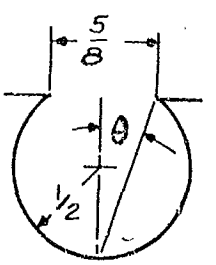

Figure 1.

Cavity Absorptivity Calculations:

$$\alpha = \frac{\epsilon_S \; 1 + (1 - \epsilon_S) \; (A/A_C - \mathrm{Sin}^2 \theta)}{\epsilon_S \; (1 - A/A_C) + (A/A_C)}$$

$$\frac{.5\,1 + .5\,(.109 - 111)}{.5\,(.891) + .109}$$

α = .90

where A_C = cavity area in.^{2}

This value is dependent upon a surface absorptivity of .5 = ϵ_S which is much higher than for a plain moly surface. Experimental results with grooved T_A and M_O have shown .5 to be reasonable.

Total cavity power is

$$P_C = A_{Con} \times SC \times \eta_R \times \eta_T \times \alpha$$

$$= 18 \times 75 \times .8 \times .82 \times .9 = 797 \text{ Watts}$$

where

A_{Con} = effective concentrator area

SC = Solar constant

η_R = Concentrator reflectivity

η_T = Bell Jar transmission

α = Cavity Absorptivity

For a 4 element calorimeter the power per element (per diode in the case of a generator) is calculated:

$$P_E = \frac{P_{Cal}}{4} = \frac{P_C - P_S - P_R}{4}$$

where

P_S = Slit loss which is proportional to $A_S/A_C \times P_C \qquad (\alpha_S = 1)$

$P_R = \sigma A \epsilon_C (T_C^4)$

where $\epsilon_C = \alpha$

$$= 5.68 \times 10^{-12} \times \frac{.625^2 \times .785}{\frac{1}{6.45}} \times .9 \times (2000^4)$$

= 161.5 Watts

$$P_E = \frac{797\ (1 - .020 \times 2 \times \pi \times 1 \times 282/360/2.794) - 161.5}{4}$$

$$= 151 \text{ Watts per element.}$$

To simulate diode radiator characteristics in the calorimeter elements a rejection temperature of 470°C will be used.

A radiator emissivity of .85 = ϵ_R will be assumed.

A first approximation of the side losses in each element is necessary to compute the size of the radiator which will be required.

Element Crossection

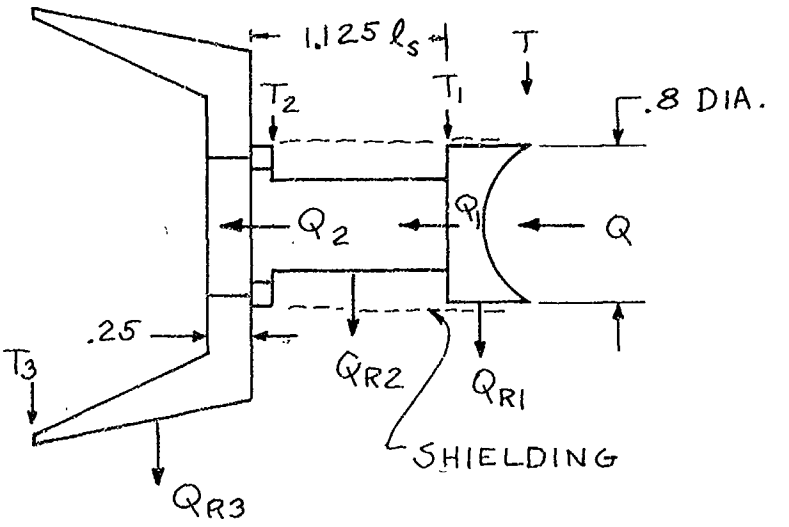

Figure 2.

$$Q = Q_1 + Q_{R1}$$

$$Q_1 = Q_2 + Q_{R2}$$

$$Q_2 = Q_{R3}$$

$$Q = Q_{R1} + Q_{R2} + Q_{R3}$$

Using a copper radiator of the type shown will result in a nearly uniform rejection temperature T_3 based on experience with similar designs. Assuming the disc area must conduct nearly all of the input heat Q to the radiator the value of T_2 may be had

For

$$Q_{R3} \approx Q_2 \approx Q_1 \approx Q$$

$$Q_{R3} = 151\ W = \frac{2\pi K \ell (T_2 - T_3)}{\ell n\, r_o/r_1}$$

where

$$T_3 = 470°C$$

$$151\ \text{Watts} = 516\ \text{BTU/hr.}$$

$$K = 218\ \text{BTU-hr.-ft}^2 - °F\text{-ft}$$

$$r_o = 2''/2$$

$$r_1 = .75''/2$$

$$\ell = .25/12\ \text{ft}$$

$$\Delta T = \frac{516 \times 12 \times .98}{6.28 \times 218 \times .25} = 17.75°F$$

$$\therefore = 895\ °F = 480°C$$

Assuming a uniform temperature gradient along the shaft and head piece we can calculate T_1 if radiation is neglected.

$$\frac{K_H A_1 (T - T_1)}{\ell_H} \approx \frac{K_S A_2 (T_1 - T_2)}{\ell_S} \approx 151\ W = 516\ \text{BTU/hr}$$

$$\Delta T_1 \approx \frac{516 \times .25 \times 12 \times}{12 \times .82 \times .785 \times} = 51.3\ °F$$

where

$$\ell_H \approx .25/12 \text{ ft}$$

$$K_H = 60 \text{ BTU/hr/ft}^2/°F/\text{ft}$$

$$d_1 = .8/12 \text{ ft}$$

and $$T_1 = 2000°K - 28.5°K = 1971.5°K = 1698.5°K$$

with

$$\ell_S = 1.125 \text{ inch}$$

$$K_S = 56 \text{ BTU/hr/ft}^2/°F/\text{ft}$$

$$A_2 = \frac{516 \times 1.125}{(3080 - 895) \times 56 \times 12} = .398 \times 10^{-3} \text{ ft}^2$$

$$d_2 = .270 \text{ inches}$$

The above calculations are made with the assumption Q_{R1} and Q_{R2} may be kept small. A check of this assumption is as follows:

$$Q_{R1} = \sigma \epsilon_1 A_{R1} (T_1^4 - T_{S1}) = \text{Power Radiated to first shield}$$

A_{R1} is stated to be $\approx 1/2 \pi d_H \ell_H$ because ofthe view of adjacent hot elements.

Considering multiple shields:

$$\frac{Q_{R1}}{\sigma A_{R1}} = \lambda (T_1^4 - T_{S1}) = \lambda (T_{S1}^4 - T_{S2}^4) --- = \epsilon_S (T_{SN}^4)$$

We can solve for Q_{R1} if T_{SN} is known or the equalities can be simplified.

with $$\lambda = \frac{1}{\frac{1}{\epsilon_1} + \frac{1}{\epsilon_S} - 1}$$

where ϵ_1 = head emissivity (for moly), and ϵ_S = ϵ_1 shield emissivity

letting $a = \epsilon_S/\lambda$

then $(T_1^4 - T_{S1}^4) = a\, T_{SN}^4$

$(T_{S1} - T_{S2}) = a\, T_{SN}^4$

$(T_{S2} - T_{S3}) = a\, T_{SN}^4$

$(T_{S(N-1)} - T_{SN}) = a\, T_{SN}^4$

Summing we get

$$T_1^4 - T_{SN}^4 = N\, aT_{SN}^4$$

and $$T_1^4 = (Na + 1)\, T_{SN}^4$$

If N is chosen to give 6 shields:

$$\frac{Q_{R1}}{\sigma A_{R1}} = \epsilon_S\, (T_{SN}^4) = \epsilon_1 \left(\frac{T_1^4}{Na+1}\right)$$

For $\epsilon_1 = .15$ for moly foil

$$Q_{R1} = 5.68 \times \frac{\pi}{2} \times 6.45 \times .25 \times .8 \times .15 \left(\frac{1.971^4}{6 \times 1.85 + 1}\right) = 2.09 \text{ Watts}$$

Similarly for the shaft:

$$Q_{R2} = \epsilon\, 1\ A_{R2}\ (\bar{T}_2^4)$$

where $\bar{T}_2$ may be taken as the average $\frac{T_1 + T_2}{2}$

Again assuming 6 shields:

$$\frac{Q_{R2}}{A_{R2}} = \epsilon_1 \left(\frac{\bar{T}_2^4}{Na+1}\right)$$

$$Q_{R2} = 5.68 \times .384 \times 1.125 \times \pi \times 6.45 \times .15 \left(\frac{1.362}{12.5}\right)^4$$

$$Q_{R2} = 1.96 \text{ Watts}$$

The calculated values of Q_{R1} and Q_{R2} give a total radiation loss of only 4.05 watts out of 151. Such small percentile losses are negligible in this approximation.

The radiator area may be calculated using the reduced value of Q_{R3}

$$Q_{R3} = Q - Q_{R1} - Q_{R2} = 146.95 \text{ Watts}$$

$$Q_{R3} = \sigma \epsilon_R A_{R3} (T_3^4)$$

$$A_{R3} = 146.95/5.68 \times .85 \times (.743)^4 = 99 \text{ cm}^2$$

Using the conical radiator design with a length of 1", an average outer diameter of 2 3/8", and an average inner diameter of 2 1/8" the following effective area is calculated.

$$(2.375 \pi \times 1 + 2.125 \times \pi \times 1 + 1\ 1/2^2 \frac{\pi}{4}) 6.45 = 93.9 \text{ cm}^2$$

The last term in the brackets is the rear disc surface. The forward surface is neglected due to the shielding effect of the calorimeter body. The 93.9 cm^2 will radiate 135 watts at 470°C. The remaining 12 watts may be reasonably attributed to conduction losses which will be associated with the mounting arrangements. Appropriate adjustments in area or emissivity will be made after preliminary calorimeter tests if necessary.

Thermocouples will be located in the shaft section 1/2 inch apart. The temperature gradient over this length will be measured with these thermocouples to determine Q, the equivalent element power input. Electron bombardment will be used to calibrate or accurately establish the various values of ΔT according to the power input level thereby providing a calorimeter function with the four elements.

APPENDIX II

[illegible]IC MOUNT COMPUTER STUDY NOTES

The following pages contain [illegible]liminary calculations of mount component characteristics used to [illegible] program the bellows-vapor pressure mount on the analogue computer.

SENSOR INPUT POWER DETERMINATION UNDER SOLAR OPERATION

The following curves are used to determine the probable sensor power input as a function of position relative to the cavity aperture.

The original flux data was obtained by radiometer measurements with the tracker and bell jar system during TRW's thermionic program tests.

The flux profile data shown in Figure 1 is summed graphically in Figures 2 and 3 to determine the total power intercepted by a sensor entering the focal spot. The sensor is assumed to be a .60 wide rectangular plate located in the focal plane. The total sensor power interception is summarized in Figure 4.

CHARGING FLUID SURVEY

A brief review of potential charging fluids has narrowed the candidates to those shown in Figure 5. Other fluids including liquid metals have been rejected because of high chemical reactivity, low temperature decomposition characteristics, or difficulties in handling or charging procedures. Of the group remaining, mercury or water appear most suitable. Mercury will be selected because its vapor pressure is reasonable for operation at the 900 to 1100°F sensor temperatures expected, it is available in a pure state, and is easily handled. The vapor pressure characteristics of mercury are given in Figure 6.

GENERATOR AND SENSOR HEAT BALANCE CALCULATION

From earlier calculations the loss through the side shields is 4.05 watt per element. The slit loss is 797 x (1 - .965) = 27.8 watts. In addition the sun will contribute some power in space, but not in the environmental chamber which encloses the rear face. The remaining heat input comes from the element radiators. The following equations apply.

AVERAGE FLUX INTENSITY (WITH BELL JAR ENCLOSED)
VERSUS DISPLACEMENT - INCHES
FROM CONCENTRATOR AXIS

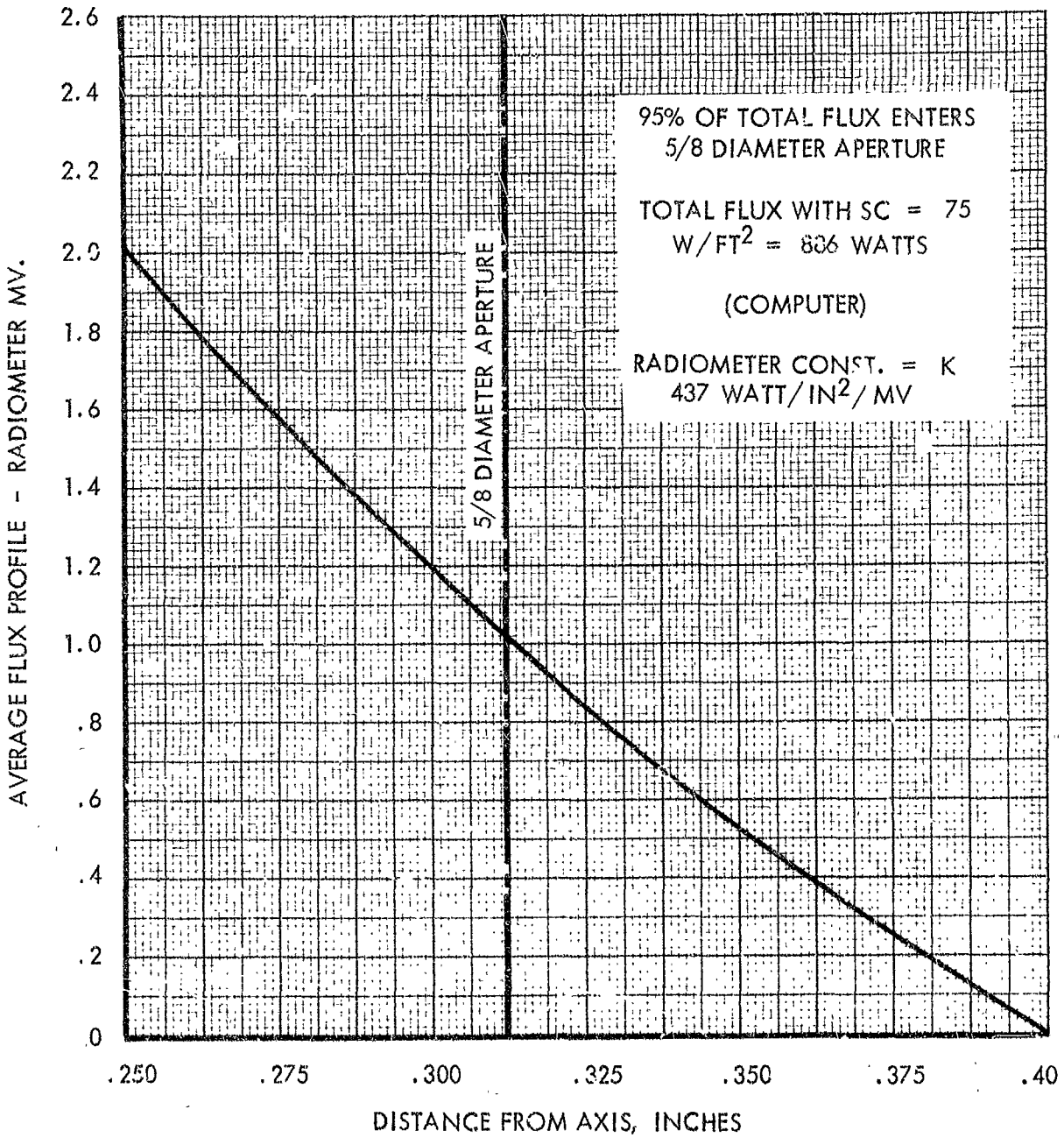

FIGURE 1

SENSOR INTERCEPTION AREA VERSUS POSITION

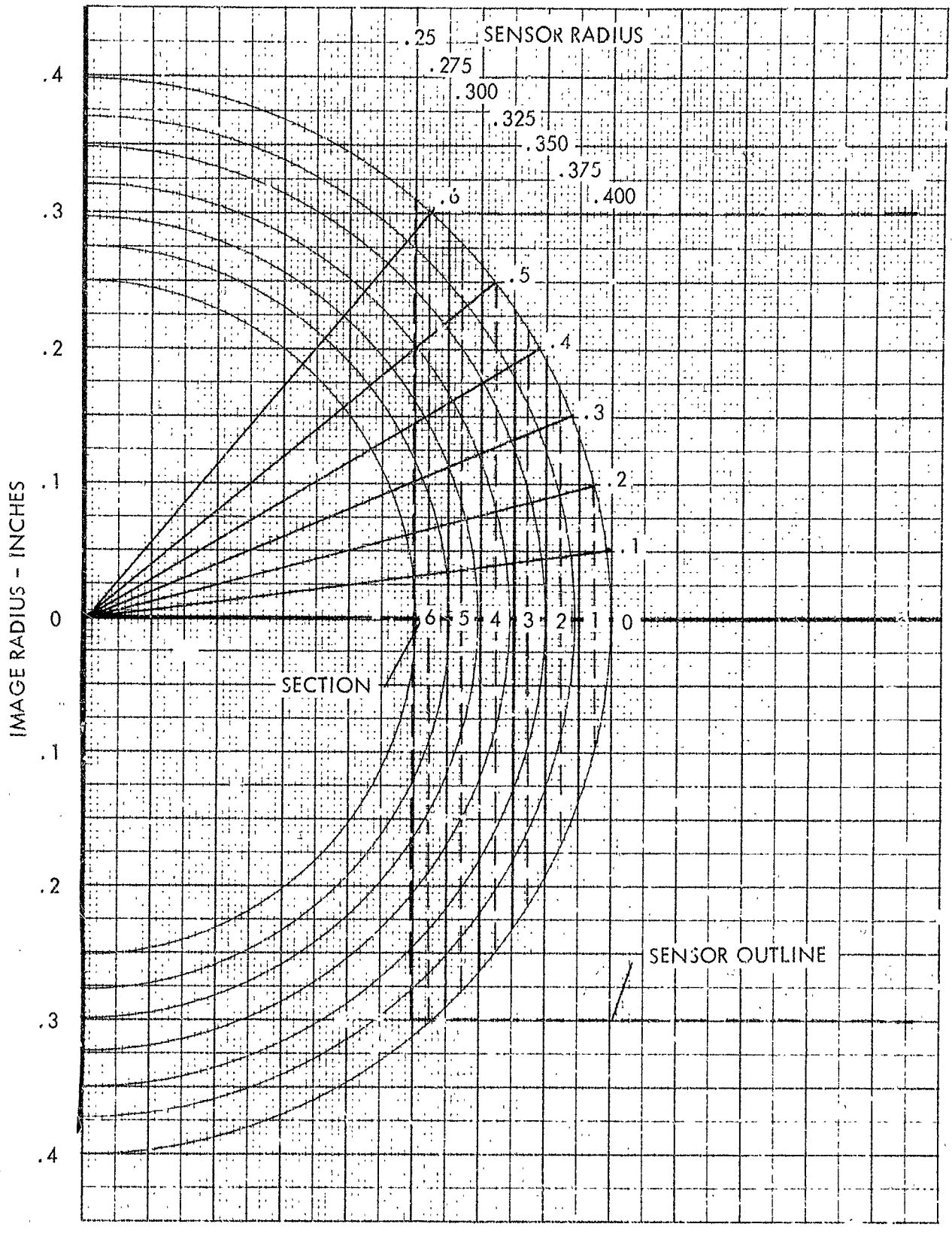

FIGURE 2

AVERAGE SECTION PROFILE

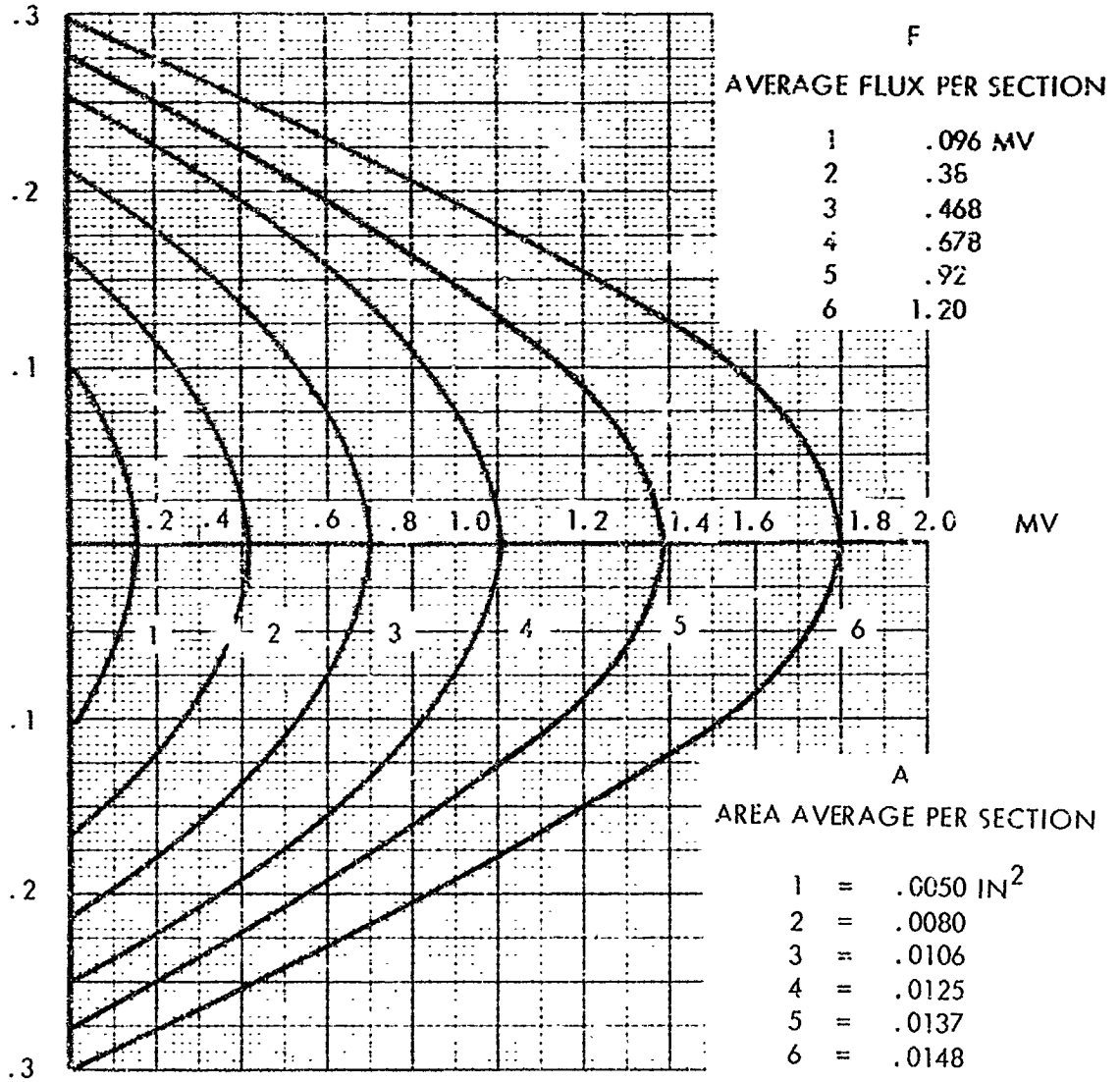

FIGURE 3

SENSOR INPUT POWER
VERSUS LOCATION

(BTU/SEC = 1.054 KW)

$P_s = \Sigma (F \times A \times K)$

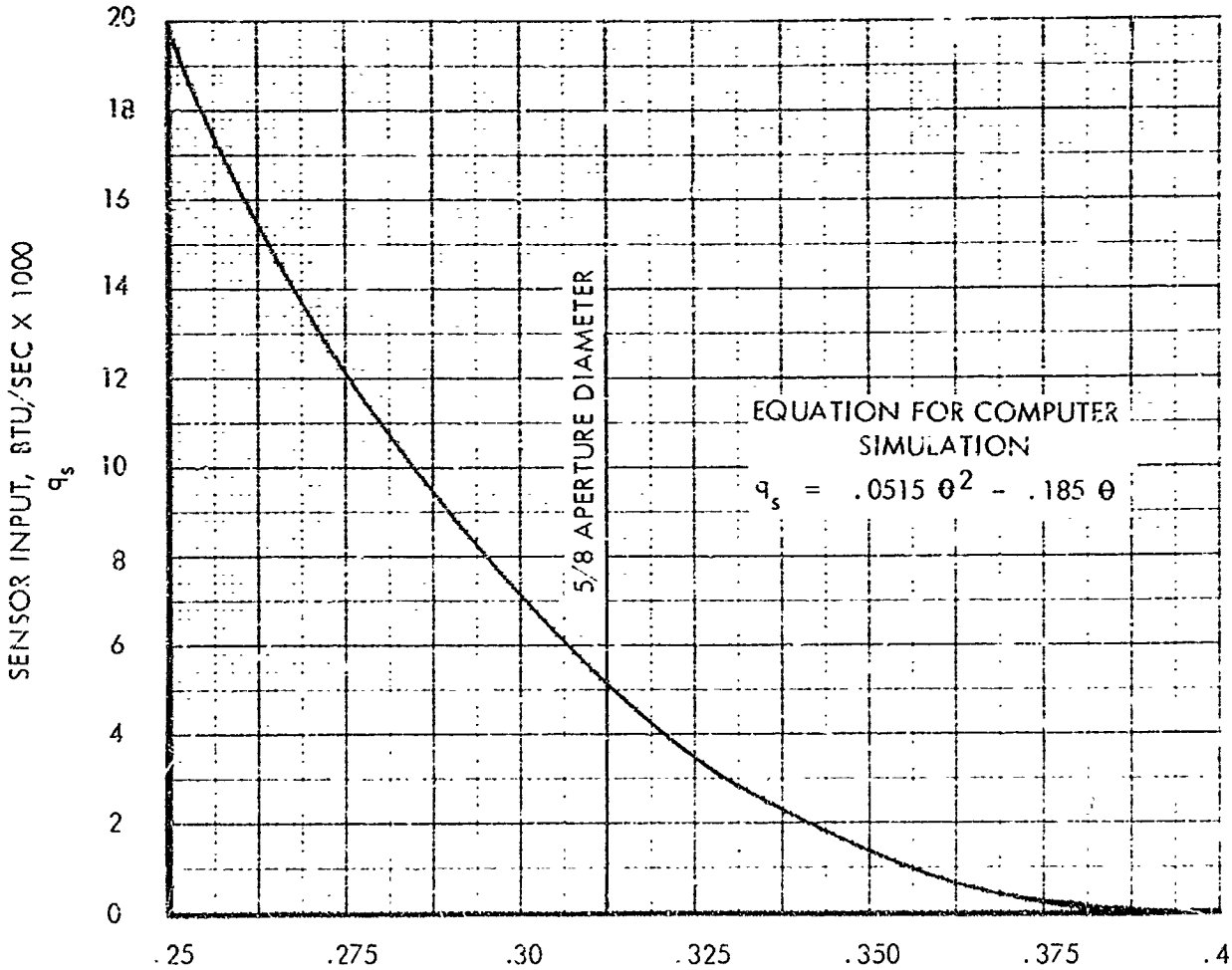

FIGURE 4

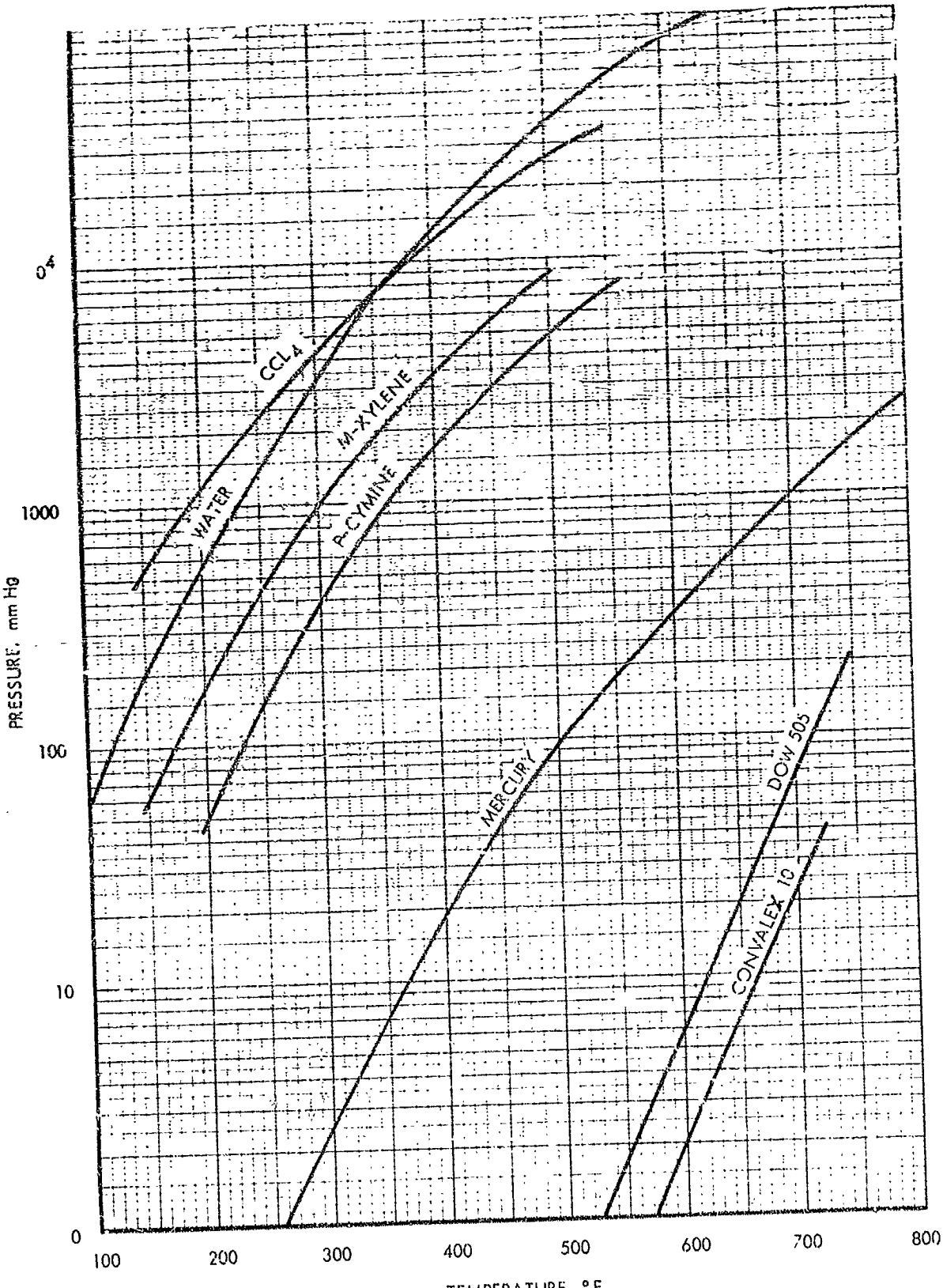
PRESSURE, mm Hg
0*
1000
100
10
0
100
200
300
400
500
600
700
800
TEMPERATURE, °F
WATER
CCL4
M-XYLENE
P-CYMENE
MERCURY
DOW 503
CONVALEX 10

FIGURE 5

VAPOR PRESSURE VERSES TMPERATURE
FOR MERCURY

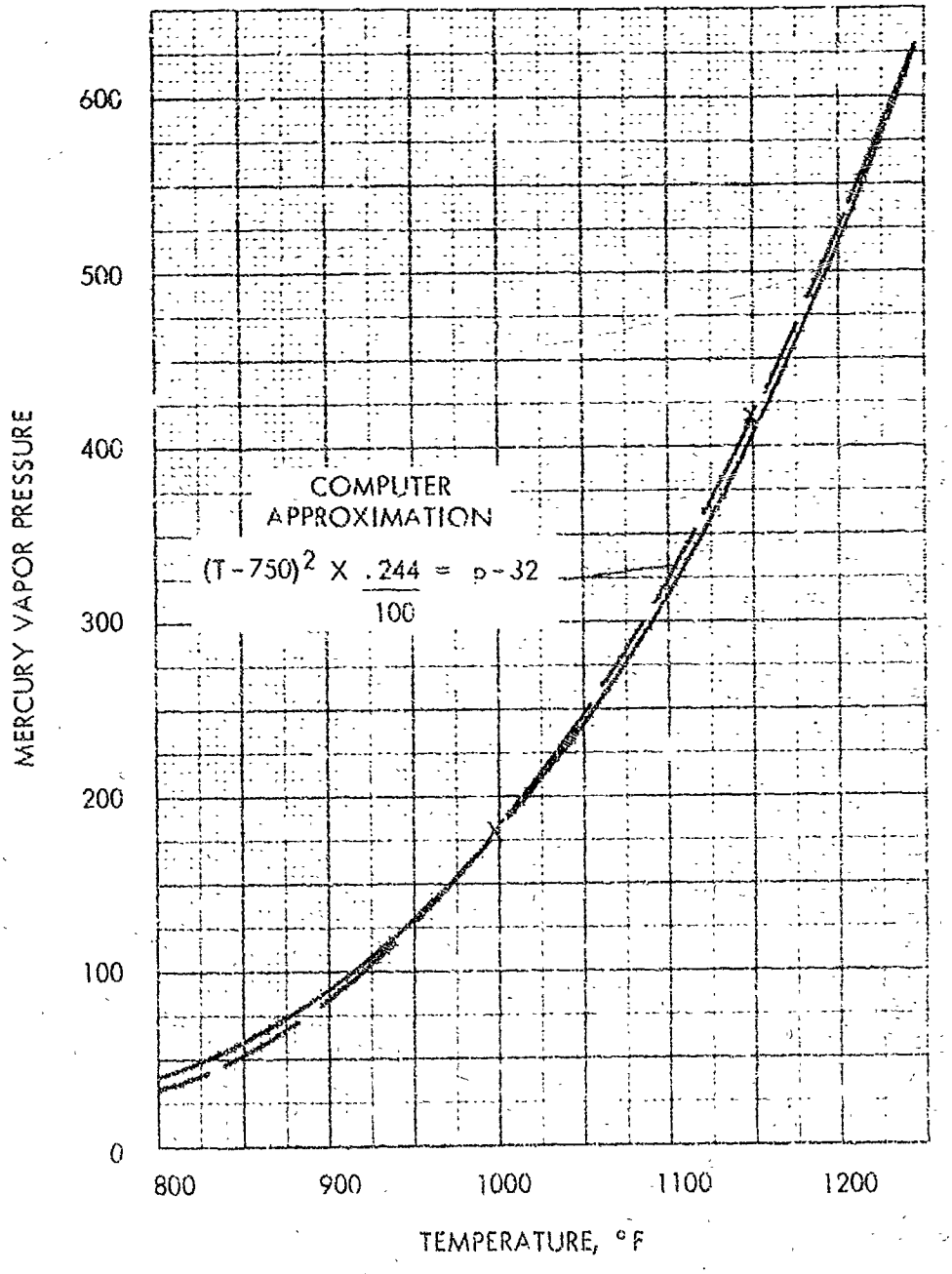

FIGURE 6

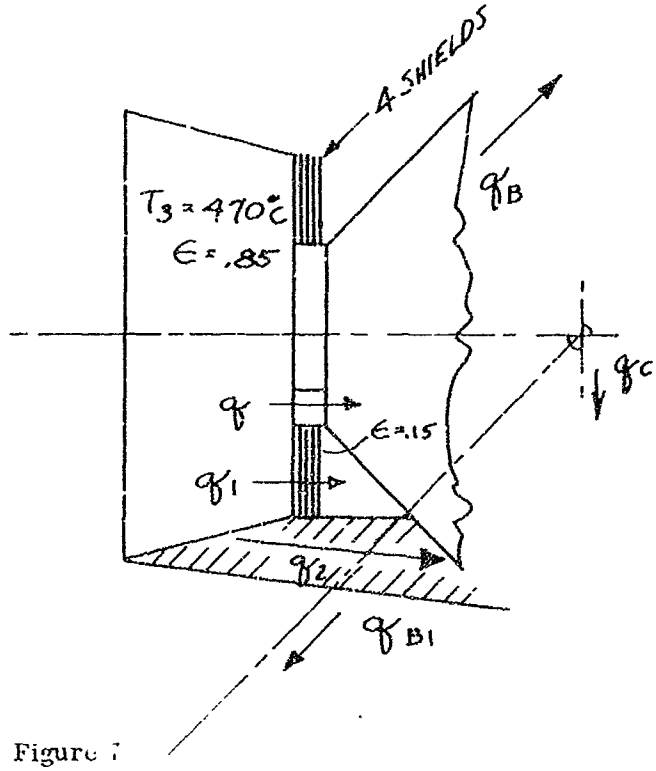

$$q_1 = \sigma \frac{\epsilon}{N} A_1 (T_3^4 - T_B^4)$$

$$q = \frac{K_I A_I (T_3 - T_B)}{l_I}$$

$$q_2 = \sigma \epsilon_2 A_2 (T_3^4 - T_B^4)$$

$$q_{B1} = \sigma \epsilon_B A_{B1} T_B^4$$

$$q_B = \sigma \epsilon_B A_B T_B^4$$

Figure 7

Radiator-Calorimeter Arrangement and Heat Flux Pattern

The heat balance in Figure 7 is given by:

$$q + q_1 + q_2 + P_{SL} + P_S = q_{B1} + q_B + q_c$$

where q = insulator conduction per element

q_1 = shield loss transfer (approximation)

q_2 = edge loss transfer

q_{B1} = edge radiation (1/4 of body)

q_B = top and bottom radiation (1/4 of body)

q_c = support conduction (to be neglected)

l_I = .6 cm avg.

A_I = 4 x 6.45 x $.146^2$ x .785 avg.

= .432 cm^2

K_I = .12/4.186 = .0287 watts cm °C

A_1 = $(\pi (2^2 - 1^2)/4) \times 6.45 = 15.2$ cm^2

A_2 ≈ 5.62 x 1/3 cm^2 estimated effective area per element including view factor

A_B = $\frac{74}{4}$ cm^2 effective area top and bottom/elem.

A_{B1} ≈ A_2

ϵ_1 = $\frac{1}{\frac{1}{.15} + \frac{1}{.15} - 1}$ Assuming a machined surface on back of rad. and body block

= .08

ϵ_2 = .62

ϵ_B = .7

σ = 5.68 watts °K^4 (For temp. x 1000°)

N = 4 shields (with uniform temp. grad.)

Substituting in the heat balance equation and solving for T_B yields

T_B = 715°K = 442°C

The body equilibrium temp is 442°C based on this approximate heat balance. It remains to establish the sensor equilibrium temperature to insure reasonable operating ambient conditions.

Assuming a cylindrical sensor reservoir with a small diameter to length and neglecting end effects we can write the heat balance for the typical geometry in Figure 8.

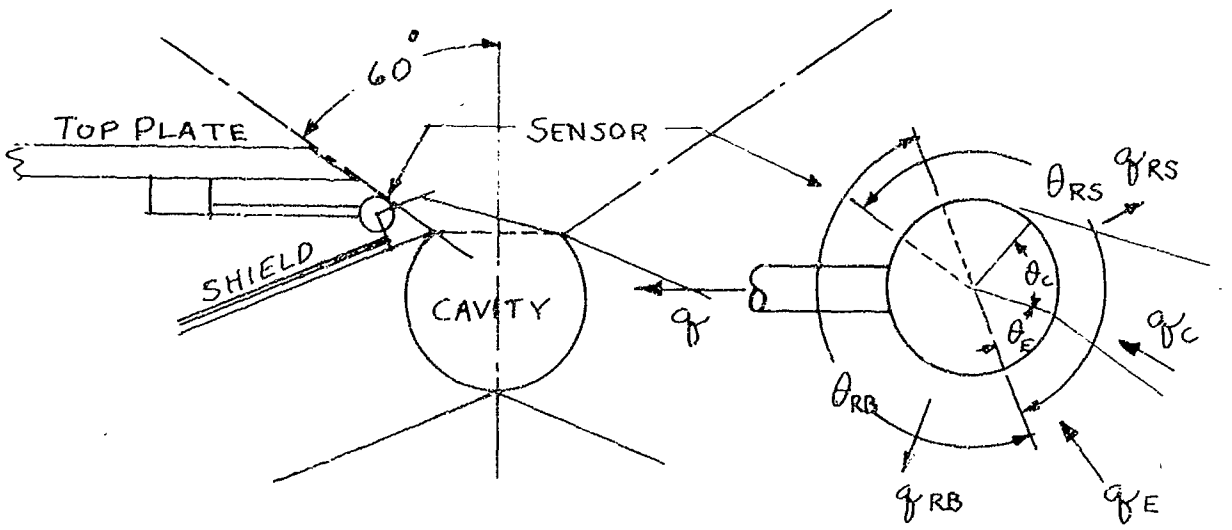

Sensor-Cavity Heat Balance

Figure 8

From Figure 8

$$q_{RS} + q_{RB} + q = q_C + q_E + q_F$$

q_F = solar flux (to be neglected in the calculation of T_S ambient)

q = heat conducted from sensor by support capillar (to be neglected due to very small value compared to radiant transfer)

It will be assumed that the sensor is blackened except for $\theta_C + \theta_E$ which is gold plated and polished.

Then,

$$q_{RS} = \sigma \epsilon_{RS} \frac{\theta RS}{360} \pi d_s l_s T_S^4$$

$$q_{RB} = \sigma \epsilon_{RB} \frac{\theta RB}{360} \pi d_s l_s (T_S^4 - T_B^4)$$

$$q_C = \sigma \epsilon_C \frac{\theta C}{360} \pi d_s l_s (T_C^4 - T_S^4)$$

$$q_E = \sigma \epsilon_E \frac{\theta E}{360} \pi d_s l_s (T_E^4 - T_S^4)$$

σ = 5.68 for T in °K x 1000

ϵ_{RS} = .9 blackened sensor

$$\epsilon_{RB} = \frac{1}{\frac{1}{.9} + \frac{1}{.7} - 1} = .65$$

$$\epsilon_C = \frac{1}{\frac{1}{.9} + \frac{1}{.05} - 1} = .0497$$

$$\epsilon_E = \frac{1}{\frac{1}{.26} + \frac{1}{.05} - 1} = .0438$$

$$\frac{\theta RS}{360} = \frac{210}{360} = .583$$

$$\frac{\theta RB}{360} = \frac{180}{360} = .5$$

$$\frac{\theta C}{360} = \frac{70}{360} = .19$$

$$\frac{\theta E}{360} = \frac{50}{360} \quad .11$$

T_B = 715°K

T_E = 2000°K

T_C = 2000°K

Substituting in the heat balance equation from Figure 8 and dividing through by $\sigma \pi d_s l_s$ we get.

$$.9 \times .583\ T_S^4 + .65 \times .5\ (T_S^4 - .715^4) = .0497 \times .19 \times (2.0^4 - T_S^4) + .0438$$

$$\times .14\ (2.0^4 - T_S^4)$$

$$.8646\ T_S^4 = .3339$$

$$T_S = 788\ ^\circ K = 959^\circ F$$

This is a reasonable sensor ambient in the absence of any signal power input. The corresponding vapor pressure with mercury as a fluid will be 140 psi. The preceding heat balance is very simplified and the actual ambient equilibrium will best be determined by test.

Using a .060 area bellows (OD = 11/32) at .9 radius the sensor volume can be calculated for ± 5° concentrator motion.

$$\partial = r\,\theta = .9 \times \frac{10}{57.7} = .156"$$

$$V_F = \partial\, A_B = .156 \times .06 = .00935\ in^3$$

For $V_S = 2\ V_F$ and $l_S = .6"$

$$d_S = \frac{2 \times .00935 \times 4}{.6} = .199\ in.$$

Then $A_{RB} + A_{RS} = .6 \times .199 \times \frac{360 - (\theta_C + \theta_E}{360}$

$$= .25\ in^2$$

Also $\epsilon_{RB} + \epsilon_{RS} \approx \frac{.9 \times .583 + .65 \times .5}{1.083} = .785$

From 959 to 1100°F the rate of change in radiated power is approximately .0046 BTU/sec °F in^2 for $\epsilon = 1$

1 watt solar input will raise T_S

$$\Delta q \approx 1\ \frac{BTU}{Sec} = .25 \times .785 \times K\,\Delta T_S$$

$$\Delta T_S = \frac{1}{.25 \times .785 \times .046} = 111^\circ F$$

It is apparent that the introduction of even 1 watt will produce a large change in T_S. It is likely that the support structure will have to be designed with sufficient cross section to stabilize T_S within reasonable limits. An additional fin to aid in radiant rejection may also be added to the enclosed portion of the sensor. A third possibility is to add a grid to shield the sensor in part from the solar flux to reduce power transfer. These options will have to be tested in the lab using dummy sensors.

Assuming the nominal sensor operating temperature will be 1070°F or 111°F above calorimeter ambient it is possible to evaluate response time in the sensor and the initial rate of change of pressure with a 1 watt signal.

Using

$$\frac{dq}{dt} = MCp \frac{dT}{dt}$$

and substituting

$$M = Vs \times \varphi = .01870 \times .29$$

$$Cp = .12 \text{ Btu/\#}$$

$$\frac{dq}{dt} \approx 10^{-3} \text{ Btu/sec}$$

The rate of change of sensor temperature is

$$\frac{dT}{dt} \approx \frac{10^{-3}}{.0187 \times .29 \times .12} = 1.52 \text{ °F/sec/watt}$$

using mercury as the fluid charge

$$\frac{dp}{dt} = 1.4 \times 1.52 = 2.1 \text{ psi/sec/watt}$$

where 1.4 is the slope of the mercury pressure-temperature curve.

The sensor response time may be approximated by

$$3TC \approx 3 \times \frac{111 \times .63}{1.52} \qquad 139 \text{ seconds}$$

Support conduction loss from the sensor along its capillary tube length is as follows.

$$q = \frac{KA}{l} (T_S - T_B)$$

$$A = .062^2 / 4 \times 6.45 = .0194 \text{ cm}^2$$

$$K = \frac{.2}{4.186} \text{ watts/°C cm}^2 \text{ cm}$$

$$l = 1\text{cm}$$

$$q = \frac{.2 \times .0194}{4.186} (848 - 715) = .124 \text{ watts}$$

The small value of q justifies dropping the quantity in sensor temperature determinations but indicates the need for larger support sections to adjust for solar flux input.

BELLOWS SELECTION

A survey of various bellows manufacturers has shown several possible standard bellows which may be of use in mount designs. These bellows are compared here to select the most appropriate for use in the design.

The bellows selected should be compatible with size and pressure requirement of the mount. Also the bellows should be of steel or monel to insure compatability with mercury, and the properties of the bellows should yield the greatest amount of useful work and require a minimum of sensor inventory volume to insure fast thermal response. By assuming a maximum angle $\theta = 5°$, a persistent torque of 5 in #, and a pressure of 270 psi at 1070°F for the sensor the various bellows can be compared using the following equations.

$$\tau = r\, p\, A - r^2 \theta \frac{K}{N}$$

where r = radius arm in.

A = effective are in^2

K = spring rate/conv. #/in. /conv.

N = number of convolutions.

Also $\partial = r\,\theta$ and $N = \partial / K_1$

where K_1 = max allowable deflection per convolution in. /conv.

Then $$\tau = r\,p\,A - \frac{r^2\,\theta\,K}{\frac{r\,\theta}{N_i}}$$

$$= r\,(p\,A - K_1\,K)$$

Table I

Table of Standard Bellows Characteristics

Bellows	OD in.	A in.^{2}	K $\frac{\#/in.}{conv.}$	p max psi	K_1 $\frac{in.\ max.}{conv.}$	N Max. conv.
1	1/4	.033	2100	1300	.033	30
2	5/16	.0485	2790	920	.002	22
3	11/32	.06	1400	1500	.005	25
4	15/32	.12	1640	619	.004	14
5	9/16	.16	660	360	.009	30

For τ = 5 in., r may be obtain along with the number of convolutions N required for the deflection of 5°.

Table II

Bellows	r in.	N	Vol. in.^{3}	Work in. #
1	2.94	29	8.4×10^{-3}	1.35
2	.663	43	2.77×10^{-3}	.592
3	.545	17	2.82×10^{-2}	.6
4	.193	22	2.0×15^{3}	.485
5	.134	10	1.85×10^{-3}	.465

$$\text{Work} = \frac{(\tau_1 + \tau\ \theta)}{2}\ \theta = \frac{(r\,A\,p + 5)}{2}\ \theta \quad \text{in. \#}$$

The above tabulation shows a definite advantage in several areas for the 3rd bellows. Also, the size, radius, number of convolutions and maximum pressure are satisfactory for use in the mount. Bellows #4 and #5 require too small a radius. Bellows #2 and #4 require convolutions in excess of the number available. Bellows #1 required a very large radius and 4 times the sensor volume of the other units.

Having selected bellows #3 as most suitable a complete set of characteristics may be tabulated.

Allowing the radius to vary from .5 to 1.5 inches and assuming a max θ of $\pm$ 6° or 12° total the following Table is made.

Table III

Radius In. r	Deflection In. ∂	Volume In.^{3} V	Diameter Sensor In. d	Convolutions N	Free Length FL In.	Spring Rate K in#/Rad.
.5	.104	6.25×10^{-3}	.115	21	.965	16.7
.75	.156	9.35×10^{-3}	.141	31	1.425	25.3
1.0	.208	12.5×10^{-3}	.163	42	1.93	33.0
1.25	.26	15.6×10^{-3}	.182	52	2.39	42.0
1.5	.312	18.7×10^{-3}	.199	62	2.86	52.0
.6	.125			25		36

Since the bellows is limited to 25 convolutions by the manufacturer. A radius of .6 is desired. Since the radius of the diode elements may be .5 inches with shielding, the bellows radius is:

$$.5 + \frac{11}{32}/2 = .672\text{" min.}$$

This indicates a slight over stressing of the bellows at $\theta > 10.7°$.

A practical design radius is chosen to be .8 inch. This allows .3 for bellow and enclosure cylinder radius in the calorimeter. With 25 convolutions the maximum stroke should be .125 or .156 radians, and .156 radians = 9°. Using Fulton Sylphon's nomographs it appears a cycle life of 12,000 may be expected because of the low operating to maximum pressure ratio with a 110% or 10° deflection.

Because deflection is really ± 5° it is likely a still greater cycle life will result although most bellows life times are specified assuming deflection in one direction only.

Design Values for Computer Program

r = .8"	K_2 = 36 in/rad.	N = 25
FL = 1.15"	P_{des} = 270 psi	A = .06 $in.^2$
θ = ± 5°	Cycle Life 12,000	P_{max} 1500 psi

Small Diameter Capillary Damping Calculation

Reorientation of a solar concentrator required the application of a force to the mass of the system. Unless the energy given the mass is somehow dissipated, continued oscillation of the concentrator will result. To prevent this small diameter capillaries are used as dampers. The analysis uses preceding calculations indicating the natural frequency of the concentrator mass - spring system.

Represent the system as follows:

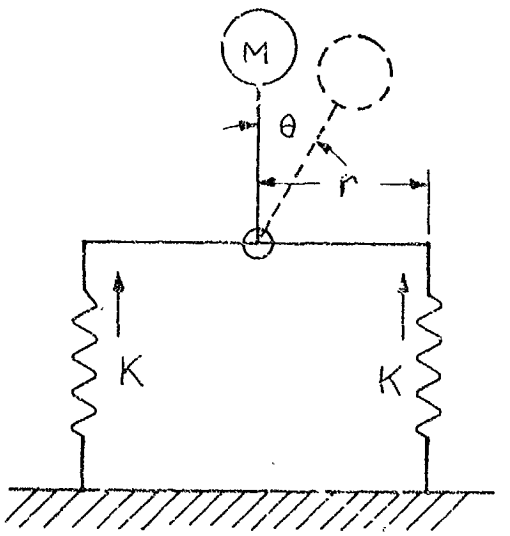

M = mass of system assumed concentrated

m collector = .0259 $\frac{sec^2}{in.}$

for a wt. of 10.

h = 26 in

r = .8 in (assumed

K_2 = stiffness of bellows

Figure 9

Restoring Torque = T = moment arm x force

$T = 2 r \times K^1 r$

$T = 2r^2 K^1 = K^1$ = torsional spring constant

for K^1 = 70 #/in. $K_2 = 72 \frac{in.\,lb}{rad.}$

The undamped differential equation of motion is

$$J\ddot{\theta} + K\theta = 0$$

The undamped natural frequency is

$$\omega_n = \sqrt{\frac{K}{J}}$$

For $K = 74 \frac{\text{in. lb}}{\text{rad.}}$ and $J = M h^2 = 17.5 \ \# \ \text{sec}^2 \ \text{in.}$

$$\omega_n = 2.1 \frac{\text{rad.}}{\text{sec.}}$$

Critical damping is $f_{cr} = 2\sqrt{KJ}$

Consider now the energy dissipated in mercury flowing in small tubes.

at 360°C, φ = density = $.00119 \ \# \frac{\text{sec}^2}{\text{in}^4}$

at 340 C, μ = viscosity = $.0134 \times 10^{-5} \ \frac{\# \ \text{sec}}{\text{in}^2}$

$$\text{head loss} = h_L = f \frac{l}{d} \cdot \frac{V^2}{2g}$$

where $f = \frac{64\mu}{Vd_p}$

l = length of tube

For the torsional system, the damping torque (c) is defined as the damping torque when the angular velocity = 1 rad. per sec.

First write c in general terms for utilization in computer program.

At $\dot{\theta}$ = 1 rad per sec

V_b = vel. bellows = r $\frac{\text{in}}{\text{sec}}$

V_c = vel. capillary fluid = $\frac{A \times V_b}{A \text{ capillary}}$

where $A_c = .785 \ d^2$

Equivalent pressure for head loss is

$$p = \gamma h_L$$

and the damping torque per capillary is

$$C = p A_b \times r = \gamma h_L A r$$

where $h_L = \dfrac{32 \mu l V_c}{g \varphi d^2}$

and $V_c = \dfrac{A V_b}{.785 d^2}$

These equations yield for $\dot{\theta} = 1$ ($V_b = 1 \times r$)

$$C = \frac{40.8 \gamma \mu l A^2 r^2}{\varphi g d^4}$$

For mercury

$$\gamma = .460 \text{ /in}^3$$

$$\varphi = .0011 \frac{\text{sec}^2}{\text{in}^2}$$

$$\mu = .0134 \times 10^{-5} \frac{\text{sec}}{\text{in}^2}$$

and for

$l = 1$ inch

$A = .060 \text{ in}^2$

$r = 1$ inch

$d = .010$ inch

$c = 1.97$ in per rad per sec. for 1 capillary, 1" long of .010" dia.

Values of c for two capillaries at several radii are plotted in Figure 10.

Using r = .8 inches and A_b = .060 in^2 the value of (capillary length) is determined from:

$$\ell = \frac{fc}{c}$$

for any capillary diameter selected.

Miscellaneous System Characteristics

Critical damping f_c = 72 in. #/rad./sec. = $\sqrt{\frac{K^1}{J} - \frac{fc^2}{4J^2}} = 0$

Bearing spring rate $K_B \approx$ 2 in #/rad.

Torsional spring rate $K^1 = 2K_2 - K_B$ = 74 in. #/rad.

Time constant $\tau c = \frac{\frac{1}{fc}}{2J}$ = .475 sec.

Natural frequency $\omega_n = \sqrt{\frac{K^1}{J}}$ = 2.1 rad/sec

Design inertial $J = M r^2 = \frac{10}{32.2 \times 12} \times 26^2$ = 17.5 in sec^2

Sensor heat capacity M_{cp} = 2.89×10^{-3} BTU/sec°F

The computer diagram is as shown in Figure 11. The initial program diagram includes all key components and uses the design values established herein.

2 Hg CAPILLARIES, 1" LONG, WITH r MOMENT ARMS

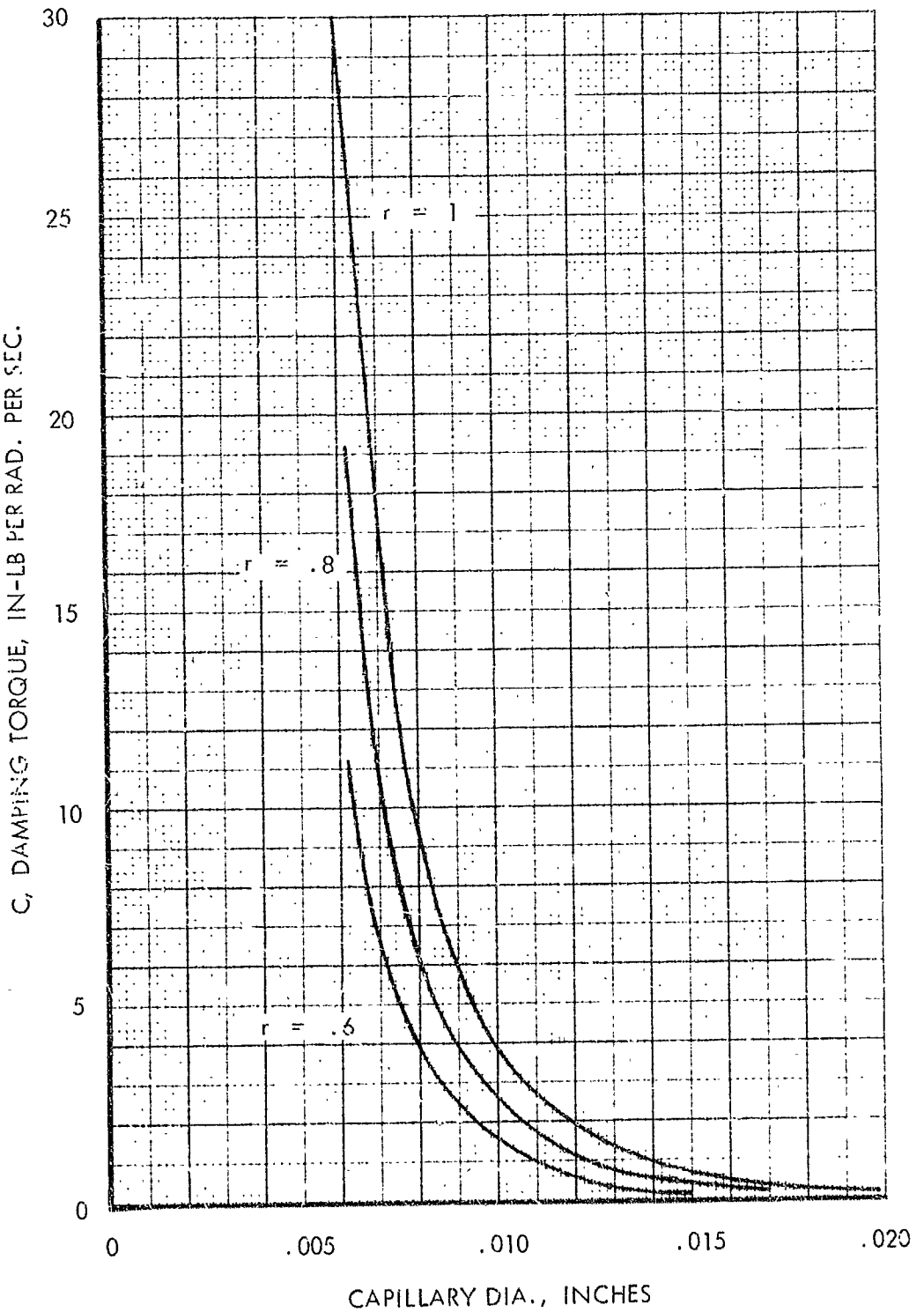

FIGURE 10

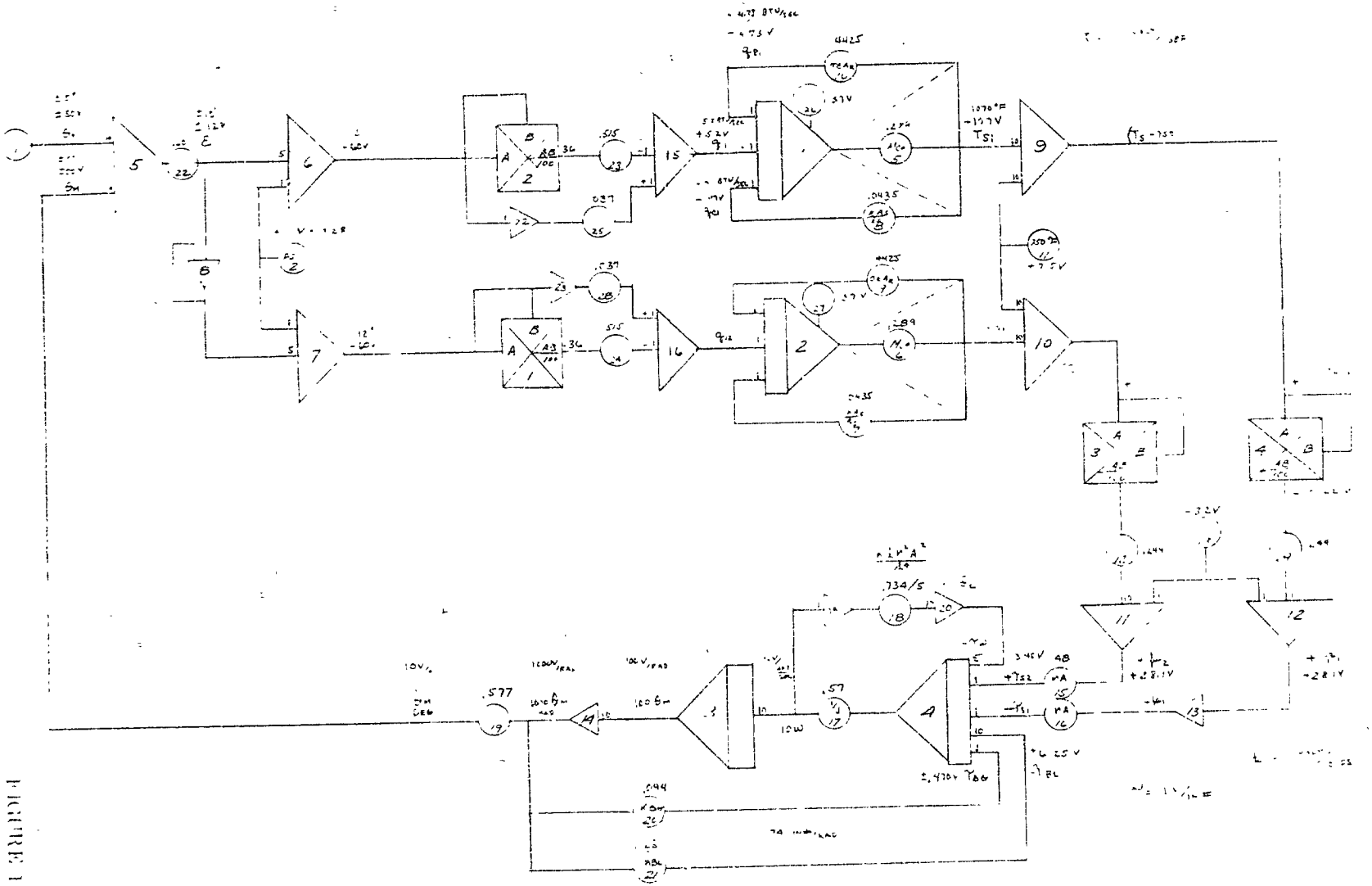

FIGURE 11

HELIOTROPIC MOUNT COMPUTER DIAGRAM